THESIS ON NATURAL AND EXACT SCIENCES B103

Formation of Properties of $CuInSe_2$ and $Cu_2ZnSn(S,Se)_4$ Monograin Powders Synthesized in Molten KI

KRISTI TIMMO

TUT PRESS

TALLINN UNIVERSITY OF TECHNOLOGY
Faculty of Chemistry and Materials Technology
Department of Materials Science
Chair of Semiconductor Materials Technology

Dissertation was accepted for the defence of the degree of Doctor of Philosophy in Natural and Exact Sciences on February 11th, 2011.

Supervisor: Leading Research Scientist Mare Altosaar, Department of Materials Science, Tallinn University of Technology

Opponents: Dr. Charlotte Platzer-Björkman, Uppsala University, Sweden

Dr. Kaupo Kukli, University of Tartu, Estonia

Defence: March 30th, 2011, at 14.00
Lecture hall: VII-226
Tallinn University of Technology, Ehitajate tee 5, Tallinn

Declaration: Hereby I declare that this doctoral thesis, my original investigation and achievement, submitted for the doctoral degree at Tallinn University of Technology has not been submitted for any academic degree.

Kristi Timmo

ISSN 1406-4723
ISBN 978-9949-23-066-2

LOODUS- JA TÄPPISTEADUSED B103

Kaaliumjodiidsulandaja keskkonnas kasvatatud monoterapulbrite $CuInSe_2$ ja $Cu_2ZnSn(S,Se)_4$ omaduste kujundamine

KRISTI TIMMO

TTÜ
KIRJASTUS

Table of Contents

LIST OF PUBLICATIONS

The present doctoral thesis is based on the following papers, which are referred to in the text by their Roman numerals **I-VI**.

I **K. Timmo**, M. Altosaar, M. Kauk, J. Raudoja, E. Mellikov, $CuInSe_2$ monograin growth in the liquid phase of potassium iodide. *Thin Solid Films*, Vol. 515 (2007) 5884-5886.

II M. Kauk, M. Altosaar, J. Raudoja, **K. Timmo**, M. Grossberg, T. Varema, E. Mellikov, Growth of $CuInSe_2$ monograin powders with different compositions, Mater. Res. Soc. Symp. Proc. Vol. 865 (2005) 463-469.

III **K. Timmo**, M. Altosaar, J. Raudoja, E. Mellikov, T. Varema, M. Danilson, M. Grossberg, The effect of sodium doping to $CuInSe_2$ monograin powder properties. *Thin Solid Films*, Vol. 515(2007) 5887-5890.

IV **K.Timmo**, M. Altosaar, J. Raudoja, M. Grossberg, M. Danilson, O.Volobujeva, E.Mellikov, Chemical etching of $Cu_2ZnSn(S,Se)_4$ monograin powder, 35th IEEE Photovoltaic Specialists Conference, Honolulu, Hawaii, June 20-25, 2010: Conference Proceedings 1982 - 1985.

V M. Altosaar, J. Raudoja, **K. Timmo**, M. Danilson, M. Grossberg, J. Krustok and E. Mellikov, $Cu_2Zn_{1-x}Cd_xSn(Se_{1-y}S_y)_4$ solid solutions as absorber materials for solar cells, *Physica Status Solidi A - Applications and Materials Science,* 205 (1) (2008) 167-170.

VI **K. Timmo**, M. Altosaar, J. Raudoja, K. Muska, M. Pilvet, M. Kauk, T. Varema, M. Danilson, O. Volobujeva, E. Mellikov, Sulfur-containing $Cu_2ZnSnSe_4$ monograin powders for solar cells, *Solar Energy Materials & Solar Cells* 94 (2010) 1889-1892.

In Appendix A, copies of the following papers are included.

Author`s own contribution

I Part of the experimental work ($CuInSe_2$ monograin powder preparation, determination of $CuInSe_2$ solubility in KI, granulometric analysis), analysis of the results and major part of writing

II Part of the experimental work ($CuInSe_2$ monograin powder preparation)

III Part of the experimental work ($CuInSe_2$ monograin powder preparation, doping with sodium) and characterization (I-V curve measurements), analysis of the results and major part of writing

IV Part of the experimental work ($Cu_2ZnSn(S,Se)_4$ monograin powder preparation, chemical etching, CBD-CdS deposition) and characterization (Raman spectroscopy, I-V curve measurements), analysis of the results and major part of writing

V Part of the experimental work ($Cu_2Zn_{1-x}Cd_xSn(Se_{1-y}S_y)_4$ monograin powder preparation, CBD-CdS deposition) and characterization (I-V curve measurements)

VI Part of the experimental work ($Cu_2ZnSn(S,Se)_4$ monograin powder preparation, chemical etching, CBD-CdS deposition) and characterization (I-V curve measurements), analysis of the results and major part of writing

List of abbreviations and symbols

MGL	Monograin layer
CISe	$CuInSe_2$
CZTS	Cu_2ZnSnS_4
CZTSe	$Cu_2ZnSnSe_4$
CZTSSe	$Cu_2ZnSn(S,Se)_4$
RF	Radio frequency
RT	Room temperature
EDXRD	Energy dispersive X-ray diffraction
PL	Photoluminescence
E_g	Bandgap energy
MGP	Monograin powder
I-V	Current-voltage
η	Solar cell efficiency
j_{sc}	Short circuit current density
V_{oc}	Open circuit voltage
FF	Fill factor
Φ_b	Barrier height of *p-n* junction
V_L	Volume of liquid phase
V_S	Volume of solid phase
XRD	X-ray diffraction
ICP-MS	Inductively coupled plasma mass spectrometry

SEM	Scanning electron microscopy
SE SEM	Secondary electron mode of SEM
EsB SEM	Energy selectiv backscattering mode of SEM
EDS	Energy dispersive spectroscopy
QE	Quantum efficiency
XPS	X-ray photoelectron spectroscopy

INTRODUCTION

The increasing demand for energy, the limited supply of fossil fuels and their unfavourable effect on the environment are the main reasons why the search for alternative sources of power is imperative. Given that there is a vast amount of energy available from the sun, devices that convert light energy into electrical energy are becoming increasingly important. Since the 1970s, solar electricity, also known as photovoltaics (PV), has shown that human race can get a substantial portion of its electrical power without burning fossil fuels (coal, oil or natural gas) or creating nuclear fission reactions. Photovoltaics has shown that it can generate electricity for a wide range of applications, scales, climates, and geographic locations [1].

For large–scale terrestrial photovoltaic applications, cost-effective processes and materials are needed. One approach to bring down the costs of solar cell production is to develop cheap non-vacuum technologies: one of them is the monograin layer (MGL) solar cell technology.

The research in this thesis is mainly directed to the regularities of the synthesize-growth of $CuInSe_2$ and $Cu_2ZnSn(S,Se)_4$ monograin powders in liquid potassium iodide as absorber materials for monograin layer solar cells. The aim of the study was to modify absorber material properties for improvement of monograin layer solar cell parameters.

This thesis is divided into four Chapters. After introduction, literature is briefly reviewed in Chapter 1. Chapter 2 describes the preparation of the $CuInSe_2$ and $Cu_2ZnSn(S,Se)_4$ monograin powders and the design of monograin layer solar cells on their bases. Additionally, the used experimental technological approaches and characterization methods are given. Chapter 3, divided into four different parts, presents experimental results and their discussion. In the first part the growth parameters of $CuInSe_2$ powder particles in potassium iodide are described. The second part deals with the effect of sodium doping to the properties of $CuInSe_2$ monograin powder as absorber material in monograin layer solar cells. The third part of this chapter presents the results of chemical treatment of $Cu_2ZnSn(Se_{1-x}S_x)_4$ monograin powder surface. The morphological and compositional properties of CZTSSe crystals surfaces depending on the chemical nature of the etchant are given in this part of the work. The fourth part describes the formation of $Cu_2ZnSn(Se_{1-x}S_x)_4$ solid solutions and how the concentration ratio of Se/S in the absorber material influences the solar cell parameters.

Finally, Chapter 4, summarizes the main results.

The work is financially supported by Estonian Science Foundation grants 6160, 6179, 7678 and SF0140099s08. Financial support was also received from Enterprise Estonia, World Federation of Scientists National Scholarship Programme and Estonian Doctoral School of Materials Science and Materials Technology (MMTDK). This doctoral thesis is based on 6 published papers.

1. LITERATURE REVIEW AND AIM OF THE STUDY

1.1 $CuInSe_2$ based solar cells

The chalcopyrite $CuInSe_2$ is a I-III-VI_2-semiconductor. It can be deposited as a polycrystalline thin film or grown as a single crystal. As a semiconductor, $CuInSe_2$ inhibits a high absorption coefficient 10^4 – 10^5 cm^{-1}. Conversion efficiencies between 12 and 15% have already been achieved for devices based on pure $CuInSe_2$/CdS/ZnO heterojunction [2,3]. The bandgap of the absorber material can be changed by using solid solutions of $CuInSe_2$ with $CuInS_2$ and $CuGaSe_2$. The bandgap of the resulting $Cu(In,Ga)(S,Se)_2$ compound semiconductor can be adjusted over a wide range: from 1.04 eV for pure $CuInSe_2$ over 1.5 eV and 1.68 eV for $CuInS_2$ and $CuGaSe_2$ [4].
The highest efficiency to date for $Cu(In,Ga)Se_2$ solar cells is 20.3%, reported by Centre for Solar Energy and Hydrogen Research (ZSW) in Stuttgart [5].

1.1.1 $Cu_2ZnSnSe_4$ and Cu_2ZnSnS_4 based solar cells

Since the availability of indium is an object of discussion regarding the large-scale production of $CuInSe_2$ solar cells, its replacement with other elements, for instance with Zn and Sn, is reconceived.
$Cu_2ZnSn(S,Se)_4$ (CZTSSe) is a new type of an absorber material for thin film solar cells. CZTSSe consists of elements that are abundant in the crust of the earth and most of them are nontoxic. This semiconductor compound can be obtained by replacing half of the indium atoms in chalcopyrite $CuInSe(S)_2$ with zinc and the other half with tin. The abundance of zinc, tin, and indium in the crust of the earth is 75, 2.2, and 0.049 ppm, respectively [6]. In 1988, Ito and Nakazawa for the first time recorded the photovoltaic effect in the heterodiode that consisted of a cadmium-tin-oxide transparent conductive film and a CZTS thin film on a stainless steel substrate. They reported the value of open-circuit voltage as high as 165 mV [7]. In 1989, by annealing the same device in air, they achieved the open-circuit voltage of 250 mV and the short-circuit current of 0.1 mA/cm^2 [8]. In 1997, Friedlmeier *et al.* fabricated CZTS thin films by thermal evaporation of the elements and binary chalcogenides in high vacuum. To form the heterojunction on this film they deposited *n*-CdS and ZnO window layers and reported the highest conversion efficiency of 2.3% and the highest open-circuit voltage of 570 mV [9]. In 2003, Seol *et al.* prepared CZTS thin films by RF magnetron sputtering. They reported that the refractive index of CZTS was 2.07, the absorption coefficient was about 10^4 cm^{-1}, and that the band gap energy was about 1.51 eV [10]. Katagiri *et al.* attained the conversion efficiency of 5.45% in 2003 [11]. In 2007, they reached up to the conversion efficiency of 5.74% [12] and in 2009 up to 6.77% using a three-sources RF co-sputtering for metal film deposition followed by annealing in sulfur

containing atmosphere [13]. At present, the best conversion efficiency of the $Cu_2ZnSn(S,Se)_4$ thin film solar cells achieved by Mitchi *et al*. is 9.66% [14].

1.2 Crystal structures of $CuIn(S,Se)_2$ and $Cu_2ZnSn(S,Se)_4$

The compounds $A^IB^{III}X_2^{VI}$ (A = Cu,Ag; B = Al,Ga,In; X = S,Se,Te) crystallize in the tetragonal chalcopyrite-type structure (space group $I\bar{4}2d$) [15]. The unit cell of $CuInSe_2$ is shown in Figure 1. The values measured for lattice parameters of CISe at room temperature are a = 5.784 Å and c = 11.618 Å [16].

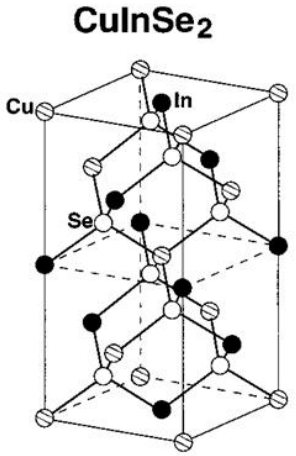

Figure 1. Chalcopyrite type unit cell of $CuInSe_2$ [15].

Lowering the symmetry one step further leads to the stannite-type structure (space group $I\bar{4}2m$) named after the mineral stannite Cu_2FeSnS_4 [17,18]. A symmetry decrease is not only achieved by an ordered substitution of the metals, but also by changing the metal ordering, i.e. the arrangement of the cations on the structural sites of the unit cell. By doing so the kesterite type structure (space group $I\bar{4}$) can be deduced from the stannite-type structure, which is named after the mineral kesterite Cu_2ZnSnS_4 [18,19]. These two structures, the stannite and kesterite type structures (see Figure 2), differ only in the distribution of Cu^+ and Zn^{2+} [19,20].

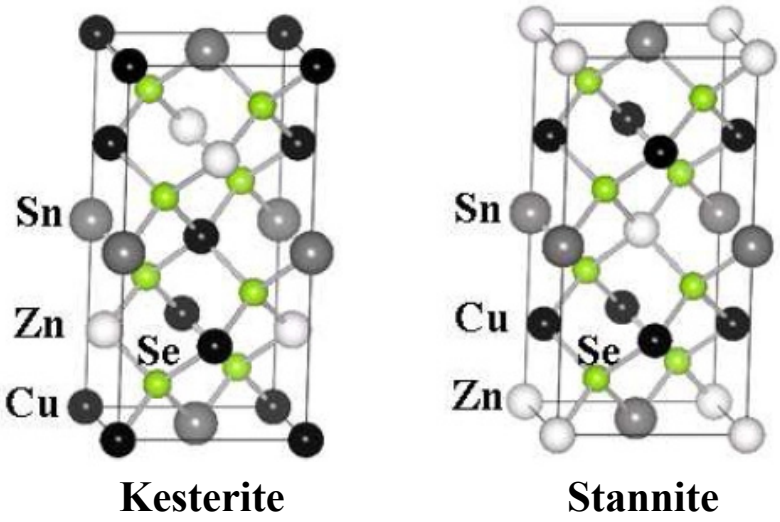

Figure 2. Crystal structures of $Cu_2ZnSnSe_4$ in kesterite and stannite phases [20].

The discussion in literature centres on photovoltaics based on In-free absorber materials, as for instance compounds belonging to the stannite-type or also kesterite-type structure family [21,22]. Chen *et al*. found that kesterite structure is the ground state structure for both CZTS and CZTSe, whereas stannite structure has higher total energies [23]. Although the kesterite structure possesses lower energy, the energy difference between the kesterite and stannite structure is small, about 3 meV/atom [23,24]. This indicates that kesterite and stannite ordering may coexist in the sythesized samples.

The calculated bandgap of CZTSe is about 0.4 eV smaller than CZTS in the same crystal structure, which is consistent with our common expectation that the selenides have smaller bandgaps than the corresponding sulfides but disagrees with the interpretation of experimental absorption data showing that the bandgaps of CZTSe are nearly the same as CZTS at about 1.5 eV [25,26,27]. The estimated energygaps are *Eg* =1.56 eV for kesterite CZTS, 1.42 eV for stannite CZTS, 1.05 eV for kesterite CZTSe, and 0.89 eV stannite CZTSe [24].

Another problem reported concerns the bandgap energy of CZTSe, where there are large discrepancies between the reported values. Several research groups have found that $Cu_2ZnSnSe_4$ has bandgap energies from 1.44 to 1.56 eV [7,25,27,28]. On the other hand, Raulot *et al.*[29] have performed *ab initio* calculation of the electronic structure of CZTSe and found a bandgap around 0.8 eV and Zoppi *et al*.[30] stated that this value ranges from 0.88 to 0.94 eV.

1.2.1 Phase diagrams

The isoelectronic, pseudobinary Cu_2Se-In_2Se_3 tie line provides a good overview of the phases involved in $CuInSe_2$ growth. The most contemporary and the most relevant for thin-film $CuInSe_2$ growth, Cu_2Se-In_2Se_3 phase diagram, is the one from Haalboom in 1998 [31] shown in Figure 3. This investigation had special focus on temperatures and compositions relevant for the preparation of thin-films. The phase diagram in Figure 3 represents the four different phases which have been found to be relevant in this range: the α-phase $CuInSe_2$, the In-rich β-phase $CuIn_3Se_5$, the δ-phase (the high-temperature sphalerite phase) and Cu_2Se. For the α-phase the existence range extends from 24-24,5 at.% Cu at room temperature [32]. At higher temperatures, the existence range of single-phase $CuInSe_2$ is broadening to the In side and does not involve the stochiometric composition with 25% Cu, as reported in [33,34]. The α-phase and Cu_2Se already coexist at a Cu content below 25 at.%. Cu_2Se is the only secondary phase present in Cu-rich compositions. For more extreme In-rich compositions, in addition to the β-phase, other ternary In rich Cu-In-Se phases can also form (e.g. $Cu_2In_4Se_7$, $CuIn_3Se_5$ and Cu_5InSe_4) [35].

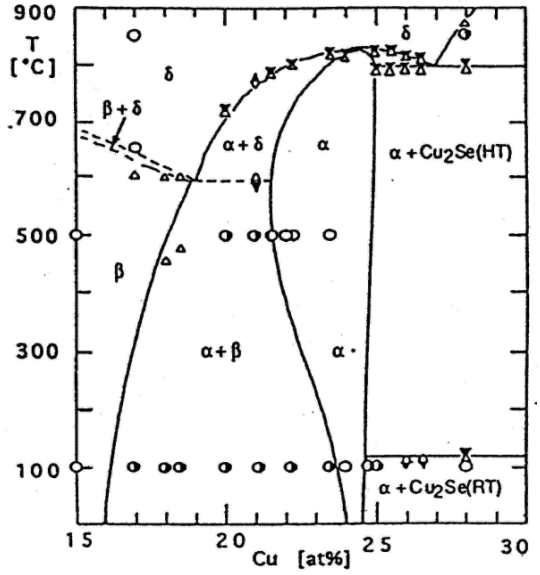

Figure 3. Quasi-binary phase diagram Cu_2Se-In_2Se_3 in the range of 15-30 at.% Cu and 20-900˚C [31].

There is no simple way to draw a quaternary phase diagram, and only few papers have been published in this regard for Cu-Zn-Sn-S/Se. Phase equilibria in the Cu_2Se-Cu_2SnSe_3-ZnSe system were investigated by L.V.Piskach *et al.* [36]. The quaternary

compound $Cu_2ZnSnSe_4$ has a homogeneity range and undergoes a polymorphous transformation ($\delta \leftrightarrow \delta'$) in the temperature interval 856–892 K (see Figure 4). In contrast to $CuInSe_2$, where it is clear that only Cu_2Se is present for compositions with [Cu]/[In]≥1, the formation of secondary phases in $Cu_2ZnSnSe_4$ for [Cu]□25 at.% depends also on the Sn content (on the [Sn]/[Zn] ratio). The polythermal $SnSe_2$–$Cu_2ZnSnSe_4$ section is quasi-binary in the subsolidus part. Its liquidus consists of two fields of primary crystallization of the β-solid solution (ZnSe) and the γ-solid solution ($SnSe_2$). The secondary crystallization $L \leftrightarrow \gamma+\beta$ and $L+\beta \leftrightarrow \delta$ is completed on the horizontal plane at a temperature of 892 K corresponding to a ternary peritectic processes. The $SnSe_2$–$Cu_2ZnSnSe_4$ section is a tie line in the quasi-ternary system and, hence, the three-phase fields 4 and 5 can be contiguous with the single-phase fields 10 and 7, respectively. The polymorphous transformation of $Cu_2ZnSnSe_4$ occurs at 856 K and its homogeneity range is smaller than 3 mol.% $SnSe_2$.

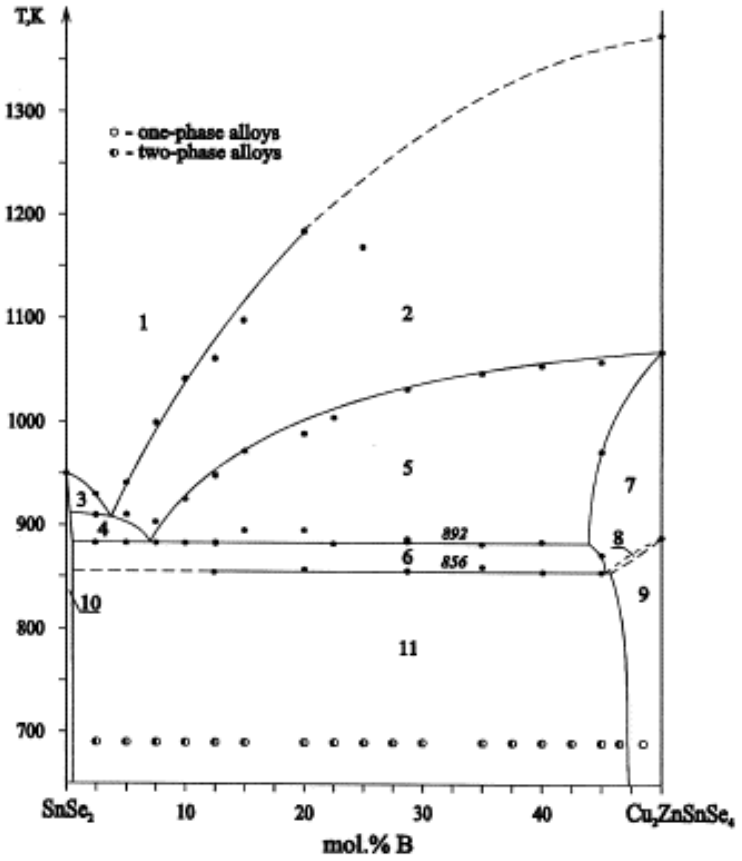

Figure 4. $SnSe_2$–$Cu_2ZnSnSe_4$ section (B, 50 mol.% Cu_2Se, 50 mol.% ZnSe): (1) L, (2) L+β, (3) L+γ, (4) L+β+γ, (5) L+β+δ, (6) γ+δ, (7) δ, (8) δ+δ′, (9) δ′, (10) γ, (11) γ+δ′ [36].

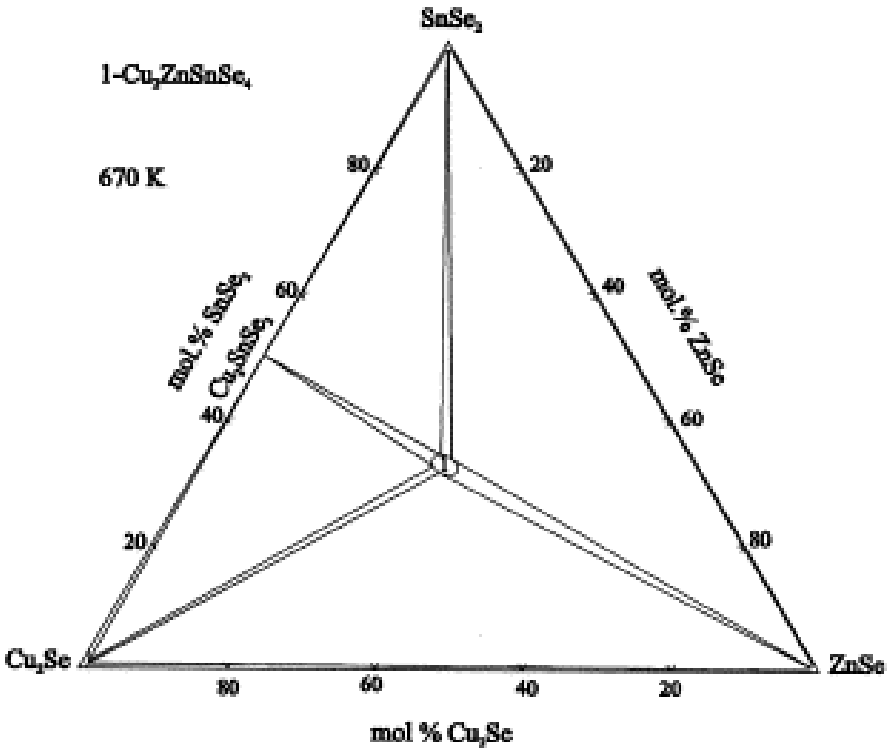

Figure 5. Isothermal section of the Cu_2Se–ZnSe–$SnSe_2$ system at 670 K [36].

The isothermal section of the quasi-ternary Cu_2Se–ZnSe–$SnSe_2$ system at 670 K (Figure 5) consists of the homogeneity ranges of the α-, β-, γ- and δ'-solid solutions of Cu_2Se, ZnSe, $SnSe_2$ and of the low-temperature modification of the quaternary compound $Cu_2ZnSnSe_4$. The solubility of $Cu_2ZnSnSe_4$ in Cu_2Se is lower than 2 mol.% and is elongated along the Cu_2Se–$SnSe_2$ boundary side, in ZnSe and $SnSe_2$ it is lower than 1 mol.%, in Cu_2SnSe_3 lower than 0.5 mol.%. The miscibility gap of $Cu_2ZnSnSe_4$ was found to be 3 mol.% along the triangulated section Cu_2SnSe_3–ZnSe, which was established according to the investigation of 20 additional alloys allocated in three sections crossing the equimolar composition of the quaternary compound.

L.V.Piskach *et al.* have investigated the phase equilibria in the Cu_2S-ZnS-SnS_2 system [37]. The vertical section Cu_2S–A (A-50 mol% ZnS, 50 mol% SnS_2) is shown in Figure 6. The liquidus consists of three lines that limit the fields of primary crystallization of the α-solid solution range of Cu_2S and β'- and β-solid solution range of the two polymorphic modifications of ZnS.

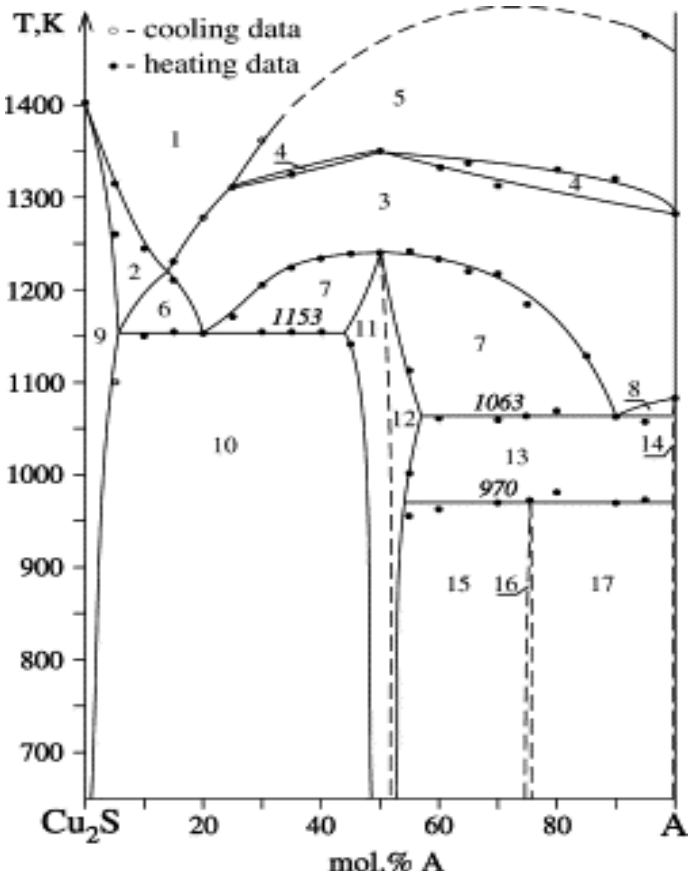

Figure 6. Phase diagram of the Cu_2S–A section: (1) L, (2) L+α, (3) L+β′, (4) L+β+β′, (5) L+β, (6) L+α+β′, (7) L+β′+δ, (8) L+β′+γ, (9) α, (10) α+δ, (11) δ, (12) β′+δ, (13) β′+γ+δ, (14) β′+γ, (15) β′+δ+$Cu_2ZnSn_3S_8$, (16) β′+$Cu_2ZnSn_3S_8$, (17) β′+γ+$Cu_2ZnSn_3S_8$ [37].

The lines of 1153 and 1063K correspond to ternary peritectic reactions L+$\beta' \leftrightarrow \delta+\alpha$ and L+$\beta' \leftrightarrow \delta+\gamma$, respectively. At these temperatures the secondary crystallization of the binary peritectics: L+$\beta' \leftrightarrow \alpha$, L+$\beta' \leftrightarrow \delta$ and the binary eutectic L$\leftrightarrow \beta'+\gamma$ terminated. The Cu_2S–Cu_2ZnSnS_4 part of the section is quasi-binary in the sub-solidus region. Therefore the single-phase region δ is limited by the three-phase region L+$\beta'+\delta$, and the line between them is two-phase $\beta'+\delta$. The homogeneity region of the α-solid solution at the annealing temperature contains approximately 1 mol% of A and tends to increase with temperatures reaching a maximum at the ternary peritectic temperature. Also, the homogeneity region of the δ-solid solution (Cu_2ZnSnS_4) has a tendency to increase slightly with temperature. At the annealing point the solubility of the δ-solid solution consists of up to 2 mol% of the initial components on either side of the stoichiometric composition of the quaternary compound.

1.2.2 Formation of $Cu_2ZnSn(S,Se)_4$

There are only few publications describing in detail the formation of Cu_2ZnSnS_4 or $Cu_2ZnSnSe_4$ [38,39,40].
A.Weber *et al.* [38] studied the phase formation during the annealing/sulfurization step of co-electroplated Cu–Zn–Sn precursors using in-situ Energy Dispersive X-ray Diffraction (EDXRD). At room temperature (RT) there were diffraction peaks which could be assigned to ZnS, CuS and also weak diffraction peaks of Cu. Only at about 150˚C they found CuS. Further heating led to the rapid crystallization of Sn_2S_3 at approximately 200˚C. The diffraction intensity of this phase remained constant until 400˚C. At about 300˚C the CuS- $Cu_{2-x}S$ transformation began. Further heating led to the abrupt phase transition from the Sn_2S_3 to the SnS phase. This SnS phase was not stable and above 400˚C decomposed gradually while strong, broad peaks appeared in the EDXRD spectra, which can be related to Cu_2ZnSnS_4. They found also Cu_2SnS_3 together with the quaternary compound. Further heating to 550˚C led to a reduction of the Cu_2SnS_3 phase. S.Schorr *et al*. [39] found that using the mixture of 2CuS+SnS+ZnS the formation of Cu_2ZnSnS_4 starts just below 300˚C, accompained by a decrease of the fraction of CuS and SnS, whereas the fraction of the ZnS phase remained.
Results by R.Schurr *et al*. [40] showed that the crystallization of kesterite Cu_2ZnSnS_4 was completed by the solid state reaction of Cu_2SnS_3 and ZnS. The formation mechanism of Cu_2SnS_3 was dependant on the binary precursor phases.
In the case of sulfurization of copper-rich metal films they found at RT Cu_3Sn and CuZn phases. The formation of SnS_2 and $Cu_{2-x}S$ began at 387˚C. Further annealing led to the formation of ZnS (500˚C). At the annealing temperature of 540˚C the formation of Cu_2SnS_3 began from the binary sulphides $Cu_{2-x}S$ and SnS_2. The crystallization of kesterite Cu_2ZnSnS_4 was completed by the solid state reaction of Cu_2SnS_3 and ZnS, starting approximately at 565˚C.
In copper-poor near stoichiometric precursors in addition to Cu_3Sn and CuZn phases Cu_6Sn_5 was detected [40]. The presence of Cu_6Sn_5 led to the preferred formation of Cu_2SnS_3 via the reaction educts $Cu_{2-x}S$ and SnS_2 in the presence of SnS_2 (Cu_4SnS_6) melt, which is the result of the decay of the Cu_4SnS_6 phase. The formation of SnS_2 began at 180˚C, induced by the transformation of Cu_6Sn_5. The further increase of the annealing temperature led to the formation of Cu_2S. The Cu_3Sn phase occured at 300˚C as a result of the transformation of Cu_6Sn_5. The formation of the Cu_4SnS_6 phase took place at 387˚C out of the binary educts Cu_2S and SnS_2 in the sulphur atmosphere. The evolved phase Cu_4SnS_6 was stable up to 540˚C and decomposed into the $Cu_{2-x}S$ and SnS_2 (melt). This was also the formation temperature of ZnS and Cu_2SnS_3. The crystallization of kesterite Cu_2ZnSnS_4 was completed by the solid state reaction between ZnS and Cu_2SnS_3, starting at 565˚C.

1.3 Monograin powder growth

The isothermal growth of II-VI, I-III-VI and I-II-IV-VI polycrystalline powders in the presence of the liquid phase of a suitable solvent material (flux) in an amount sufficient for repelling initial crystallites leads to the formation of semiconductive materials with single-crystalline grain structure and narrow-disperse granularity, so called monograin powders [41]. Thus, it is possible to form many little perfect single crystals in one process. The driving force in this process is the difference of the surface energy of crystals of different sizes. The criterion of single grain growth is a sufficient amount of flux for filling the whole free space between initial particles. Otherwise there can occur molten or gaseous phase sintering, The sintering is determined by capillary forces in the solid-liquid phase boundary.

The analogous processes - crystal growth and sintering - proceed also during the heat treatment of semiconductor thin films for solar cells and they are essential for the production of dense and well-oriented crystalline thin films. The presence of the liquid phase of a fluxing agent enables the fast recrystallization and sintering of primary crystals during the heat treatment of films due to the fast diffusion of components through the molten phase [42]. In dense and well recrystallized films a high concentration of inherent defects, particularly in the intergrain region, where a considerable part of photogenerated charge carriers is lost due to the recombination, is reduced.

On the other hand, the liquid phase of the flux represents a source of doping impurities which are easily incorporated into the crystal during the growth process. The level of doping depends on the time and temperature of heating and is limited by the solubility of impurities [43]. The growth of monocrystalline powder grains can proceed at temperatures higher than the melting point of the used flux materials and at lower temperatures than the phase transition or the melting point of the synthesized semiconductor compound. Once the powder grains have the desired size, quenching stops the growth and the fluxing agent has to be removed.

Research directed to the development of $CuIn(S,Se)_2$ monograin powder technology for solar cell application began at TUT in the Laboratory of Semiconductor Materials in 1994. Already the first results indicated to a possibility of producting CISe monograin powders by the recrystallization of polycrystalline powders in isothermal ampoules in the presence of liquid selenium [44].

Afterwards the recrystallization of polycrystalline powders was replaced by a similar process where the synthesis of the compound and the growth process were combined and proceeded in the CuSe-Se liquid phase [45]. From the technological point of view, the process of flux removal is also of great importance. Due to this Se and CuSe-Se as flux materials were later substituted by water soluble potassium iodide.

The developed monograin powder technology [41-45] appears to be a relatively simple, inexpensive and convenient method to produce powder materials for monograin layer solar cell applications. The advantages of the powder crystals growth in a liquid flux are: single-crystalline structure of every grain, uniform

distribution of doping impurities and the homogeneous composition of grains in the whole patch.
As the large scale production of copper-indium chalcopyrite based solar cells for terrestrial use in future is limited due to the high price and lack of indium, the replacement of In in $CuIn(Se,S)_2$ by equal parts of Zn and Sn atoms is preferred. Starting from 2005 the investigations have mainly been directed to the $Cu_2ZnSnSe_4$, Cu_2ZnSnS_4 and their solid solutions as possible absorber materials.

1.4 Effect of sodium on the properties of $CuInSe_2$

In the case of vacuum deposited $Cu(In,Ga)Se_2$ thin film solar cells, the presence of Na in the absorber correlates with numerous changes in the material and device quality. In most cases Na diffuses from the glass substrate into the absorber, but there are also approaches where Na is incorporated by the use of Na-containing precursors such as Na_2Se, Na_2O_2, NaF and Na_2S [46]. The most obvious effects of Na incorporation are improvements in the open-circuit voltage [47,48], preferential grain orientation [48], increased grain size and carrier concentration [49,50]. Using the photoluminescence (PL) measurements, Kimura *et al*. [51] found that the self compensation of $CuInSe_2$ was reduced by Na incorporation due to the suppression of donor-type defects.
The addition of 0.1-0.2 at.% sodium has been found to extend the region of single phase existence of polycrystalline α-$CuInSe_2$ by 2 % towards the Cu_2Se side in the quasibinary phase diagram [32]. A widening of the existence region is beneficial because the synthesis of the single phase semiconductor material is simplified if the product compound tolerates slight deviations from stoichiometry.

1.5 Surface modification by chemical treatments

The active interface of the *p*-type absorber and the *n*-type buffer layer plays a key role in solar cell performace. Different research groups have studied the influence of various chemical etchants on $CuInSe_2$, but detailed surface analytical studies have not been carried out to understand the surface modifications and chemical changes occuring on the $Cu_2ZnSn(S,Se)_4$ monograins surface.
Due to the segregation of Cu-Se binaries, it is necessary to remove these phases with strongly selective etchant that only attacks Cu-Se and does not harm $CuInSe_2$. The only chemical etchants, which are presently known to fulfil this condition, are cyanide containing solutions such as potassium cyanide (KCN) [52,53,54,55] or sodium cyanide (NaCN) [56]. It has been found that efficient removal of surface oxides can be achieved by NH_3 treatment [57]. Bromine etching is an oxidative etching and leaves elemental Se on crystal surfaces [58,59]. The influence of HCl treatment on CISe surface was investigated by Nelson *et al*. [59]. They found that after HCl etching the surfaces appeared to be unoxidized and Se rich. At the same time it does not affect the surface morfology significantly.

1.6 Summary of the literature review and the aim of the study

Monograin layers are perspective for the development of inexpencive solar cells. Monograin powders of $CuInSe_2$ can be applied as absorber materials in monograin layer solar cells. The isothermal growth of $CuInSe_2$ monograin powders takes place in the presence of the liquid phase of a suitable solvent material (flux). In this process the chemical nature of the liquid (molten) phase of the used solute material inhfluences certain properties of the obtained absorber material. The system $CuInSe_2$-KI had not been studied yet.

Chalcopyrite-type semiconductors like $Cu(In,Ga)S_2$ or $Cu(In,Ga)Se_2$ have very beneficial properties for photovoltaic applications [2,3,4], which in turn have led to a strong scientific interest in thin film solar cells based on these materials. Obtained efficiencies are remarkably high, up to 20.3% [5] however, gallium and indium used for the preparation of the active layer are very rare and expensive elements. This could lead to a shortage in the supply of these elements and would inhibit a cost-effective large-scale production. To overcome these limitations, alternative materials are intensively researched in order to substitute the expensive elements In and Ga. Among these materials, $Cu_2ZnSnSe_4$ (CZTSe) is one of the most promising materials, as it consists of abundant and relatively cheap elements. The formation of $Cu_2ZnSn(Se_{1-x}S_x)_4$ solid solutions has not been investigated yet.

Neither has the behaviour of $Cu_2ZnSn(S,Se)_4$ in different etching solutions been studied.

The objectives of the present doctoral thesis were:

- To study the growth process of $CuInSe_2$ in potassium iodide.

- To study the effect of sodium doping on the electrical and photoluminescence properties of $CuInSe_2$ monograin powders with nearly stoichiometric composition in order to clarify the influence of sodium on the parameters of $CuInSe_2$ monograin layer devices.

- To study the effect of chemical treatments on the surface composition of $Cu_2ZnSn(S,Se)_4$ monograin powders.

- To study the formation of $Cu_2ZnSn(Se_{1-x}S_x)_4$ solid solutions with the aim to find out the best composition of an absorber material for monograin layer solar cells.

2 EXPERIMENTAL

The main experimental features are briefly presented in this section. For details of the experiments, see publications I-VI.

2.1 Preparation of $CuInSe_2$ and $Cu_2ZnSn(S,Se)_4$ monograin powders

The initial Cu-In alloys (in molar ratio 1:1.1) were synthesized from the elemental metal precursors of 5N purity in carbon-coated quartz ampoules for synthesis growth of $CuInSe_2$. The syntheses of Cu-In alloys were made in dynamic vacuum (continious pumping) at the temperature of 10 70K. Cu-In alloy ingots were triturated in the agate mortar and sieved through the 100 μm sieve. Ground Cu-In alloy (1:1.1) and elemental Se in proportions providing stoichiometry of $CuInSe_2$ were mixed with KI. The amount of components for $CuInSe_2$ and the amount of KI were nearly equal to provide a sufficient liquid phase for the monograin growth (V_S=V_L). Samples were sealed into evacuated quartz ampoules, annealed isothermally at various temperatures and annealing times and quenched to room temperature. The minimum growth temperature was limited by the melting temperature of the used flux material KI (953-959K) [60] and the maximum growth temperature was limited by the temperature of the phase transition of $CuInSe_2$ (1083K) [31]. The flux material was removed by leaching with deionized water. Finally, the well-dried powders were sieved into narrow fractions from 38μm to 112μm.

The $Cu_2ZnSn(S,Se)_4$ powder materials were synthesized from binaries Cu(S,Se), Zn(S,Se), Sn(S,Se) and KI as flux material. The binary precursor compounds for synthesis of $Cu_2ZnSn(S,Se)_4$ and KI were mixed and ground in planetary ball mill. The mixture was degassed and sealed into quartz ampoules. The recrystallization temperature was 1000K. More detailed description of the procedure of materials preparation is presented in papers [IV,V,VI].

2.2 Doping with sodium

The $CuInSe_2$ monograin powder used for doping with sodium was synthesized in the molten phase of CuSe to avoid the contamination of material with K and Na from KI. The synthesized material was subdivided into several portions and placed into the quartz ampoules. The doping solution of NaI as a source of Na-dopant was added to each portion directly into the quartz ampoules. Solution of NaI in deionizated water was dosed in controlled amounts in the range of 5×10^{16} – 1×10^{20} atoms of Na per cm^3 of $CuInSe_2$. The amount of doping solution was kept constant by sequential diluting. The materials were dried, InI as flux was added and ampoules were vacuum-sealed and heated at 800 K for 48 hours. The materials recrystallized in the presence of molten InI that provided an homogeneous redistribution of Na.

After annealing, the ampoules were quenched to room temperature in water. The flux was removed by 3.7% aqueous solution of HCl [III].

2.3 Chemical treatment

The grown $Cu_2ZnSn(S,Se)_4$ monograin powders were divided into several parts and each of them passed through different etching procedures. Concentrated HCl, 10% aqueous solution of KCN, 1% Br_2-MeOH (bromine in methanol) solution and 2M NH_4OH solution were used as etchants. All the chemical etchings were performed at room temperature. After etching the powders were washed in deionized water and dried [IV].

2.4 Preparation of monograin layer solar cells

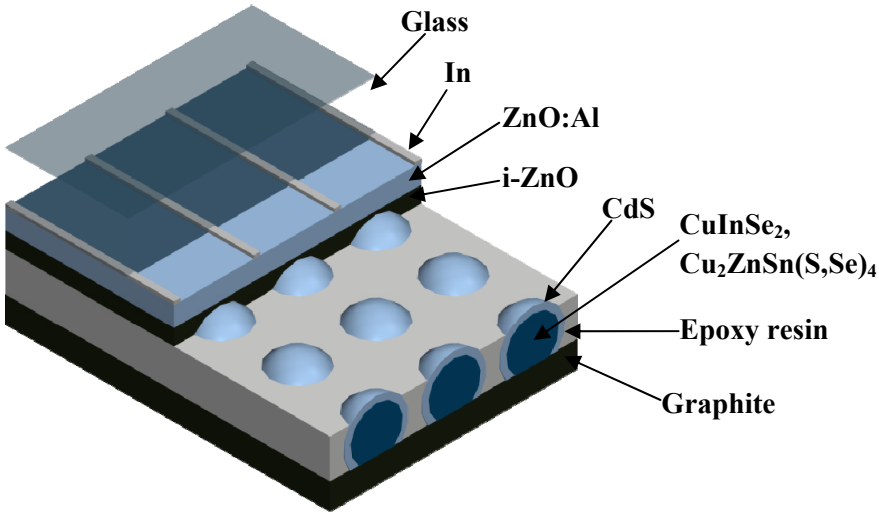

Figure 7. Schematic illustration of the standard structure of monograin layer solar cell.

To form a monograin layer (see Figure 7) of nearly unisize $CuInSe_2$ or $Cu_2ZnSn(S,Se)_4$ powder crystals preliminarily covered with chemically deposited CdS are poured onto a thin layer of epoxy resin so that the upper part of crystals remains untouched with epoxy. After the polymerization of epoxy, i-ZnO and conductive ZnO:Al are deposited by RF-sputtering. The solar cell structure is completed by the evaporation of 1-2 μm thick In grid contacts onto the ZnO window layer. After glueing the structures on glass substrates, the back contact area of

crystals that was still covered with epoxy is opened by etching epoxy off with concentrated H_2SO_4 (see Figure 8) and by additional abrasive treatment of absorber crystals. The back contact is made using graphite paste.

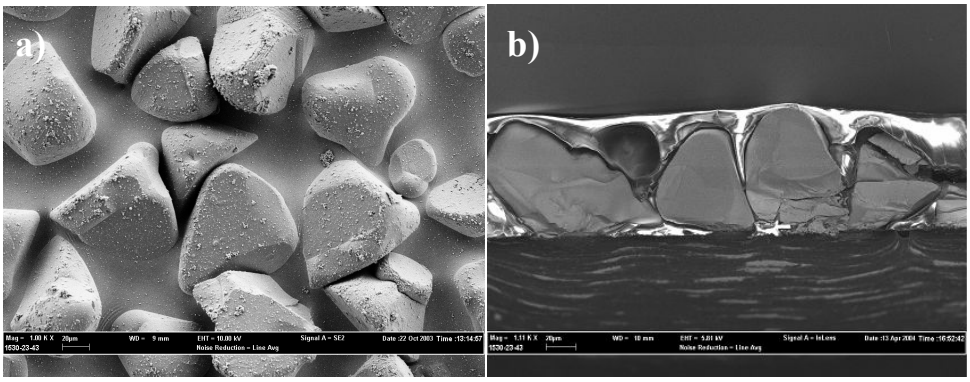

Figure 8. SEM photos of monograin layer (MGL) solar cells: a) surface of front contact side before glueing on glass and b) cross-section of MGL on glass (upper dark layer) and with graphite back contact (lower dark layer).

2.5 Current-voltage characterization of solar cells

The most important parameters that describe the performance of a solar cell - efficiency η, open circuit voltage V_{oc}, short circuit current density j_{sc} and fill factor FF - can be derived from the I-V curve measured under standard test conditions (AM 1.5, 100 mW/cm^2).
The efficiency of a solar cell is defined as the ratio of maximum (electrical) power density delivered by the cell to the power density of the illuminating light source. It is the most important characteristic of a solar cell, given by Eq. (2.5.1.)

$$\eta = \frac{P_{\max}}{P_{in}} = \frac{j_{sc} \cdot V_{oc} \cdot FF}{P_{in}}, \qquad (2.5.1)$$

where P_{in} is the power of the standard illumination of AM 1.5 (100 mW/cm^2). The fill factor (FF) is often used to characterize the quality of a solar cell junction, calculated by Eq. (2.5.2).

$$FF = \frac{j_m \cdot V_m}{j_{sc} \cdot V_{oc}}, \qquad (2.5.2)$$

where j_m is current density at maximum power output and V_m is voltage at maximum power output.

2.5.1 Characterization techniques

The analytical techniques used for the characterization of monograin powders and monograin layer solar cells are summarized in Table 1. More detailed information about the instrumentation and measurements can be found in the experimental sections of References I-VI.

Table 1.

	Properties	Used techniques	Apparatus	Ref.
MATERIAL	composition	POL	Metrhom polarograph	[I,II,IV]
	elemental composition	EDS	ZEISS ULTRA 55	[II,IV-VI]
	morphology	SEM	ZEISS ULTRA 55	[I-VI]
	phase composition	Raman	Horiba LabRam HR	[IV-V]
	elemental composition	XPS	Kratos Axis Ultra DLD Al Kα	[IV]
	optical properties	PL	Photoluminescence measurement system	[II,III,V]
	phase composition	XRD	Bruker AXS D5005	[I,II,IV,VI]
MGL SC	SC output parameters	I-V	Keithley 2400	[II-VI]
	SC quality	QE	Autolab PGSTAT 30	[V,VI]
	carrier concentration	C-V	Autolab PGSTAT 30	[III]
	barrier height	V_{oc} vs. T	Autolab PGSTAT 30	[VI]

3 RESULTS AND DISCUSSION (CISe, CZTSSe)

3.1 $CuInSe_2$ monograin growth in the liquid phase of potassium iodide

In high performance solar cells slightly In-rich $CuInSe_2$ is used as an absober material. Cu-rich $CuInSe_2$ displays the segregation of a secondary Cu_ySe ($y<2$) phase preferably at the material surface. Even after removal of the Cu containing phase from the surface by etching the absorber in KCN, the use of this material for photovoltaic applications is limited, most probably due to the high doping density in the bulk [46]. The growth of $CuInSe_2$ MGP-s in CuSe-Se flux results in near-stoichiometric compositions of material grains [45]. This is in accordance with the Cu-side borderline of $CuInSe_2$ phase existence range of Cu_2Se-In_2Se_3 phase diagram [31]. The use of Se as a flux material allows us to grow the MGP in the large range of deviations from stoichiometric composition. The technological difficulty is the removal of Se flux from powder batch. Therefore, in order to obtain In-rich compositions of MGP-s in a shorter time consuming process, the growth of MGP-s in KI as a flux material that is easily removable by leaching with DI water was studied. $CuInSe_2$ was synthesized from high-purity elements Cu, In and Se (Cu and In were prior melted and used as the CuIn alloy as precursor of metals for the CISe sythesis) [I, II].

3.1.1 Growth parameters of $CuInSe_2$ in the KI flux

The regularities of growth and formation parameters of $CuInSe_2$ monograins in the KI flux are presented in paper [I].

The formation of $CuInSe_2$ monograins takes place in the amount of liquid phase of a flux that exceeds the limit of sintering of initial crystals [61]. The formed liquid phase consists of the molten salt used as a flux material and the product of synthesis dissolved in it. It means that in order to determine the amount of added KI and the volume of liquid phase in the recrystallization process we have to know the solubility of CISe in KI. Therefore, we determined the solubility of CISe in KI at the growth temperature by the weight loss method. Large pieces of polycrystalline $CuInSe_2$ were weighed and sealed with 5 times larger amount of dried KI into quartz ampoules. The ampoules were annealed at 990 K for 120 hours and then quenched in water. The undissolved $CuInSe_2$ was gathered and weighed. From the weight loss we found the solubility of $CuInSe_2$ in KI. For comparison the data of CISe solubilities in Se and CuSe-Se are given in Table 2.

Table 2. Solubility of $CuInSe_2$ in different fluxes: Se, CuSe-Se and KI.

Flux material	Se [62]	CuSe-Se [45]	KI (this work)
Temperature, K	970	800	990
Solubility, wt. %	28.5 ± 0.5	8.8 ± 0.5	0.17 ± 0.05

Considering the low solubility of $CuInSe_2$ in KI and the densities of KI (3.12 g/cm^3) [63] and CISe (3.0 g/cm^3) [64] we found that the equal masses of both materials guarantee the ratio of $V_S/V_L \geq 0.6$, satisfying the condition for single crystalline growth of grains [61]. The dissolution of KI revealed uniform, nonaggregated microcrystals of tetragonal shape with smooth surfaces and sharp edges (Figure 9), indicating their growth from individual seed crystals rather than from the aggregates of crystallization nuclei.

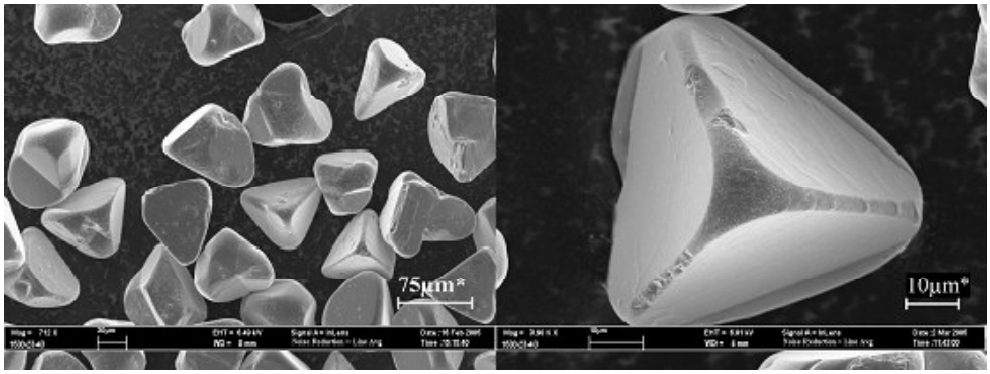

Figure 9. SEM photos of $CuInSe_2$ monograin powder crystals grown in KI at 990 K for 76 hours.

The X-ray diffraction (XRD) spectra of the formed $CuInSe_2$ monograin powder (Figure 10) showed only the peaks of chalcopyrite $CuInSe_2$.

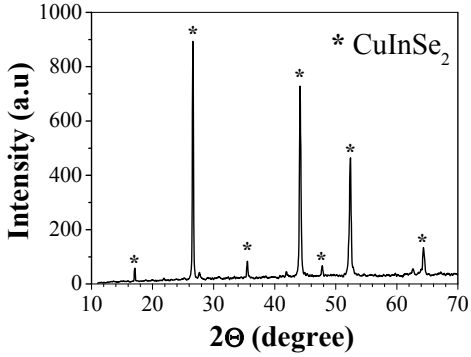

Figure 10. The X-ray diffraction pattern of $CuInSe_2$ monograin powder grown in KI at 990 K for 76 hours.

In order to find out the growth parameters of $CuInSe_2$ in KI, the precursors for synthesis of CISe (Cu-In, Se) and KI were ground and sealed into evacuated quartz ampoules and annealed isothermally at various temperatures (970, 990, 1010 and 1050K) and for different annealing times (30, 76, 270 and 334 h). The sieve analysis method was used to determine the particle size distribution. The median particle size was found graphically from the particle size distribution data on the log-normal probability graph [65].

The composition of $CuInSe_2$ powder materials grown at various temperatures and for different times was analysed polarographically. The composition of $CuInSe_2$ monograin powder materials was Cu:In:Se = 23.3:25.5:51.2 ([Cu]/[In] = 0.91). The results revealed that the composition remained unchanged by changing the growth temperature and duration. The solubility of potassium and iodine in $CuInSe_2$ at 990 K was 0.094 wt. %, and 0.0086 wt. %, respectively (results of ICP-MS). All the as-grown monograin powders had *p*-type conductivity.

The particle size distribution of samples grown at 1010 K for different recrystallization durations is shown in Figure 11. The particle size distribution of all the samples depending on the process duration follows a log-normal distribution.

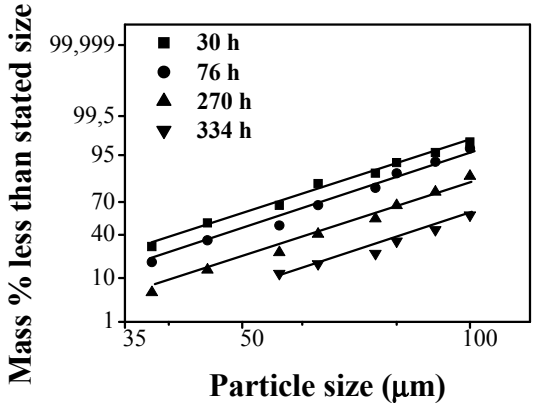

Figure 11. Particle size distribution of $CuInSe_2$ monograin powders grown in KI at 1010 K for different time periods.

It allows the use of the median particle size d_m to describe the grain growth according to the equation:

$$d_m = At^{1/n}exp(-E_d/kT), \qquad (3.1.1.1)$$

where A is a constant for a given flux and compound, k is the Boltzman constant, T is the growth temperature (K), E_d is the activation energy for linear crystal growth and n is the geometric factor of growth mechanism [42].

From the Arrhenius plot of the median grain diameter d_m the activation energy for the linear crystal growth E_d = 0.25 ± 0.05 eV was determined. If the growth is controlled by one growth mechanism (diffusion), then n = 3. The power of the time dependence of crystal growth l/n = 0.25 ± 0.06, n = 3.9 ± 0.93 was found from the time dependencies of d_m. The value of n = 3.9 ± 0.93 indicates that the growth process of $CuInSe_2$ particles in KI flux is limited by diffusion processes on the surfaces of sintered grains [66].

3.1.2 Growth of $CuInSe_2$ monograin powders with different Cu/In ratio

The aim of this part of experiments was to clarify the limits for the single-phase growth of $CuInSe_2$ in flux materials of different chemical nature and to study the possibilities to tailor CISe properties in the growth process. In order to grow $CuInSe_2$ MGP-s with different compositions, precursor Cu-In alloys with different Cu/In concentration ratios (0.5 - 1.1) were prepared and annealed with Se in sealed ampoules in KI flux. It was found that KI as a flux material allows the growth of In-rich $CuInSe_2$ monograin powders. The obtained results show that the single-phase powder crystals can be grown from precursor Cu-In alloys with Cu/In concentration ratio values between 1>Cu/In>0.7. The powders from precursor Cu-In alloys with Cu/In<0.67 were found to consist of crystals with two different compositions: Cu/In = 0.92 and Cu/In = 0.66. This indicates that this precursor composition is in the region of the multiphase area of $CuInSe_2$ phase diagram (see Figure 3). Selenium content in the grown powders increases almost linearly with the decreasing Cu/In ratio of the materials.
The samples with nearly stoichiometric or slightly In-rich compositions showed *p*-type conductivity and exhibited PL spectrum with dominant peak at 0.93 eV. In contrast, the samples with Cu/In<0.7 had n-type conductivity and exhibited two broad bands in PL spectra with the peak positions at 0.86 eV and 0.93 eV. Results of this research of modifying CISe monograin powder growth in the KI flux in the single-phase region of CISe phase diagram are described in more detail in paper [II].

3.2 The influence of sodium doping on $CuInSe_2$ monograin powder properties

The results of the research in this field have been published and are described in paper [III].
Sodium has been found to improve the performance of $Cu(In,Ga)Se_2$ solar cells [48-51]. As the monograin powder growth takes place in the liquid phase of potassium iodide the question arises: if the effect of K on the solar cell output parameters is similar to the effect of Na.
The best results of I-V measurements of solar cells made from powders synthesized in the liquid phase of InI and in the liquid phase of mixture of KI and InI are

presented in Table 3. It can be seen that the presence of KI in the flux improves solar cell parameters.

Table 3. Comparison of solar cell parameters for $CuInSe_2$ synthesized in the InI flux and in the InI/KI flux material.

Flux material	V_{oc}, (mV)	J_{sc},(mA)	FF, %
InI/KI	481	0.43	45
InI	357	0.22	38

Results of ICP-MS analysis showed that the concentration of sodium in $CuInSe_2$ synthesized at 990 K in KI was about 6 times higher than the concentration of potassium. The used potassium iodide contains sodium as impurity at a high level and sodium can dissolve in $CuInSe_2$ at the saturation concentration. The explanation can be in the difference of ionic radii of K and Na [49]. The ionic radii of K (see Table 4) is much larger than the ionic radii of Na and sodium fits very well on Cu site.

Table 4. Ionic radii of elements.

Element	Cu	In	I	Se	Na	K
Å (charge)	0.96 (+1)	0.81 (+3)	2.16 (-1)	1.91 (-2)	0.97 (+1)	1.33 (+1)

A.Rockett *et al*. [67] found that there is an optimal concentration of sodium that improves solar cell output parameters. Following our previous results a serie of experiments was planned to determine the optimal sodium concentration in monograin CISe powders. To study the effect of doping we varied sodium concentration ($5x10^{16}$-$1x10^{20}$ at/cm^3) in the absorber by adding the solutions of NaI of different sodium concentrations as a source of Na.

3.2.1 Photoluminescence study of sodium doped $CuInSe_2$ powders

The photoluminescence spectra (T = 10 K) of all monograin materials show a broad band with its maximum around 0.99 eV (Figure 12). The peak position of the PL band at 0.99 eV depends on the dosed sodium doping level, as shown in Figure 13. The peak position shifts to higher energy values with increasing sodium concentration up to 1×10^{19} cm^{-3}. With further increase in the level of sodium doping, a sharp decrease of the PL peak energy values was observed.

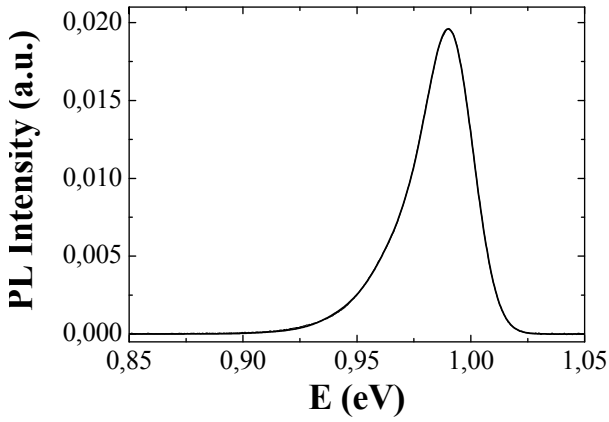

Figure 12. The PL spectrum of Na doped $CuInSe_2$ monograin powder.
Dosed [Na] = 3×10^{18} at Na/cm^3 $CuInSe_2$.

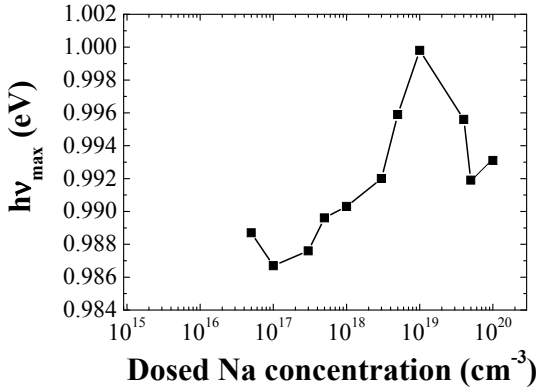

Figure 13. The peak position of the PL band depending on the dosed sodium doping.

It was found in [47] that Na does not create shallow acceptor levels in $CuInSe_2$. Na incorporation could result in the formation of a solid solution with $CuInSe_2$ in the form of $Na_xCu_{1-x}InSe_2$ with higher bandgap energy than $CuInSe_2$. For $CuGaSe_2$, in [68] the formation of a quaternary Na-Cu-Ga-Se compound on the base of defect-chalcopyrite structure in which Cu vacancies are partially filled by Na atoms was proposed. To explain the obtained results we can follow a presumption similar to the abovementioned concerning the formation of a solid solution of $CuInSe_2$ with Na. The formed new Na containing phase locates on the surface of our crystals and has slightly higher bandgap energy as compared to CISe. SEM image (Figure 14)

indicates to the segregation of a phase in our sodium doped samples and supports this presumption.

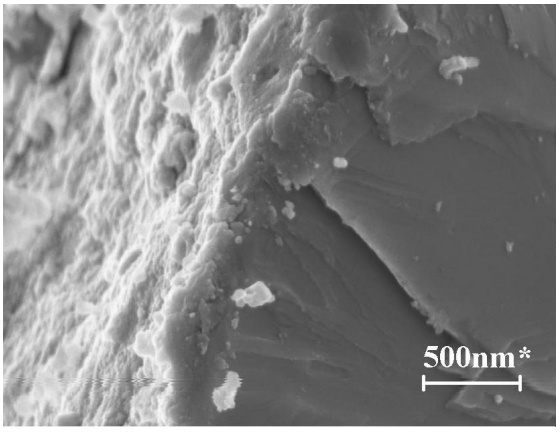

Figure 14. SEM image of a broken $CuInSe_2$ crystal with a dosed sodium content $10^{19}cm^{-3}$.

The bandgap energy of a quaternary $Na_xCu_{1-x}InSe_2$ solid solution increases with the increasing sodium doping level. At doping concentrations higher than $10^{19}cm^{-3}$, the PL peak position shifts to lower values of energies. More detail analysis are needed to explain this behaviour.

3.2.2 Solar cell parameters

The solar cells on the base of undoped and doped with sodium up to $3\times10^{17}cm^{-3}$ absorber materials had low value of shunt resistance (Figure 15). These materials were etched with 10% KCN aqueous solution. After KCN etching the solar cells showed better diode behaviour. The KCN solution is known as a selective etchant for Cu-Se binary phases [69]. Starting from $3\times10^{17}cm^{-3}$ and higher concentrations of sodium there was no need to etch $CuInSe_2$ materials with KCN. Therefore we suppose that the segregation of the Cu-Se phase occurs in powders with added Na concentration less than $3\times10^{17}cm^{-3}$. It is known that sodium incorporation widens the area of the α-($CuInSe_2$) phase existance in the phase diagram [31]. In our case, starting from the doping level of $3\times10^{17}cm^{-3}$ the increase of sodium content in $CuInSe_2$ widens the single phase area of $CuInSe_2$ towards Cu-rich composition. In undoped materials or in materials with Na concentration up to $3\times10^{17}cm^{-3}$, the Cu-Se phase segregation is possible.

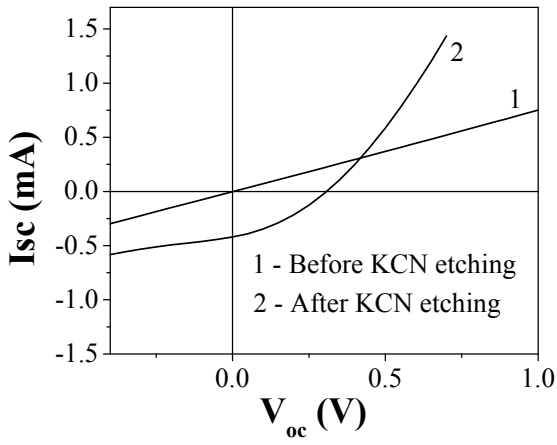

Figure 15. I-V curves of $CuInSe_2$ solar cells without sodium and low sodium concentrations before and after KCN etching.

The values of the open-circuit voltage of solar cells (Figure 16) increase with dosed sodium concentration from $5\times10^{16}cm^{-3}$ to $3\times10^{18}cm^{-3}$. At Na concentrations higher than $3\times10^{18}cm^{-3}$ the open-circuit voltage decreases down to a constant value. Solar cells on the base of absorber material with the doped sodium concentration $3\times10^{18}cm^{-3}$ were found to result in the highest open-circuit voltage values. Wei *et al.* [47] found theoretically that Na on Cu site does not create levels in the band gap, while Na on In site creates acceptor levels that are shallower than Cu_{In}. The major effect of Na is the elimination of the In_{Cu} defects and the resulting increase of the effective hole densities.The theoretical assumption was supported by the experimental work of Kimura *et al*. [51]. However, as the Na concentration increases to the level where most of the In_{Cu} defects have been eliminated, it starts to fill in vacant lattice places in Cu sublattice and diminishing the concentration of the acceptor defect V_{Cu} This process reduces the hole density [47] and leads to the reduction in the solar cell performance at Na contents higher than dosed $3\times10^{18}cm^{-3}$.

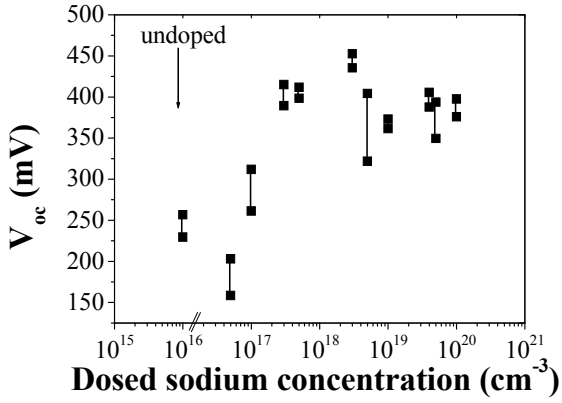

Figure 16. The open circuit voltage of solar cells depending on the dosed sodium concentration.

3.2.3 Carrier concentration

Sodium incorporation enhances the carrier concentration [70]. The carrier concentration in our monograin materials was determined by room-temperature capacitance-voltage measurements (Figure 17). We found that the maximum carrier concentration 2×10^{17} cm^{-3} was in materials with the doped sodium concentration of 1×10^{19} cm^{-3}. Further increase in sodium concentration resulted in the decreased carrier concentration. As seen in Figure 16, a similar tendency was observed in the values of open-circuit voltage.

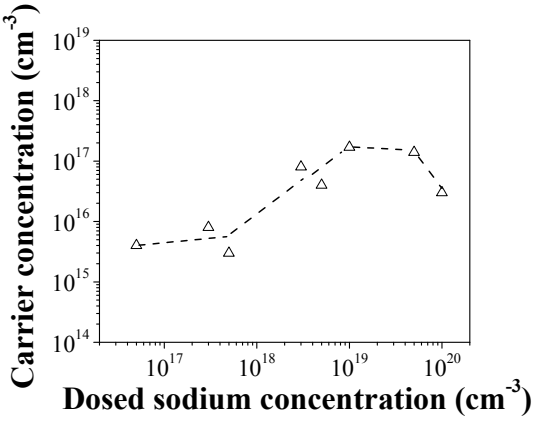

Figure 17. Carrier concentration depending on the dosed sodium doping level.

In conclusion, solubility of $CuInSe_2$ in KI at 720ºC was found to be 0,17 weight %. Crystals of $CuInSe_2$ grown in KI flux have a shape of polyhedrons. The facets of the crystals are smooth. The single-phase powder crystals can be synthesized from precursor Cu-In alloys with the Cu/In ratio values between 1> Cu/In>0.7. From the Arrhenius plot of the median grain diameter d_m the activation energy for the linear crystal growth E_d = 0.25(±0.05) eV was obtained. From the time dependencies of d_m the power of the time dependence of crystal growth $1/n$ = 0.25(±0.06), n = 3.9(±0.93) was found.

It was shown that the output parameters of the solar cells are dependent on the Na doping level of the absorber material. Sodium concentration 3×10^{18} at/cm^3 was found to result in the best open-circuit voltage and fill factor values. The PL spectra of Na doped CISe powders showed that the peak position of the PL band shifted depending on the Na doping level. The peak position of the PL band with maximum energy was observed when sodium concentration was 1×10^{19} at/cm^3. The same material had the highest carrier concentration 2×10^{17} cm^{-3}.

3.3 $Cu_2ZnSn(S,Se)_4$ monograin growth in the liquid phase of potassium iodide

The $Cu_2ZnSn(Se_{1-x}S_x)_4$ (CZTSSe) powder materials with different x values were synthesized from CuSe(S), ZnSe(S) and SnSe(S) in appropriate relations as precursors for CZTSSe in molten KI, as it was described in section 2.1. The recrystallization temperature was 1000 K. The crystal size was controlled by the duration of the crystallization process. The results of studies on chemical etching and the formation of solid solution of $Cu_2ZnSn(Se_{1-x}S_x)_4$ in the form of monograin powders are presented in [IV,V,VI].

3.3.1 Process description

In the process of monograin growth, monograins of a semiconductor compound are formed in the liquid phase of the used flux material. The criteria for the monograin growth is the following: the volume of the molten phase V_L between grains has to exceed the limit of sintering - $V_L \geq 0.6\ V_S$, where V_S is the volume of solid phase. In this case the liquid phase separates the initial solid particles from each other and the individual single crystals grow [61]. Due to solubility, the precursors and the formed CZTSSe dissolve in the molten flux salt at the used recrystallization temperature and some part of it can re-precipitate on the surface of the formed crystals during the cooling period. These precipitations change the surface morphology and the composition of the crystal surface. On the other hand, it is well known that the active interface of a *p*-type absorber and a *n*-type buffer layer plays a key role in solar cell performace. Therefore, an in-depth understanding of the chemical treatment of CZTSSe monograin powder crystals' surfaces with different etchants is very important for tailoring the absorber crystal's surface composition and finally the parameters of solar cells on their base.
The results of chemical treatment of $Cu_2ZnSn(S,Se)_4$ are presented in paper [IV].

3.3.1.1 The morphology and surface composition of asgrown $Cu_2ZnSn(S,Se)_4$

$Cu_2ZnSn(S,Se)_4$ monograin powder crystals had tetragonal shape with rounded grain edges (see Figure 18) and homogeneous chemical composition of crystals bulk through the whole patches.

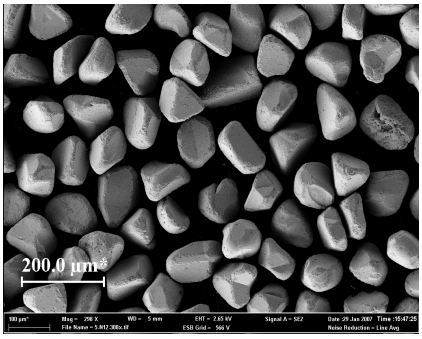

Figure 18. SEM micrograph of $Cu_2ZnSn(S,Se)_4$ monograin powder**.**

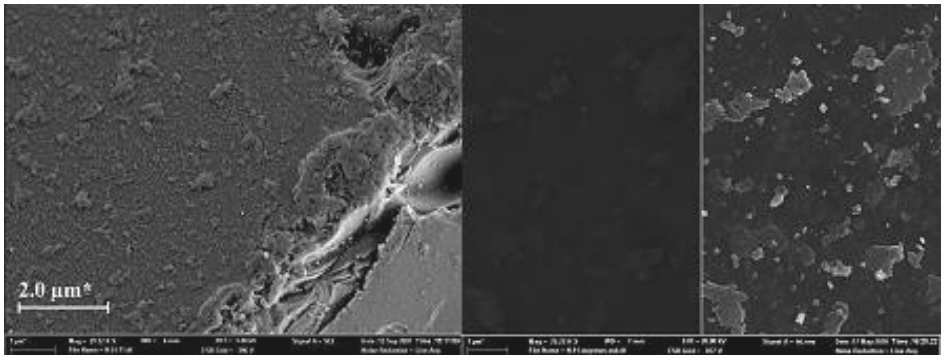

Figure 19. SE SEM images (left) and EsB SEM images (right) of a crystal surface of $Cu_2ZnSn(S,Se)_4$ as-grown monograin powder.

SE and EsB SEM images exposed the inhomogeneity of crystal's surface of as-grown $Cu_2ZnSn(S,Se)_4$ monograin powders (see Figure 19). The comparison of the crystal's surface composition with the bulk by using EDS revealed that the surface of as-grown CZTSSe crystals is Sn-rich while the bulk of crystals is Zn-rich (see Table 5).

Table 5. Compositions of chemically untreated CZTSSe crystals' surfaces and their bulk (polished cross-section of powder crystals) as determined by EDS.

Material	Cu/Zn+Sn	Zn/Sn	Se+S/Met
Crystal's surface	0.94	0.86	1.01
Crystal's bulk	0.88	1.03	1.03

The difference in the surface and the bulk compositions can be taken as a hint of material precipitation from components dissolved in the flux at the growth-temperature onto the surface of the grown crystals during cooling. After the removal of the flux the remaining solid phase consists of well formed crystallites of CZTSSe and an amorphous material that was originally dissolved in KI at the recrystallization temperature. Some part of the material dissolved in KI at the growth

temperature could precipitate onto the surface of crystals during the cooling period. The composition of the amorphous deposit was analysed by EDS and it was Cu : Zn : Sn : S+Se = 25 : 3 : 20 : 53. This Zn poor elemental composition of the amorphous phase could be a source for formation of compounds like $Cu_2Sn(S,Se)_3$ and $Sn(S,Se)_2$ on the surface of monograins.
The surfaces of CZTSSe monograins were locally covered with islands (Figure 20). EDS spot measurements revealed the composition of the islands as $Sn_x(S,Se)_y$ with elemental ratio Sn : Se/S = 40 : 60.

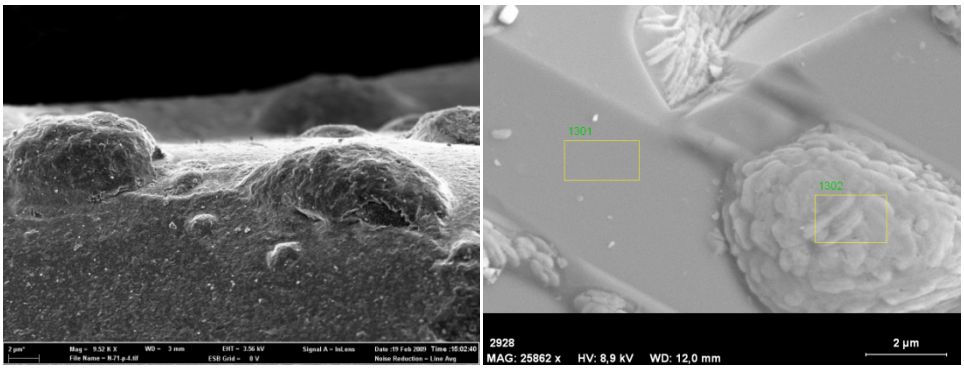

Figure 20. SEM images of CZTSSe monograins surfaces.

3.3.1.2 Raman study of $Cu_2ZnSnSe_4$ monograins

The phase composition of as-grown $Cu_2ZnSnSe_4$ monograin powders was additionally studied by room temperature micro-Raman spectroscopy. As Raman spectra of CZTSSe materials have the bimodal behaviour and show the Raman peaks of both components ($Cu_2ZnSnSe_4$ and Cu_2ZnSnS_4) we used for Raman studies only $Cu_2ZnSnSe_4$ materials.
Figure 21 shows normalized RT Raman spectra taken from the surface of powder crystals and Raman spectra of the bulk of $Cu_2ZnSnSe_4$ monograins taken from polished samples, together with a normalized Raman spectrum of precipitated amorpheus material. The polished cross-sections of $Cu_2ZnSnSe_4$ monograins were used to measure Raman spectra of the bulk material.

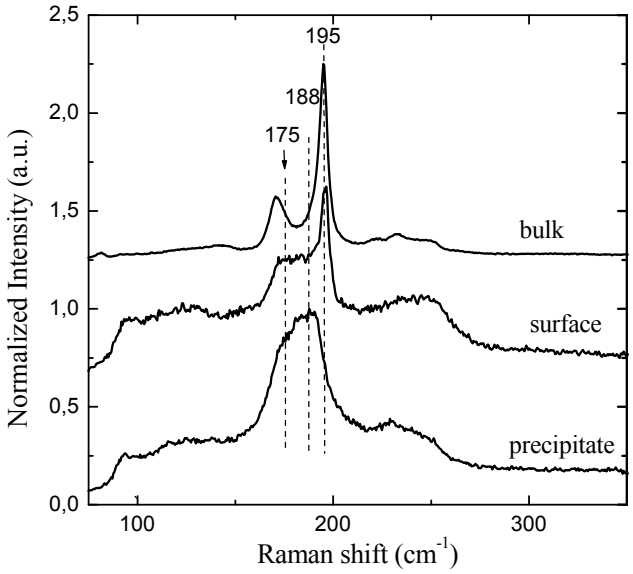

Figure 21. Raman spectra of a $Cu_2ZnSnSe_4$ crystal's bulk (polished cross-sections of crystals), of the crystal's surface and of the solid amorphous precipitate.

Two dominating modes of $Cu_2ZnSnSe_4$ [V] can be found at 195 and 171 cm^{-1} in the Raman spectra of the bulk of crystals. These modes can also be found in the spectra of the surface of monograins. However, there are some additional modes around 188 cm^{-1} and 175 cm^{-1} in the Raman spectra of the crystal's surface, indicating the presence of other phases on the crystal's surface. These additional peaks are also present in the Raman spectra of the precipitate, which confirms our assumption that the material that was dissolved in the molten phase precipitates onto the crystal's surface in the cooling process. The Sn-rich chemical composition of the crystal's surface and a Raman peak around 188 cm^{-1} led to an assumption that $SnSe_2$ (A_1 mode at 186 cm^{-1} [71]) is a main component of the precipitate [IV]. In the Raman spectra of as-grown CZTSe monograin powders (Raman modes at 173 cm^{-1}, 196 cm^{-1} and 231 cm^{-1}) the presence of an additional Cu_2SnSe_3 phase was also detected (Raman peak at 180 cm^{-1}) [72]. The frequencies of the A1 Raman modes of Cu_2SnSe_3 and CZTSe are 180 cm^{-1} and 196 cm^{-1}, respectively (see Figure 22) [V]. The conclusion drawn here about the presence of Cu_2SnSe_3 on the surface is supported also by the results of EDS analysis.

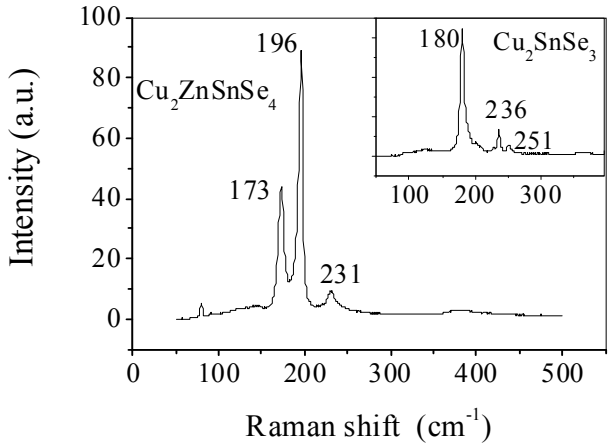

Figure 22. Room temperature Raman spectrum of $Cu_2ZnSnSe_4$ monograin powder. Raman spectrum of polycrystalline Cu_2SnSe_3 is shown in the upper right corner.

3.3.1.3 Chemical etching of $Cu_2ZnSn(S,Se)_4$ powder crystal surfaces

Chemical treatments with several etchants (HCl, KCN, Br_2-MeOH and NH_4OH) were performed in order to remove other phases from the $Cu_2ZnSn(Se_{1-x}S_x)_4$ (x = 0, 0.45) monograins' surfaces and to improve the active interface of the *p*-type $Cu_2ZnSn(S,Se)_4$ solar cell performance.

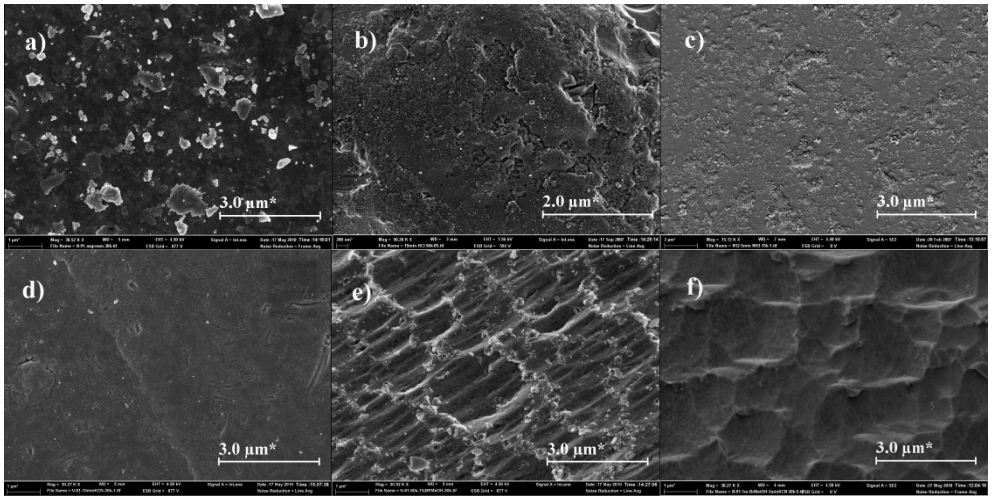

Figure 23. SEM micrographs of as-grown $Cu_2ZnSn(S,Se)_4$ monograin powder surfaces (a) and after treatment with b) HCl, c) NH_4OH, d) KCN, e) Br_2-MeOH, and f) Br_2-MeOH+KCN etchants.

SEM micrographs of the CZTSSe surface after treatment with different etchants (see Figure 23 b) show that after etching with HCl the surfaces of $Cu_2ZnSn(S,Se)_4$ powder crystals are rough and covered with microparticles. We were unable to determine the elemental composition of these microprecipitates by EDS due to their very small size. The etching with NH_4OH resulted in relatively flat surfaces (Figure 23 c). The surfaces of KCN-etched crystals seem to be quite smooth without any precipitates (Figure 23 d). After etching with Br_2-MeOH the surfaces of CZTSSe monograins were covered by crater-like areas with microparticles on their edges (Figure 23 e). Additional etching of the Br_2-MeOH treated powders with KCN removed these precipitates and resulted in clean crystal surfaces (Figure 23 f).

The polarographic analysis data (see Table 6) of the leaching solutions indicated that preferably Sn and chalcogen have been removed by HCl-etching, probably due to the complexation of tin in HCl solution and formation of $[SnCl_4]^{2-}$ [73]. The KCN etching is known as a process to remove preferably Cu-Se binary phases [69]. In our experiments with KCN treatment we found also tin in the leaching solutions of $Cu_2ZnSnSe_4$ monograin materials. The used ammonia solution removed selectively Cu and chalcogen in an approximate ratio 1:2.

Table 6. Composition of elements in leaching solution as determined polarographically.

Etchant	Cu	Zn	Sn	Se
KCN	1.0	no	0.36	1.5
HCl	1.0	0.11	5.8	6.5
NH_4OH	1.0	0.17	no	2.2
Br_2-MeOH	1.0	0.83	0.66	0.33

Figure 24 represents XPS spectra of the as-grown and Br_2-MeOH-etched $Cu_2ZnSn(S,Se)_4$ monograin surfaces. The intensity of Cu2p, CuLMM peaks decreases and the intensity of the Sn and O1s peaks increases after etching materials with Br_2-MeOH. Zn2p and ZnLMM peaks are almost undetectable for materials etched with Br_2-MeOH. The relative atomic concentrations of zinc, copper, tin and selenium were determined from integrated peak areas of high-resolution XPS core level spectra. The S2p peak area was determined by core level curve-fitting procedures since this peak overlaps with the Se3p core level. The composition of the $Cu_2ZnSn(S,Se)_4$ monograin surface etched in Br_2-MeOH solution was determined by XPS and it was: Cu: Zn : Sn : S+Se : O = 1.23 : 1.16 : 37.05 : 12.83 : 47.72 at.%. Comparison of the XPS spectra of the as-grown and the Br_2-MeOH-etched samples allows us to conclude that Br_2-MeOH-etching mainly removes Cu and Zn. This fits well with the results of the polarographic analysis of the leaching solutions.

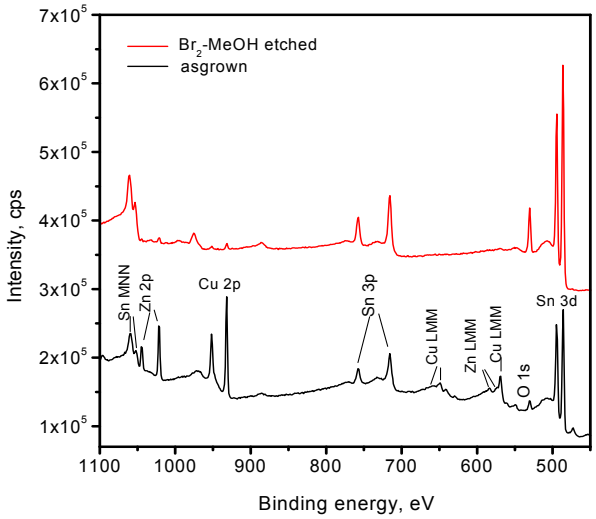

Figure 24. XPS spectra of the as-grown and Br_2-MeOH etched $Cu_2ZnSn(S,Se)_4$ monograin surfaces.

I-V dependences of solar cells made from chemically treated $Cu_2ZnSn(S,Se)_4$ monograin powders are given in Table 7. All the etched powders were post-heat-treated to improve the crystal surface structure.

Table 7. Performance characteristics of $Cu_2ZnSn(S,Se)_4$ monograin layer solar cells made from nonetched and etched absorber crystals.

Etchant	V_{oc}, mV	I_{sc}, mA/cm^2	FF, %
None	300	10	40
Conc. HCl	342	11.5	48
2M NH_4OH	422	10.5	44
10% KCN	490	13.5	49
1% Br_2-MeOH	563	8.5	54
1% Br_2-MeOH +10% KCN	575	13.75	55

It can be seen that etching of the powder crystals improves the parameters of monograin layer solar cells. Solar cells that were made from combined etched materials have the highest values of V_{oc}, I_{sc} and fill factor. The efficiencies of the best solar cells in etching experiments were in the order of 4 %.

3.3.2 $Cu_2ZnSnSe_4$ - Cu_2ZnSnS_4 solid solutions in monograin powder form for solar cells

The first monograin layer solar cells in the structure of ZnO/CdS/$Cu_2ZnSnSe_4$/graphite had low output parameters, their conversion efficiency was 1.8 % [74] and relatively low value of V_{oc}. The results of PL and Raman measurements combined with a detailed analysis of the solar cell parameters enabled us to conclude that $Cu_2ZnSnSe_4$ actually has a bandgap much lower than 1.44 eV as it was reported by Matsushita [25]. According to the PL results, it is proposed that the bandgap energy of CZTSe is around 1.02 eV at T=10K [72] that does not allow high values of V_{oc} to be obtained. These considerations led us to the study of the formation of $Cu_2ZnSn(Se_{1-x}S_x)_4$ solid solutions in the form of monograin powders to find out the optimal composition for an absorber of monograin layer solar cells.

$Cu_2ZnSn(Se_{1-x}S_x)_4$ materials were prepared with the composition x = 0, 0.25, 0.45, 0.75, 0.85, and 1. The ratio of Cu to other metals Cu/(Zn+Sn) was 0.925 and the Zn to Sn ratio was kept constant and equal to 1.0.

Monograin growth in molten KI resulted in a homogeneous composition of the $Cu_2ZnSn(Se_{1-x}S_x)_4$ powders in the region of sulfur content x = 0 to x = 0.85 (Figure 25).

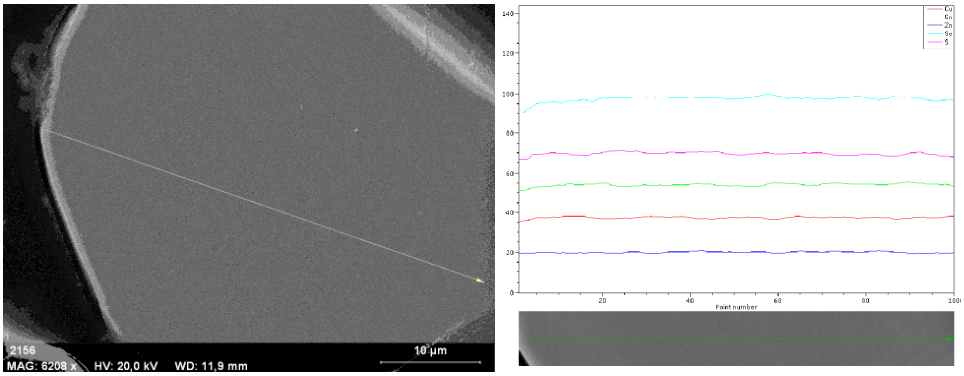

Figure 25. EDS scan over polished individual $Cu_2ZnSn(Se_{1-x}S_x)_4$ powder crystal.

This statement was derived from the XRD analyses and from the EDS scan data over polished individual CZTSSe ($0 \leq x \leq 0.85$) powder crystals.

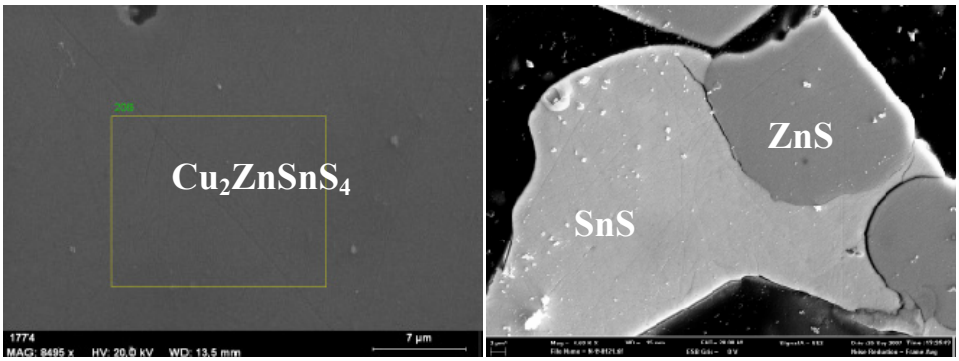

Figure 26. EDS analysis of polished individual crystals of CZTS powder showing existance of different phases.

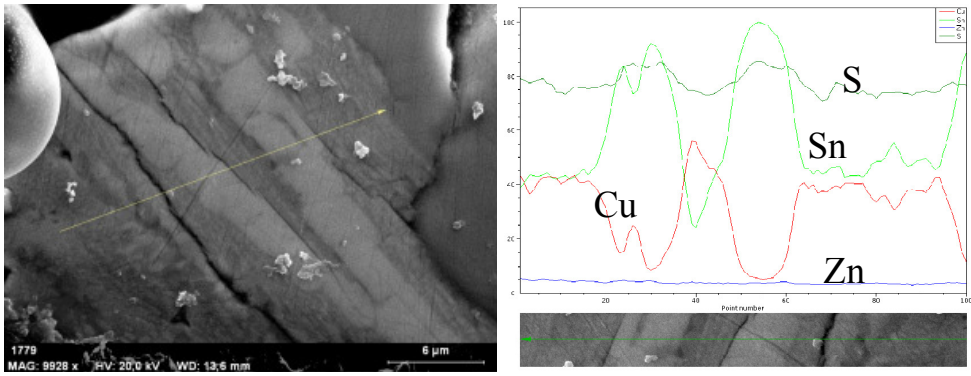

Figure 27. EDS scanning over a polished multiphase Cu_2ZnSnS_4 powder crystal.

For x = 1, synthesized powder crystals were multiphase, as can be seen from the SEM photos and from the curves of the distribution of constituent elements (Figure 26, 27). Here, the results of EDS analysis also indicate the presence of separate phases besides the Cu_2ZnSnS_4 phase: Cu_2SnS_3 ([Cu]=32.9 %, [Sn]=17.2 %, [S]=49.8 %), SnS ([Sn]=51.5 %, [S]=48.45 %) and ZnS ([Zn]=50 %, [S]=50 %). The results of XRD investigations confirm that in addition to the dominating CZTS phase, powders contain SnS in small quantities (Figure 28).

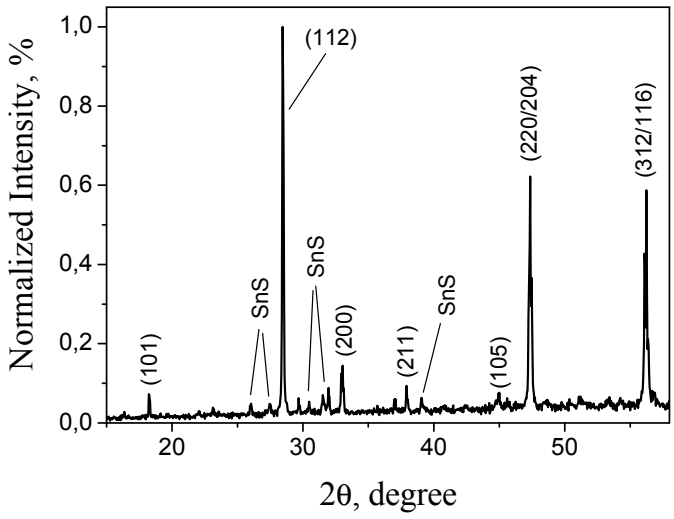

Figure 28. X-ray diffraction pattern of the Cu_2ZnSnS_4 monograin powder.

The XRD pattern did not indicate to the existence of Cu_2SnS_3 and ZnS. In the system Cu-Zn-Sn-S the diffraction signals of the phases Cu_2SnS_3 and ZnS cannot be distinguished from the phase Cu_2ZnSnS_4 due to their structural similarity (the diffraction peaks of these phases can overlap) [75]. One possible explanation for the existence of different phases in synthesized pure CZTS (x=1) is that the homogeneity range of Cu_2ZnSnS_4 is much narrower than that of $Cu_2ZnSnSe_4$ (see Figure 29), resulting therefore in a higher probability for the formation of other phases during the synthesis and the growth process of the Cu_2ZnSnS_4 (x=1) monograin powders of the same initial composition as the $Cu_2ZnSn(Se_{1-x}S_x)_4$ materials with ($0 \leq x \leq 0.85$). Chen *et al*. [76] demonstrated by the first principles of electronic structure calculations that the chemical potential range for the formation of Cu_2ZnSnS_4 without secondary phases is very small. This is in agreement with our experimental results.

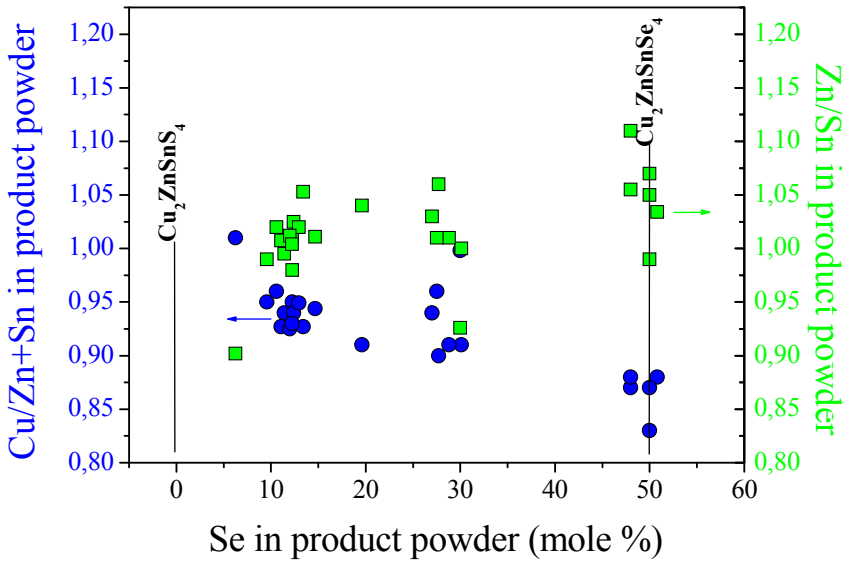

Figure 29. Change in composition of $Cu_2ZnSn(Se_{1-x}S_x)_4$ monograin powders depending on the Se/S concentration ratio.

X-ray diffraction patterns of the monograin powders with different Se/S concentration ratio are presented in Figure 30.

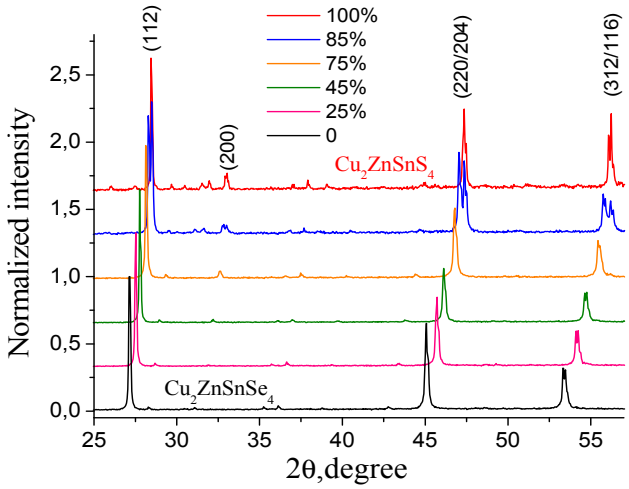

Figure 30. XRD patterns of $Cu_2ZnSn(Se_{1-x}S_x)_4$ monograin powders with different x values.

The diffraction peaks were identified as belonging to the Cu_2ZnSnS_4 compound (x=1) with kesterite structure (space group $I\bar{4}$) and to the $Cu_2ZnSnSe_4$ (x=0) with stannite structure (space group $I\bar{4}2m$) [25, 77]. The reflection Miller indexes were assigned according to Matsushita [24]. The ratio of reflection intensities was in correspondence to that measured by Olekseyuk [77]. An exchange of Se with S shifts the peak positions from the stannite structure to the kesterite structure. At a ratio of S to Se of 85 : 15 mole % the XRD pattern shows a splitting of peaks, which could be a sign of existance of two crystal phases at the same time. From the calculated total energy difference $\Delta Et = Et$ (stannite) - Et (kesterite) the most stable phase is the kesterite structure for both the S-based and the Se-based compounds. This is in accordance with most of the recent experimental data [10,22,27] but it has been suggested that it is possible to grow also the stannite structure [25,77,78]. However, the total energy of the kesterite S-based compounds is only ~1.3 meV/atom lower than the corresponding stannite structure. Similarly, the total energy of the kesterite Se-based compounds is ~3.3 meV/atom lower than their stannite structure. This indicates that kesterite structure should be formed under equilibrium growth conditions, but since the total energy, lattice parameters, and bonds of kesterite and stannite are very similar, both phases may coexist and it should be relatively easy to grow materials with mixed phases depending on the growth method and growth conditions.

3.3.2.1 Solar cell characterization

The prepared monograin powders were used as absorber materials in monograin layer (MGL) solar cell structures: ZnO/CdS/CZTSSe/graphite, where every crystal works as an individual solar cell. All the as-grown powders were post-heat-treated to improve the crystal surface structure.

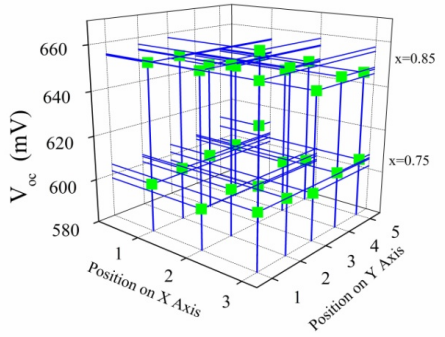

Figure 31. Distribution of V_{oc} values of two different $Cu_2ZnSn(Se_{1-x}S_x)_4$ solar cells with x=0.75 and x=0.85 over a 1 cm (x-axis) by 1.5 cm (y-axis) cell measured in equal distances. Area of every point is 4 mm^2.

Solar cells showed a uniform distribution of solar cell parameters over the whole working area of 1x1.5 cm^{-2} samples (Figure 31).

Open circuit voltages of $Cu_2ZnSn(Se_{1-x}S_x)_4$ monograin layer solar cells increased with increasing sulfur content in the monograin powders, from 283 mV for x=0 to 660 mV for x=0.85 (Figure 32).

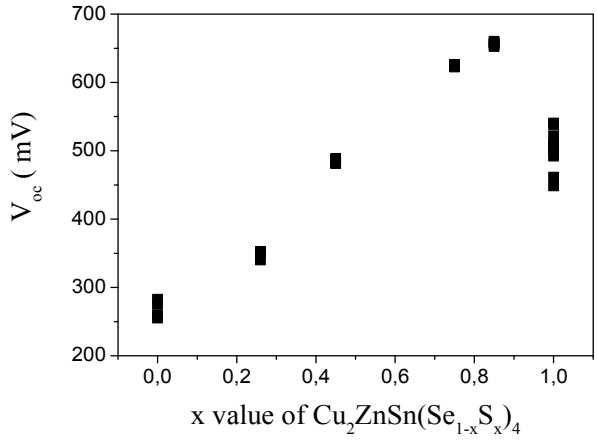

Figure 32. Maximum V_{oc} values of $Cu_2ZnSn(Se_{1-x}S_x)_4$ monograin layer solar cells in depending on Se displacement by S. Data points describe measurement results from graphite back contacts of 4 mm^2 of 1x1.5 cm^2 cell.

The pure Cu_2ZnSnS_4 absorber material resulted in lower V_{oc} (541 mV) probably due to the secondary phases formed. An increase of the open circuit voltage values points to a widening of the bandgap of $Cu_2ZnSn(Se_{1-x}S_x)$ with increasing S concentration. Solar cell structures based on monograin powders with the S/Se concentration ratio of 85 mole % sulfur to 15 mole % selenium yielded in the highest values of the open circuit voltage 660 mV. The $Cu_2ZnSn(S,Se)_4$ solid solution with 75 mole % sulfur and 25 mole % selenium gave the best solar cell with parameters: V_{oc}=622 mV, j_{sc}=15.87 mA/cm^2, *FF*=60 %, η=5.9 %.
The quantum efficiency of solar cell structures was measured as a function of the wavelength of the incident light. The normalized quantum efficiency (QE) spectra of solar cells on the base of $Cu_2ZnSn(Se_{1-x}S_x)_4$ monograin powders show the shift of the absorption edge to shorter wavelengths as well as a change in the short wavelengths response with increasing S content in the absorber material, as shown in Figure 33.

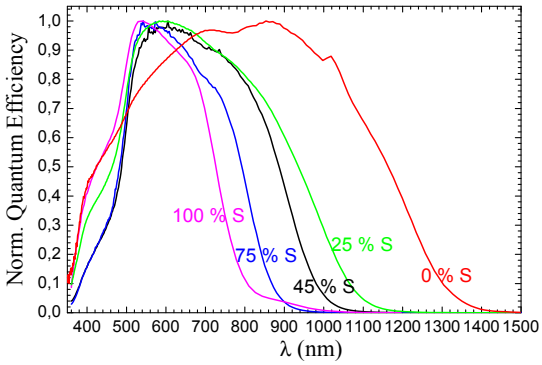

Figure 33. Normalized quantum efficiency spectra of MGL solar cell devices with different S/Se concentration ratio in the used absorber material.

It is known that the open-circuit voltage V_{oc} vs T curves are linear at RT and capable of being used to determine the main path of current losses in solar cells. The open circuit voltage can be given by the following equation:

$$V_{oc} = \frac{\Phi_b}{q} - \frac{AkT}{q} ln\left(\frac{qS_pN_v}{j_{sc}}\right), \qquad (3.3.2.1.1)$$

where Φ_b is the barrier height for holes, A is the diode ideality factor, S_p is the interface recombination velocity for holes, j_{sc} is the short-circuit current density, q is the elementary charge, and N_v is the effective density of states in the valence band. For bulk recombination, $\Phi_b \approx E_g$ [79]. The temperature dependent open circuit voltage measurements were performed to determine the barrier height of the *p-n* junction (Φ_b) (Figure 34).

The barrier height of the solar cells increases as expected with increasing the S content in $Cu_2ZnSn(Se_{1-x}S_x)$ monograin powders.

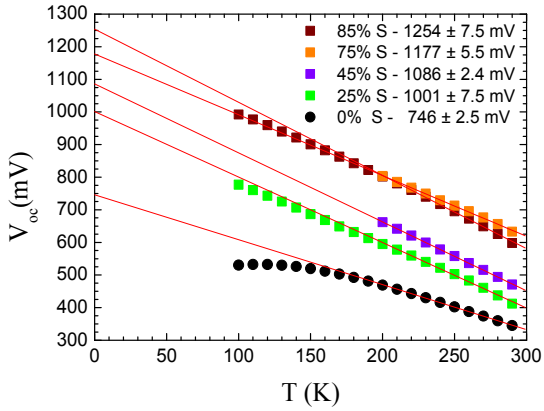

Figure 34. V_{oc} vs. T for $Cu_2ZnSn(Se_{1-x}S_x)_4$ monograin layer solar cells with different x values in the monograin powders.

For CZTSe, quite different bandgaps have been reported. Mostly, it is proposed that the bandgap energy lies between 1.4 eV and 1.56 eV. However, it was suggested by our group that the bandgap energy of CZTSe is about 1.02 eV according to PL analysis [72].

Grossberg *et al.* [80] observed a nearly linear shift of the PL emission towards higher energies with increasing S concentration in $Cu_2ZnSn(Se_xS_{1-x})_4$ solid solutions up to a total value of 0.4 eV.

Considering the increase in the open circuit voltage values, the linear shift of the PL emission towards higher energies, the quantum efficiency spectra shift to the shorter wavelengths and the increase of barrier height of solar cells with increasing S content in the absorber material gives us an assertion that the published $Cu_2ZnSnSe_4$ bandgap energies: 1.44-1.56 eV should be much lower than Cu_2ZnSnS_4 bandgap energies: 1.45-1.51 eV. During the time of writing this thesis, other groups have obtained similar results [14,81,82]. Ahn *et al.* [81] proposed that the possible overestimation of the E_g value is caused by the existence of ZnSe in the coevaporated films.

In conclusion, it has been shown that monograin powder technology enables to grow $Cu_2ZnSn(S,Se)_4$ materials with homogeneous composition usable for monograin layer solar cells. It has been found that the surface and the bulk compositions of as-grown CZTSSe monograin powder crystals are not identical. The chemical treatments before the deposition of CdS are important to improve the $Cu_2ZnSn(S,Se)_4$ monograin layer solar cell performance. The increasing sulfur content in $Cu_2ZnSnSe_4$ monograin powder absorber materials improves the values of open circuit voltages of MGL solar cells and shifts the QE curves to the higher energy side. The $Cu_2ZnSn(S,Se)_4$ solid solution with 75 mole % sulfur and 25 mole% selenium gave the best solar cell with parameters: V_{oc}=622 mV, j_{sc}=15.87 mA/cm^2, FF=60 %, η=5.9 %.

CONCLUSIONS

$CuInSe_2$

1 The growth of $CuInSe_2$ powder crystals in KI results in single crystalline tetragonal particles and the process can be described by the formula: $d_m \sim t^{1/n} exp(-E_d/kT)$. From the Arrhenius plot of the median grain diameter d_m the activation energy for linear crystal growth E_d = 0.25 ± 0.05 eV and from the time dependance of the median grain diameter $d_m \sim t$ at constant temperature the power of the time dependence of crystal growth $1/n$ = 0.25 ± 0.06 and n = 3.9 ± 0.93 were determined. n value is indicating that mass diffusion through the liquid phase and sintering of formed grains by material surface diffusion are dominating in the growth process of monograin powder crystals.

2. The single-phase powder crystals can be synthesized from precursor Cu-In alloys with Cu/In ratio values between 1>Cu/In>0.7. The solubility of $CuInSe_2$ in KI at 720ºC was found to be 0.17 weight %.

3. In the case of Na doping it was found that the peak position of the PL band of Na doped CISe powders shifted depending on the Na doping level and showed the maximum energy when sodium concentration was 1×10^{19} at/cm^3. The same material had the highest carrier concentration 2×10^{17} cm^{-3}. The Na doping level of the absorber material had strong influence on solar cell parameters and added sodium concentrations 3×10^{18} at/cm^3 resulted in the highest open-circuit voltage and fill factor values.

$Cu_2ZnSn(S,Se)_4$

1. In the case of $Cu_2ZnSn(S,Se)_4$ growth in molten KI the bulk and the surface compositions of formed CZTSSe crystals were found to be non-identical. The chemical treatments before the deposition of CdS were found to be important to improve the performance of the $Cu_2ZnSn(S,Se)_4$ monograin layer solar cell.

- The analysis of leaching solutions showed that Sn and chalcogen are removed preferably by HCl etching. Leaching solutions after KCN-etching contain Cu, Sn and chalcogen. From XPS measurements we found that etching with 1% Br_2-MeOH resulted in Sn-rich material surfaces.
- The combination of chemical treatments (1% Br_2-MeOH + 10% KCN) before the deposition of CdS gave the best $Cu_2ZnSn(S,Se)_4$ monograin layer solar cells with efficiencies in the order of 4 %.

2. Monograin powder technology enables us to grow $Cu_2ZnSn(Se_{1-x}S_x)_4$ materials with homogeneous composition in the region of sulfur content x = 0 to x = 0.85 usable for monograin layer solar cells.

3. Increase in the sulfur content in $Cu_2ZnSnSe_4$ monograin powder absorber materials improves the values of open circuit voltages of MGL solar cells and shifts the QE curves to the higher energy side. The barrier height of solar cells increasis also with the increase of S content in $Cu_2ZnSn(Se_{1-x}S_x)_4$ monograin powders.

4. Solar cell structures based on monograin powders with a S/Se concentration ratio of 85 mole% sulfur to 15 mole% selenium yielded in the highest values of open circuit voltage: 660 mV. The $Cu_2ZnSn(S,Se)_4$ solid solution with 75 mole % sulfur and 25 mole % selenium gave the highest parameters of solar cell: V_{oc} = 622 mV, j_{sc} = 15.87 mA/cm^2, FF = 60 %, η = 5.9 %.

ACKNOWLEDGEMENTS

This thesis is based on the experimental work carried out in the Laboratory of Semiconductor Materials Technology at the Department of Materials Science, Tallinn University of Technology.

Above all, I would like to express my deepest gratitude to my supervisor Leading Research Scientist Mare Altosaar for her support, excellent guidance and encouragement over the years.

I would also like to thank Prof. Enn Mellikov, Head of the Department of Materials Science, for giving me the opportunity to join the research group at the Chair of Semiconductor Materials Technology and to work in his laboratory.

This work would not have been possible without contribution and help from my colleagues from the Laboratory of Semiconductor Materials Technology.
Special thanks go to Dr. Jaan Raudoja for teaching me the monograin powder technology both in theory and in practice. I am very thankful to Dr. Marit Kauk for being always ready to help and to answer my questions. I wish to thank Dr. Tiit Varema, Dr. Maarja Grossberg, PhD student Mati Danilson, Dr. Karin Kerm, Prof, Jüri Krustok, Dr. Malle Krunks, Dr. Olga Volobujeva, MSc. Rainer Traksmaa, PhD student Katri Muska, Dr. Kaia Ernits, PhD student Liina Kaupmees and PhD student Maris Pilvet, who supported me with their work and friendship.

I appreciate greatly the acceptance of Dr. Charlotte Platzer-Björkman, University of Uppsala, Sweden and Dr. Kaupo Kukli, University of Tartu, for accepting to be opponents of this thesis.

Financial support from the Estonian Science Foundation grants No. 6160, 6179, 7678, Estonian Ministery of Education and Science target financing project SF0140099s08, Enterprise Estonia, World Federation of Scientists National Scholarship Programme, and Estonian Doctoral School of Materials Science and Materials Technology (MMTDK) is gratefully acknowledged.

My warmest gratitude belongs to my family.

Tallinn, February 2011

Kristi Timmo

ABSTRACT

Formation of properties of $CuInSe_2$ and $Cu_2ZnSn(S,Se)_4$ monograin powders synthesized in molten KI

This thesis is focused on the research of regularities of formation of $CuInSe_2$ (CISe) and $Cu_2ZnSn(S,Se)_4$ (CZTSSe) monograin powders in liquid potassium iodide (flux). The variation of elemental composition, chemical surface treatment and doping with sodium were used to modify absorber materials properties for monograin layer solar cells (MGL).

The developed $CuInSe_2$ and $Cu_2ZnSn(S,Se)_4$ powders were characterized by EDS, SEM, XRD, ICP-MS, XPS, Raman, polarographic analyses and photoluminescence spectroscopy. The monograin powders were used as absorber materials in monograin layer solar cells. The solar cells were characterized by the dark and light current-voltage (I-V), capacitance-voltage, QE and by V_{oc} vs. T measurements.

In the growth process of monograin powders the chemical nature of the liquid (molten) phase of the used flux material impacts the powder crystals growth parameters and properties of the obtained absorber materials. It was found that the growth of powder crystals can be described by the formula: $d_m \sim t^{1/n} \exp(-E_d/kT)$. From the Arrhenius plot of the median grain diameter d_m the activation energy for linear crystal growth E_d = 0.25 ± 0.05 eV and from the time dependance of the median grain diameter $d_m \sim t$ at constant temperature the power of the time dependence of crystal growth $1/n$ = 0.25 ± 0.06 and n = 3.9 ± 0.93 were determined. The value of n = 3.9 ± 0.93 indicates that mass diffusion through the liquid phase and sintering of formed grains by material surface diffusion were dominating in the growth process of monograin powder crystals. Crystals of $CuInSe_2$ grown in KI flux had a shape of polyhedrons with smooth facets. By variation of the Cu/In ratio (0.5 - 1.1) in initial Cu-In alloys the area of single-phase $CuInSe_2$ was determined to be between 1>Cu/In>0.7.

The processes of the synthesis and isothermal growth of $CuInSe_2$ monograin powders proceed at elevated temperatures in KI as a flux material and lead to the doping of the grown materials with iodine and potassium (also with Na as impurity in KI) from the flux. The doping with K and Na influences the surface composition, the defect structure and electrical and optical properties of the materials. The peak position of the PL band of Na doped CISe powders shifted depending on the Na doping level and showed the maximum energy when sodium concentration was 1×10^{19} at/cm^3. The same material had the highest carrier concentration 2×10^{17} cm^{-3}. The Na doping level of the absorber material had strong influence on the solar cell parameters and the added sodium concentrations 3×10^{18} at/cm^3 resulted in the highest open-circuit voltage and fill factor values.

In the case of $Cu_2ZnSn(S,Se)_4$ growth in molten KI the bulk and the surface compositions of formed CZTSSe crystals were found to be non-identical. This difference in bulk and surface compositions is caused by the different solubilities of the precursors in the molten flux. As a result, different precursor components precipitate out from the flux during the cooling period onto the surface of the grown crystals. The influence of different chemical treatments of powder crystals on the chemical composition of crystals surface was studied to control the surface composition and to improve the parameters of the $Cu_2ZnSn(S,Se)_4$ monograin layer solar cell. The analysis of the leaching solutions showed that tin and chalcogen can be removed preferably by HCl etching. The leaching with KCN leads to the removal of Cu, Sn and chalcogen from the surface. From the XPS measurements we found that etching with 1% Br_2 in methanol resulted in Sn-rich material surface. The combination of chemical treatments (1% Br_2-MeOH + 10% KCN) resulted in $Cu_2ZnSn(S,Se)_4$ monograin layer solar cells with the highest values of parameters.

It was shown that monograin powder technology in the use of KI flux enables us to grow $Cu_2ZnSn(Se_{1-x}S_x)_4$ materials with homogeneous composition in the region of sulfur content x = 0 to x = 0.85. The increasing of sulfur content in $Cu_2ZnSn(S,Se)_4$ monograin powder absorber materials led to the increase of the forbidden band of material and improved the values of open circuit voltages of MGL solar cells. Solar cell structures based on monograin powders with the concentration ratio of 85 mole% sulfur to 15 mole% selenium yielded in the highest values of V_{oc} = 660mV. The $Cu_2ZnSn(S,Se)_4$ solid solution with 75 mole % sulfur and 25 mole % selenium gave the highest parameters of solar cell V_{oc} = 622 mV, I_{sc} = 15.87 mA/cm^2, FF = 60 %, η = 5.9 %.

KOKKUVÕTE

Kaaliumjodiid-sulandaja keskkonnas kasvatatud $CuInSe_2$ ja $Cu_2ZnSn(S,Se)_4$ monoterapulbrite omaduste kujundamine

Käesolevas töös uuriti $CuInSe_2$ (CISe) ja $Cu_2ZnSn(S,Se)_4$ (CZTSSe) monoterade sünteeskasvatust ja nende omaduste kujunemist kaaliumjodiidsulandaja (KI-sulandaja) keskkonnas. Sünteesitud materjali omaduste modifitseerimiseks, eesmärgiga parandada monoterakihtide baasil valmistatavate päikeseelemetide väljundparameetreid, kasutati absorbermaterjalide CISe ja CZTSSe lähteainete varieerimist, keemilist pinnatöötlust ja legeerimist naatriumiga.

CISe ja CZTSSe monoterade omaduste uurimisel kasutati EDS, SEM, XRD, ICP-MS, XPS ja polarograafilise analüüsi meetodeid, aga ka Raman- ja fotoluminestsents-spektroskoopiat. Monoterapulbrite baasil valmistatud päikeseelementide iseloomustamiseks kasutati valgustundlikkuse spektroskoopiat (QE), V_{oc} vs. T mõõtmisi, mahtuvusspektroskoopiat ja volt-amper kõverate mõõtmisi.

CISe ja CZTSSe monotera kristallide sünteesi ja seega saadava materjali omadusi mõjutab väga suurel määral protsessis kasutatava KI-sulandaja keemiline koostis. Töös leiti CISe kristallide mediaanse diameetri suurenemist väljendava valemi – $d_m \sim t^{1/n} exp(-E_d/kT)$ - näitajad E_d ja $1/n$ KI- sulandaja puhul alljärgnevalt: kristallide mediaanse diameetri d_m suurenemise aktivatsioonienergia E_d = 0,25 ± 0,05 eV ja aja t astmenäitaja $1/n = 0.25 \pm 0.06$. Mediaanse diameetri ajasõltuvuse astendaja väärtusest n = 3,9 ± 0,93 järeldub, et CISe monoterapulbrite sünteeskasvatusel KI-sulandajas esineb lisaks aine massidifusioonile läbi sulandaja vedelfaasi ka prekursor-osakeste paakumine koos pinnadifusiooniga. $CuInSe_2$ lahustuvuseks KI-sulandajas saadi 0,17 kaal %. Kasvanud üksikkristallide tetragonaalne kuju viitab samuti $CuInSe_2$ väikesele lahustuvusele KI-sulandajas. Varieerides vase ja indiumi kontsentratsioonide suhet Cu-In prekursorsulamis piirides [Cu]/[In] = 0,5-1,1 leiti, et ühefaasilise koostisega CISe absorbermaterjale saab sünteesida vahemikus 1>[Cu]/[In]>0,7.

CISe ja CZTSSe kasvatamisel KI-sulandaja keskkonnas toimub kaaliumi ja joodi difusioon moodustuvatesse kristallidesse kuni kasvatustemperatuurile vastava küllastuseni. Uuriti ka Na mõju kasvavate kristallide pinnakoostisele, defektstruktuurile, elektrilistele ja optilistele omadustele. Na mõju uurimiseks $CuInSe_2$ monoterade omadustele kasvatati CISe monoterapulbrid CuSe sulandajas ja seejärel legeeriti Na-ga kasutades selleks erineva kontsentratsiooniga/suhtega NaI vesilahuseid. Fotoluminestsentsspektrite mõõtmisel selgus, et Na kontsentratsiooni suurenemisega toimub PL ribade maksimumi asukoha nihkumine suuremate energiaväärtuste poole. Kõige suurema energiaväärtusega fotoluminestsentsi maksimum oli materjalil, millele oli naatriumit lisatud 1×10^{19} at/cm^3. Sellise lisatud

Na koguse juures oli laengukandjate kontsentratsioon CISe absorbermaterjalis 2×10^{17} cm^{-3}. Päikeseelemendi parim avatud vooluringi pinge saadi CISe absorbermaterjaliga, kus lisatud Na kontsentratsioon oli 3×10^{18} at/cm^3.

$Cu_2ZnSn(S,Se)_4$ kui teise väga perspektiivse absorbermaterjali sünteeskasvatuse uurimisel KI-sulandajas saadi samuti tetragonaalse kujuga pulbrikristallid. EDS ja XPS analüüside alusel leiti, et üksikkristallide sisu- ja pinnakoostised erinevad teineteisest. Koostise erinevus tuleneb sellest, et pärast sulandaja eemaldamist veega on kristallide pind kaetud vedelfaasis lahustunud ja jahtumise käigus kristallide pinnale sadenenud amorfse materjaliga. Selle amorfse materjali eemaldamiseks ja $Cu_2ZnSn(S,Se)_4$ kristallide pinnakoostise modifitseerimiseks kasutati erinevaid keemilisi söövituslahuseid. Söövituslahuste polarograafiline analüüs pärast $Cu_2ZnSnSe_4$ kristallide söövitamist näitas, et soolhappeline söövitus eemaldas peamiselt Sn ja kalkogeeni, KCN-söövitus aga Cu, Sn ja kalkogeeni. XPS mõõtmistest selgus, et söövitamine Br_2-metanool lahusega jättis kristallide pinna O-, Sn- ja kalkogeenirikkaks. Parimad päikeseelemendi väljundparameetrid saadi kasutades kombineeritud söövitusrežiime, kus Br_2-metanool-söövitusele järgnes söövitamine KCN vesilahusega.

Leiti, et kasutades sünteesiprotsessis sulandajana kaaliumjodiidi, on võimalik kasvatada (sarnaselt $CuInSe_2$-le) homogeense koostisega CZTSSe tahkeid lahuseid $Cu_2ZnSn(Se_{1-x}S_x)_4$ (x = 0, 0.25, 0.45, 0.75, 0.85, 1.0) kuni S sisalduseni x = 0.85, mis on sobilikud kasutamiseks *p*-tüüpi absorbermaterjalina päikeseelementides. Näidati, et väävli kontsentratsiooni suurendamine materjalis viib kasvatatud ja uuritud CZTSSe absorbermaterjalide keelutsooni laienemisele. Väävli kontsentratsiooni suurendamine $Cu_2ZnSn(Se_{1-x}S_x)_4$-s parandas avatud vooluringi pinge väärtusi. Parimad avatud vooluringi pinge väärtused (V_{oc} = 660 mV) saadi materjaliga, kus x = 0.85. Parima päikeseelemendi kasuteguri η = 5.9 % andis materjal, kus väävli ja seleeni sisaldus oli 75 mool% S ja 25 mool% Se (x = 0.75). Parima kasuteguriga päikesepatarei teised parameetrid olid: V_{oc} = 622 mV, I_{sc} = 15.87 mA/cm^2, FF = 60%.

REFERENCES

1) A. Luque, S. Hegedus, Handbook of Photovoltaic Science and Engineering, 2002.
2) H. Du, C.H. Champness, I. Shih, *Thin Solid Films*, 480-481 (2005) 37-41.
3) V. Alberts, M.L. Chenene, *Phys.D: Appl. Phys.*32 (1999) 3093-3098.
4) U. Rau, H.W. Schock, *Appl. Phys. A* 69 (1999) 131-147.
5) http://www.pv-tech.org/news/_a/zsw_sets_another_new_cigs_997_solar_cell_record/
6) J. Emsley, *The Elements* (3rd ed.), Oxford Univ. Press, Oxford (1998), p. 289.
7) K. Ito and T. Nakazawa, *Jpn. J. Appl. Phys.* 27 (1988), 2094-2097.
8) K. Ito and T. Nakazawa, *Proceedings of the 4th International Conference of Photovoltaic Science and Engineering, Sydney* (1989), p. 341.
9) Th.M. Friedlmeier, N. Wieser, T. Walter, H. Dittrich and H.-W. Schock, *Proceedings of the 14th European Conference of Photovoltaic Science and Engineering and Exhibition, Bedford* (1997), p. 1242.
10) J.S. Seol, S.Y. Lee, J.C. Lee, H.D. Nam and K.H. Kim, *Sol. Energy Mater. Sol. Cells* 75 (2003), p. 155.
11) H. Katagiri, K. Jimbo, K. Moriya and K. Tsuchida, *Proceedings of the 3rd World Conference on Photovoltaic Solar Energy Conversion, Osaka* (2003), p. 2874.
12) K. Jimbo, R. Kimura, T. Kamimura, S. Yamada, W.S. Maw, H. Araki, K. Oishi, H.i Katagiri, *Thin Solid Films* 515 (2007), p. 5997–5999.
13) K. Jimbo, R. Kimura, T. Kamimura, S. Yamada, H. Katagiri, W. Shwe Maw, K. Oishi, M. Yamazaki, H. Araki, A. Takeuchi, *Thin Solid Films* 517 (2009) 2455-2460.
14) T.K. Todorov, K.B. Reuter, D.B. Mitzi, *Adv. Mater. (Weinheim, Ger.)*, 22 (2010) 1-4.
15) G. Kühn, H. Neumann, *Z.Chem.* 27 (1987) 197.
16) W. Paszkowicz, R. Lewandowska, R. Bacewicz, *Journal of Alloys and Compounds* 362 (2004) 241-247.
17) S.R. Hall, J.T. Szymanski, J.M. Stewart, *Can. Mineral.* 16 (1978) 131.
18) S. Chen, X.G. Gong, A. Walsh, S.H. Wei, *Phys. Rev B* 79 (2009) 165211.
19) S.Schorr, *Thin Solid Films* 515 (2007) 5985-5991.
20) T. Maeda, S. Nakamura, T. Wada, *Mater. Res. Soc. Symp. Proc. Vol.* 1165 (2009).
21) H. Katagiri, *Thin Solid Films* 480–481 (2005) 426.
22) H. Katagiri, K. Saitoh, T. Washio, H. Shinohara, T. Kurumadani, S. Miyajima, *Sol. Energy Mater. Sol. Cells* 65 (2001) 141.
23) S. Chen, X.G. Gong, A. Walsh, S.H. Wei, *Appl. Phys. Lett.* 94 (2009) 041903.
24) C. Persson, *J. Appl. Phys.* 107 (2010) 053710.

25) H. Matsushita, T. Maeda, A. Katsui, T. Takizawa, *J. Cryst. Growth* 208 (2000) 416-422.
26) R.A. Wibowo, E.S. Lee, B. Munir, K.H. Kim, *Phys. Status Solidi A* 204 (2007) 3373.
27) G.S. Babu, Y.K. Kumar, P.U.Bhaskar, V.S. Raja, *Semicond. Sci. Technol.* 23 (2008) 085023.
28) R.A. Wibowo, W.S. Kim, E.S. Lee, B. Munir, K.H. Kim, J. Phys. Chem. Solids 68 (2007) 1908–1913.
29) J.M. Raulot, C. Domain, J.F. Guillemoles, *J. Phys. Chem. Solids* 66 (2005) 2019-2023.
30) G. Zoppi, I. Forbes, R.W. Miles, P.J. Dale, J.J. Scragg, L.M. Peter, *Prog. Photovoltaics* 17 (2009) 315-319.
31) T. Haalboom, T. Gödecke, F. Ernst, M. Rühle, R. Herberholz, H.W. Schock, C. Berlharz, K.W. Benz, *Inst. Phys. Conf. Ser. No 152: Section B: Thin Film Growth and Characterization* (1998) 249-252.
32) R. Herberholz, U. Rau, H.W. Schock, T. Haalboom, T. Gödecke, F. Ernst, C. Beilharz, K.W. Benz, D.Cahen, *Eur. Phys. J. AP* 6 (1999) 131-139
33) C.H. Champness, *Journal of Materials Science: Materials in Electronics* 10 (1999) 605-622.
34) U.C. Boehnke, G.Kühn, *J. Mater. Sci*. 22 (1987) 1635.
35) M.L. Fearheiley, *Solar Cells* 16 (1986) 91-100.
36) I.V. Dudchak, L.V. Piskach, *Journal of Alloys and Compounds* 351 (2003) 145-150.
37) I.D. Olekseyuk, I.V. Dudchak, L.V. Piskach, *Journal of Alloys and Compounds* 368 (2004) 135-143.
38) A. Weber, I. Kötschau, S. Schorr, H.W. Schock, *Mater. Res. Soc. Symp. Proc.* 1012 (2007) 1012-Y03-35.
39) S. Schorr, A. Weber, V. Honkimäki, H.W. Schock, *Thin Solid Films* 517 (2009) 2461-2464.
40) R. Schurr, A. Hölzing, S. Jost, R. Hock, T. Voβ, J. Schulze, A. Kirbs, A. Ennaoui, M. Lux-Steiner, A. Weber, I. Kötschau, H.W. Schock, *Thin Solid Films* 517 (2009) 2465-2468.
41) J. Hiie, M. Altosaar, E. Mellikov, P. Kukk, J. Sapogova, D. Meissner, Physica Scripta. Vol. T69 (1997) 155-158.
42) J. Hiie, M. Altosaar, E. Mellikov, *Solid State Phenomena Vol.* 67-68 (1999) 303-308.
43) J. Hiie, M. Altosaar, E. Mellikov, D. Meissner, T. Brammer, *2nd WCEPSEC* (1998) 732-734.
44) M. Altosaar, J. Hiie, E. Mellikov, J. Mädasson, *Cryst. Res. Technol.* 31 (1996) 505-508.
45) M. Altosaar, E.Mellikov, *Jpn. J. Appl. Phys.* 39 (2000) 65-66.
46) U. Rau, H.W. Schock, *Appl. Phys. A* 69 (1999) 131-147.

47) Su-Huai Wei, S.B. Zhang, A. Zunger, *J. Appl. Phys*. 85 (1999).
48) D. Braunger, D. Hariskos, G. Bilger, U. Rau, H.W. Schock, *Thin Solid Films* 361-362 (2000) 161-166.
49) M.A. Contreras, B. Egaas, P. Dippo, J. Webb, J. Granata, K. Ramanathan, S. Asher, A. Swartzlander, R. Noufi, *26th IEEE Photovoltaic Specialists Conference* (1997) 359-363.
50) B.M. Keyes, F. Hasoon, P. Dippo, A. Balcioglu, F. Abulfotuh, *26th IEEE Photovoltaic Specialists Conference* (1997) 479-482.
51) R. Kimura, T. Nakada, P. Fons, A. Yamada, S. Niki, T. Matsuzawa, K. Takahashi, A. Kunioka, *Sol. Energy Mater. Sol. Cells* 67 (2001) 289-295.
52) U. Störkel, M. Aggour, M. Weber, R. Scheer, H.J. Lewerenz, *Thin Solid Films* 387 (2001) 182-184.
53) Y. Hashimoto, N. Kohara, T. Negami, M. Nishitani, T. Wada, *Jpn. J. Appl. Phys*. 35 (1996) 4760-4764.
54) R. Klenk, R. Menner, D. Cahen, H.W. Schock, *Proceedings of 21st IEEE Photovoltaic Specialists Conference* (1990) 481-486.
55) T. Wada, Y. Hashimoto, K. Kusao, N. Kohara, T. Negami, M. Nishitani, *Mat. Res. Soc. Symp. Proc.* 426 (1996) 291-296.
56) R.Pal, K.K. Chattopadhyay, S. Chaudhuri, A.K. Pal, *Thin Solid Films* 254 (1995) 111-115.
57) R. Hunger, T. Schulmeyer, M. Lebedev, A. Klein, W. Jaegermann, R. Kniese, M. Powalla, K. Sakurai, S. Niki, *Proceedings of WCPSEC*, Osaka (2003).
58) B. Canava, J.F. Guillemoles, J. Vigneron, D. Lincot, A. Etcheberry, *J. Phys. Chem. Solids* 64 (2003) 1791-1796.
59) A.J. Nelson, C.R. Schwerdtfeger, G.C. Herdt, D. King, M. Contreras, K. Ramanathan, W.L. O`Brien, *J. Vac. Sci. Technol. A* 15 (1997) 2058-2062.
60) Справочник химика Т. II изд. "Химия", (1964).
61) E.Mellikov, J.Hiie, M.Altosaar, *SPIE Proc.* 222 (1994) 177-185.
62) T.I. Koneshova, A.A. Babitsyna, V.T. Kalinnikov, *Izv. Akad. Nauk. SSSR, Neorg. Mater.* 18 (1982) 1483.
63) D.R. Lide, Handbook of Chemistry and Physics, 78th Edition 1997-1998.
64) A. Bouraiou, M.S. Aida, E. Tomasella, N.Attaf, *J. Mater. Sci.* 44 (2009) 1241-1244.
65) L. Ozawa, *J. Electrochem. Soc.: Sol. State Sci. Technol.* 124 (1977) 413.
66) J. Geguzin, Physics of Sintering, Nauka, Moscow, 1984, p. 37.
67) A. Rockett, J.S. Britt, T. Gillespie, C. Marshall, M.M. Al Jassim, F. Hasoon, R. Matson, B. Basol, *Thin Solid Films* 372 (2000) 212-217.
68) V. Nadenau, G. Lippold, U. Rau, H.W. Schock, *J. Cryst. Growth* 233 (2001) 13.

69) R. Scheer, T. Walter, H.W. Schock, M.L. Fearheiley, H.J. Lewerenz, *Appl. Phys. Lett*. 63 (1993) 3294-3296.
70) A. Rockett, *Thin Solid Films* 480-481 (2005) 2-7.
71) G. Lucovsky, J.C. Mikkelsen, W.Y. Liang, R.M. White, R.M. Martin, *Phys. Rev. B 4*, 14 (1976) 1663-1669.
72) M. Grossberg, J. Krustok, K. Timmo, M. Altosaar, *Thin Solid Films*, Vol. 517 (2009) 2489-2492.
73) M. Pourbaix, Atlas of Electrochemical Equilibria in Aqueous Solutions II (1974).
74) M. Altosaar, J. Raudoja, K. Timmo, M. Danilson, M. Grossberg, M. Krunks, T. Varema, E. Mellikov, *in: Proceedings of the 2006 IEEEWCPEC-4*, Havaii, 2006.
75) A. Weber, R. Mainz, H.W. Schock, *J. Appl. Phys.* 107 (2010) 013516.
76) S. Chen, X.G. Gong, A. Walsh, S.H. Wei, *Appl. Phys. Lett.* 96 (2010) 021902.
77) I.D. Olekseyuk, L.D. Gulay, I.V. Dydchak, L.V. Piskach, O.V. Parasyuk, O.V. Marchuk, *J. Alloys Compd.* 340 (2002) 141–145.
78) T. Tanaka, T. Nagatomo, D. Kawasaki, M. Nishio, Q. Guo, A. Wakahara, A. Yoshida, H. Ogawa, *J. Phys. Chem. Solids* 66 (2005) 1978–1981.
79) J. Krustok, M. Danilson, A. Jagomägi, M. Grossberg, J. Raudoja, *Optical Materials and Properties, Proceedings of the SPIE*, 5946 (2005) 236-242.
80) M. Grossberg, J. Krustok, J. Raudoja, K. Timmo, M. Altosaar, T. Raadik, *Thin Solid Films* (2010) doi:10.1016/j.tsf.2010.12.099.
81) S. Ahn, S. Jung, J. Gwak, A. Cho, K. Shin, K. Yoon, D. Park, H. Cheong, J.H. Yun, *Appl. Phys. Lett.* 97 (2010) 021905.
82) P.M.P. Salome, P.A.Fernandes, A.F.da Cunha, J.P. Leitao, J. Malaquias, A. Weber, J.C. Gonzalez, M.I.N.da Silva, *Sol. Energy Mater. Sol. Cells* 94 (2010) 2176-2180.

APPENDIX A

PAPER I

K. Timmo, M. Altosaar, M. Kauk, J. Raudoja, E. Mellikov, $CuInSe_2$ monograin growth in the liquid phase of potassium iodide. *Thin Solid Films*, Vol. 515 (2007) 5884-5886.

Available online at www.sciencedirect.com
ScienceDirect
Thin Solid Films 515 (2007) 5884–5886
www.elsevier.com/locate/tsf

$CuInSe_2$ monograin growth in the liquid phase of potassium iodide

K. Timmo *, M. Altosaar, M. Kauk, J. Raudoja, E. Mellikov

Department of Materials Science, Tallinn University of Technology, Ehitajate tee 5, 19086 Tallinn, Estonia

Available online 19 January 2007

Abstract

The results of monograin $CuInSe_2$ synthesis from Cu–In alloy and Se in liquid KI are presented. The amounts of $CuInSe_2$ and KI were nearly equal to fulfil the criterion for the monograin growth (all free volume between the particles has to be filled with liquid). All the grown powder materials with narrow-disperse granularity were chalcopyrite $CuInSe_2$. The grown crystallites had tetrahedral shapes and homogeneous composition. Particle size distribution was used to describe the growth process. The activation energy of linear growth of crystals was $E_d = 0.25 \pm 0.05$ eV, and the power of time dependence of the crystal growth was $l/n = 0.26 \pm 0.06$. The solubility of $CuInSe_2$ in KI at 990 K was 0.17±0.05 wt. %. The solubility of potassium and iodine in $CuInSe_2$ at 990 K was 0.094 wt. %, and 0.0086 wt. %, respectively. As a result, homogeneous p-type $CuInSe_2$ monograin materials were synthesised in KI solvent.

Keywords: Crystallization; $CuInSe_2$; Halides; Growth mechanism

1. Introduction

Monograin powders of $CuInSe_2$ have found application as absorber materials in monograin layer solar cells [1]. Till now, monograin layer solar cells with the structure of graphite/CIS/CdS/ZnO have shown open-circuit voltage (*V*oc) values up to 530 mV and fillfactors up to 65%. The isothermal growth of $CuInSe_2$ monograin powders in the presence of liquid phase of a suitable solvent material (flux) leads to the formation of semiconductor materials with single-crystalline grain structure and narrow-disperse granularity, so called monograin powders [2]. The growth of $CuInSe_2$ monograin powders in CuSe-Se flux results in near-stoichiometric compositions of material grains [2]. This is in accordance with the Cu-side borderline of $CuInSe_2$ phase existence range of Cu_2Se-In_2Se_3 phase diagram [3]. The use of Se as flux material allows to grow the monograin powder in the large range of compositions [4]. The removal of Se from the powder batch is technologically difficult. Therefore, in order to obtain In-rich compositions of monograin powders in a less time consuming process, we studied the growth of monograin powders in different flux materials containing alkali metal compounds that are removable by deionizated water. In this study $CuInSe_2$ compound was synthesized from high-purity elements Cu, In and Se (Cu and In were prior melted and used as Cu–In alloy) and the growth process of $CuInSe_2$ crystals in the liquid phase of molten potassium iodide (KI) as the flux material is described.

2. Experimental

The initial Cu–In alloys were synthesized from the precursors of 5N purity in quartz ampoules. The synthesis were made in a dynamic vacuum at the temperature of 1070 K. Cu–In alloy ingots were triturated in the agate mortar and sieved through the 100 μm sieve. Grinded Cu–In alloy (1:1.1) and elemental Se was mixed with KI. The amount of components for $CuInSe_2$ and the amount of KI were nearly equal for providing enough liquid phase for the monograin growth. The minimum growth temperature was limited by the melting temperature of the used flux material and the maximum growth temperature was limited by the temperature of the phase transition of $CuInSe_2$. The samples were sealed into evacuated

Table 1
Experimentally determined solubility data of $CuInSe_2$ in Se, CuSe-Se and KI

Flux material	Se [7]	CuSe-Se [2]	KI (this work)
Temperature, K	970	800	990
Solubility, wt %	28.5±0.5	8.8±0.5	0.17±0.05

* Corresponding author.
E-mail address: timmokas@yahoo.com (K. Timmo).

0040-6090/$ - see front matter © 2007 Elsevier B.V. All rights reserved.
doi:10.1016/j.tsf.2006.12.085

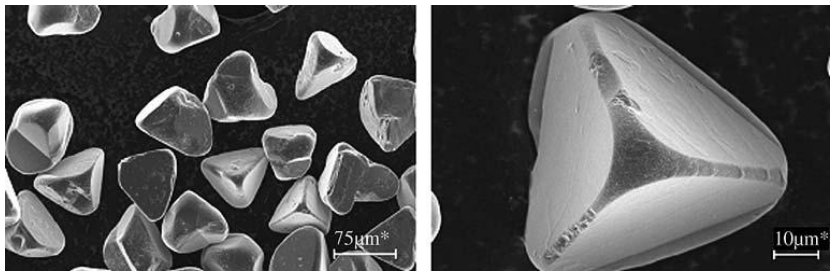

Fig. 1. The scanning electron microscopy photos of $CuInSe_2$ monograin powder crystals grown in KI at 990 K for 76 h.

quartz ampoules, annealed isothermally at various temperatures (970, 990, 1010 and 1050 K) and annealing times (30, 76, 270, 334 h) and quenched to the room temperature. The flux was removed by deionizated water.

The samples were characterised by the X-ray diffraction, the scanning electron microscopy, the photoluminescence and electrical measurements. The X-ray diffraction patterns were recorded by the Bruker AXS D5005 diffractometer with a monochromatic Cu Kα radiation in the 2θ interval of 12–90 deg using the step of 0.04 deg and counting time of 2 s/step.

For the photoluminescence measurements, the excitation source was a He-Cd laser with the wavelength of 441 nm. The powder crystals were mounted inside the closed cycle He cryostat (T=9–300 K). The photoluminescence spectra were recorded with the computer-controlled SPM-2 grating monochromator (f=0.4 m). The signal was detected with InGaAs detector using the conventional lock-in technique.

The composition of $CuInSe_2$ powders was determined polarographically. The solubility of potassium and iodine in $CuInSe_2$ was determined by the inductively coupled plasma mass spectrometry. The shape and surface morphology were studied by the high-resolution scanning electron microscopy LEO SUPRA 35. The conductivity type was determined by the hot-probe method. The sieve analysis method was used to determine the particle size distribution. The median particle size was determined graphically from sieving analyze data on the log-normal probability graph [5]. Solubility of $CuInSe_2$ in KI at 990 K was determined by the weight loss method.

3. Results and discussion

The formation of $CuInSe_2$ monograins take place in the liquid phase of flux that exceeds the limit of sintering of the initial crystals [6]. The flux consists of a molten substance used and the product of synthese dissolved in it. To find the volume of the liquid phase we need to know the solubility. Therefore, we determined the solubility of $CuInSe_2$ in KI by the weight loss method. Big pieces of polycrystalline $CuInSe_2$ were weighed and sealed with 5 times bigger amount of dried KI into quartz ampoules. The ampoules were annealed at 990 K for 120 h and then quenched in water. The undissolved $CuInSe_2$ was weighed. From the weight loss we found the solubility of $CuInSe_2$ in KI. Results are presented in Table 1. For a comparison there is also the data of $CuInSe_2$ solubility in Se [7] and CuSe-Se [2] in Table 1.

Considering the low solubility of $CuInSe_2$ in KI we used equal amounts of both materials in our growth studies.

The dissolution of the flux revealed uniform, mainly nonaggregated micro crystals of tetragonal shape with smooth surfaces (Fig. 1), indicating their growth from individual seed

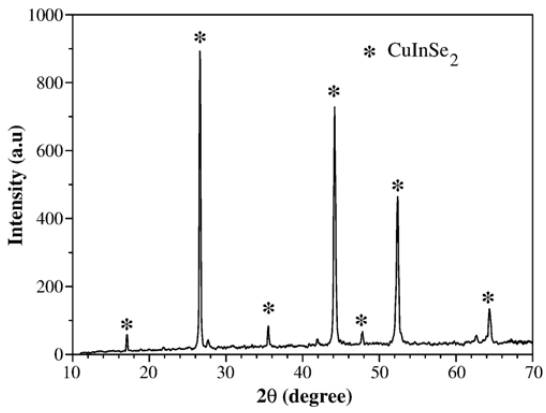

Fig. 2. The X-ray diffraction pattern of $CuInSe_2$ monograin powder grown in KI at 990 K for 76 h.

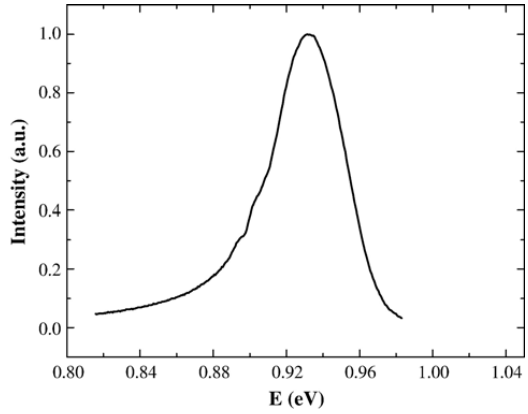

Fig. 3. The photoluminescence spectrum of the $CuInSe_2$ monograin powder grown in KI at 990 K for 76 h.

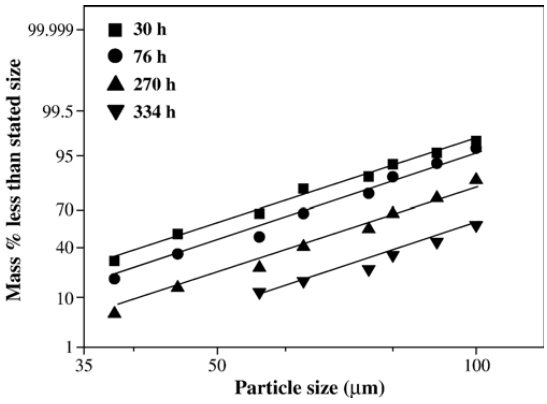

Fig. 4. Particle size distribution of $CuInSe_2$ monograin powders grown in KI at 1010 K for different time periods.

crystals rather than from the aggregates of crystallization nuclei.

The X-ray diffraction spectra of formed $CuInSe_2$ monograin powder (Fig. 2) showed the peaks of chalcopyrite $CuInSe_2$ only.

The composition of $CuInSe_2$ powder materials, which were grown at various temperatures and different times, were analysed polarographically. The results revealed that the composition did not change by changing the growth parameters temperature and time. The composition of $CuInSe_2$ monograin powder materials were Cu:In:Se=23.3:25.5:51.2 (Cu/In=0.91). The inductively coupled plasma mass spectrometry analysis data showed that the solubility of potassium and iodine in $CuInSe_2$ at 990 K was 0.094 wt. %, and 0.0086 wt. %, respectively. All the asgrown monograin powders had p-type conductivity.

The photoluminescence (PL) spectrum of our CIS crystals grown in liquid KI is shown in Fig. 3. A broad asymmetric band characterizes the typical PL spectrum of In-rich CIS with the maximum around 0.93 eV.

The sieve analysis was used to determine the particle size distribution. Fig. 4 shows the particle size distribution of the samples grown at 1010 K for different periods. The particle size distribution of all the samples follows a log-normal distribution in which the distribution shifts with growth duration t. It allows the use of the median particle size d_m to describe the grain growth according to the equation:

$$d_m = At^{l/n}\exp(-E_d/kT), \quad (1)$$

where A is a constant for a given flux and compound, k is the Boltzman constant, T is the growth temperature, E_d is the activation energy for linear crystal growth and n is the geometric factor of growth mechanism [8]. If the growth is controlled by one growth mechanism (diffusion) then $n=3$. From the time dependencies of d_m we found the power of the time dependence of crystal growth $l/n=0.25\pm0.06$, $n=3.9\pm0.93$. From the value of $n=3.9\pm0.93$ we suppose that the growth process of $CuInSe_2$ particles in KI flux is limited by diffusion processes on the surfaces of sintered grains (compare with [9]).

From the Arrhenius plot of the median grain diameter d_m we obtained the activation energy of the linear crystal growth $E_d=0.25\pm0.05$ eV.

4. Conclusions

From Cu–In (1:1.1) alloy, Se and KI it is possible to synthesize and grow p-type $CuInSe_2$ powder materials with single-crystalline grain structure and narrow-disperse granularity. From the Arrhenius plot of the median grain diameter d_m activation energy for linear crystal growth $E_d=0.25\pm0.05$ eV was determined. The power of time dependence of the crystal growth $l/n=0.26\pm0.06$, $n=3.9\pm0.93$ was determined from the time dependencies of d_m. Crystals of $CuInSe_2$ grown in KI flux had mainly tetragonal shapes with smooth surfaces.

Acknowledgements

Financial support of the European Union by Energy program and of Estonian Science Foundation under contracts No. 6160 and 6179 are gratefully acknowledged. The authors would also like to thank Prof. M. Krunks for the X-ray diffraction measurements and Mrs. O. Volobujeva for her help with the scanning electron microscopy studies.

References

[1] M. Altosaar, A. Jagomägi, M. Kauk, M. Krunks, J. Krustok, E. Mellikov, J. Raudoja, T. Varema, Thin Solid Films 431–432 (2003) 466.
[2] M. Altosaar, E. Mellikov, Jpn. J. Appl. Phys. 39 (Supplement 39–1) (2000) 65.
[3] T. Haalboom, T. Gödecke, F. Ernst, M. Rühle, R. Herberholz, H.W. Schock, C. Berlharz, K.W. Berz, Inst. Phys. Conf. Ser. No. 152: Section B: Thin Film Growth and Characterization, 1998.
[4] M. Altosaar, J. Hiie, E. Mellikov, J. Mädasson, Cryst. Res. Technol. 31 (2) (1996) 505 Spec. Issue.
[5] L. Ozawa, J. Electrochem. Soc.: Sol. State Sci. Technol. 124 (1977) 413.
[6] E. Mellikov, J. Hiie, M. Altosaar, SPIE Proc. 2228 (1994) 177.
[7] T.I. Koneshova, A.A. Babitsyna, V.T. Kalinnikov, Izv. Akad. Nauk. SSSR, Neorg. Mater. 18 (1982) 1483.
[8] J. Hiie, M. Altosaar, E. Mellikov, Solid State Phenom. 67–68 (1999) 303.
[9] J. Geguzin, Physics of Sintering, Nauka, Moscow, 1984, p. 37, (in Russian).

PAPER II

M. Kauk, M. Altosaar, J. Raudoja, **K. Timmo**, M. Grossberg, T. Varema, E. Mellikov, Growth of $CuInSe_2$ monograin powders with different compositions, Mater. Res. Soc. Symp. Proc. Vol. 865 (2005) 463-469.

Growth of $CuInSe_2$ monograin powders with different compositions

Marit Kauk, Mare Altosaar, Jaan Raudoja, Kristi Timmo, Maarja Grossberg, Tiit Varema, Enn Mellikov
Institute of Materials Science, Tallinn University of Technology,
Ehitajate Rd 5, 19086 Tallinn, Estonia

ABSTRACT

$CuInSe_2$ monograin powders (MGP) were synthesized from Cu-In alloys of different Cu/In concentration ratios and elemental Se in liquid phase of flux material in evacuated quartz ampoules. The surface morphology, phase structure, and composition of the powder crystals were analyzed by scanning electron microscopy, X-ray diffraction, and energy-dispersive X-ray analysis respectively. Bulk composition was analyzed polarographically. Photoluminescence spectra were measured at 9 K. It was found that the composition of MGP material (Cu/In concentration ratio) can be controlled by the concentration ratio of precursor Cu-In alloys. Single phase $CuInSe_2$ growth is realisable between $0.7<Cu/In<1$ at the growth temperature of 1000 K. Photoluminescence spectra of near-stoichiometric materials had one dominant peak at 0.93 eV, which is typical to In-rich $CuInSe_2$. Samples with high In content exhibited two broad bands with peak positions at 0.86 and 0.93 eV.

INTRODUCTION

The monograin powders of $CuInSe_2$ (CIS) have found application as absorber material in monograin layer solar cells [1]. The monograin layer consists of one crystal thick layer of grains embedded into an organic resin. The advantages of the developed powder materials are the single-crystalline structure of every grain, the uniform distribution of doping impurities and narrow granulometric composition. Till now, monograin layer solar cells with the structure of graphite/CIS/CdS/ZnO have shown open-circuit voltage (V_{oc}) values up to 530 mV and fill factors up to 60% [2]. The growth of $CuInSe_2$ MGP-s in CuSe-Se flux [3] results in near-stoichiometric compositions. This is in accordance with the Cu-side borderline of α- ($CuInSe_2$) phase existence range of Cu_2Se-In_2Se_3 phase diagram [4]. Therefore, in order to obtain more In-rich compositions of MGP-s, we studied the growth of MGP-s in different flux materials containing alkali metal compounds.

The structural, morphological, electrical and optical properties of CIS materials depend highly on the composition and the method of preparation. Cu-rich CIS are usually p-type materials. As the material becomes indium rich a conversion to n-type conductivity often occurs. Noufi *et al.* have shown that the conductivity type depends not only on the Cu/In concentration ratio but also on the Se content of the material [5].

The Cu concentration of absorbers in highly efficient solar cells varies typically between 22 to 24 %. At growth temperatures this composition lies within the single-phase region of α-phase. However, by cooling to the room temperature, this composition enters the two-phase $\alpha+\beta$ region

of equilibrium phase diagram. Fortunately, there are some results, where Na incorporation allows to widen the range of the α-($CuInSe_2$) phase in the phase diagram [6].

In order to grow $CuInSe_2$ MGP-s with different compositions we prepared Cu-In alloys with different Cu/In concentration ratios (0.5- 1.1) as precursor materials. Our aim was to clarify the limits for the single-phase growth of $CuInSe_2$ in flux materials of different chemical nature and to study the possibilities to tailor CIS properties in growth conditions.

EXPERIMENTAL DETAILS

Crystals growth

$CuInSe_2$ monograin powder growth was proceeded from synthesised Cu-In alloys and elemental selenium. All used precursors had 5N purity. The syntheses of Cu-In alloys were made in carbon-coated quartz tubes under dynamic vacuum (continuous pumping) at temperature of 1070 K. Cu-In alloy ingots were ground in a mortar. Powdery alloys with different Cu/In ratios, Se and flux material for solution growth of $CuInSe_2$ were loaded into quartz ampoules. Different alkali halides were used as flux materials. As it is shown in Ref. [3], the formation of $CuInSe_2$ monograins takes place in the amount of liquid phase of flux that exceeds the limit for crystals sintering. The melting temperature of the used flux material limits the minimum growth temperature and the temperature of phase transition of CIS limits the maximum growth temperature. In the present study the samples in sealed evacuated quartz ampoules were annealed isothermally at 1000 K for 96 hours and then quenched to the room temperature. The flux material was removed by dissolution in deionisated water.

The X-ray diffraction (XRD) spectra of formed Cu-In alloys showed $Cu_{11}In_9$ and indium phases. According to Ref. [7, 8] the metallic precursors of Cu-In alloys (with the indium composition of 47,62 at. %-60 at.%) have been identified as the mixtures of $Cu_{11}In_9$ compound and indium with the solidus temperature of 153°C. The presence of metallic In in In-rich precursors corresponds also to the equilibrium phase diagram [9]. Above the melting point of In, the equilibrium phases are liquid indium with dissolved Cu and solid Cu-In alloy. It has been observed by several investigators that $Cu_{11}In_9$ is the most commonly observed phase for Cu–In alloys [10].

Characterization

The bulk composition of each powder was determined polarographically and by energy-dispersive X-ray analysis (EDS). The surface morphology and crystalline phases were examined by scanning electron microscopy (SEM) and XRD respectively. For the photoluminescence (PL) measurements the closed-cycle He cryostat (T = 9 - 300 K) and the He-Cd laser were used. The PL signal was detected using a standard lock-in technique, computer-controlled SPM-2 grating monochromator (f = 40 cm) and an InGaAs detector. The signal detected was corrected in conformity with the grating efficiency and detector sensitivity spectra. The grain resistances were determined by pressing the grain between two indium contacts. The ohmic behaviour of indium contacts with CIS has been proven by linearity of I-V measurements. The conductivity type was determined by hot-probe method.

RESULTS AND DISCUSSION

Composition of the grown crystals

The Cu/In concentration ratios of Cu-In alloys, deviation from molecularity ($\Delta m=[Cu]/[In]-1$), and deviation from stochiometry ($\Delta s=(2[Se]/([Cu]+3[In]) -1$), as calculated from the polarographic analysis data of grown powders and the conductivity type of developed powders are presented in Table I. The Cu/In concentration ratios of the grown powders (determined polarographically) versus the one of the Cu-In alloys are shown in Fig. 1. In the case of In-rich precursor alloys ([Cu]/[In]<1), Cu/In ratios in the grown powders correspond nearly (or slightly less indium-rich) to the Cu/In ratios of initial Cu-In alloys. Powder materials from the Cu-rich ([Cu]/[In] ≥1) initial compositions "have lost" some amount of copper after KCN etching. This indicates the entering of material into multiphase region of phase diagram. Additionally, we determined Cu, In, and Se concentrations in the flux material leaching solutions and found that relative Cu concentrations in leaching solutions were in the range of 25-26 % while the corresponding In concentrations were 21-23%. Consequently, in growth conditions some chemical reactions between the flux material and precursor components are going on that result in water-soluble compounds.

The EDS analysis of single powder grains showed that the materials with Cu/In ≥ 0.71 consisted of the crystals with uniform composition. At the same time, the powder with Cu/In=0.67 consisted of crystals with two different compositions: with Cu/In = 0.92 and with Cu/In=0.66. This indicates that the growth process result in multiphase solid material.

Table I. [Cu]/[In] in Cu-In alloy, powder analysis data, Δm and Δs (calculated from polarographic analysis data) and conductivity type of $CuInSe_2$ monograin powders.

[Cu]/[In] in Cu-In alloy	Cu, at%	In, at%	Se, at%	Δm	Δs	Conductivity type
1.1	25.8	24.9	49.4	0.04	-0.02	p
1	24.1	25.6	50.4	-0.06	0.00	p
0.92	23.7	25.6	50.7	-0.07	0.01	p
0.83	22.7	26.2	51.0	-0.13	0.01	p
0.71	20.6	27.1	52.3	-0.24	0.03	p
0.66	19.1	29.0	51.9	-0.34	-0.02	p , n
0.59	18.0	30.3	51.6	-0.40	-0.05	n
0.5	15.7	33.1	51.2	-0.52	-0.11	n

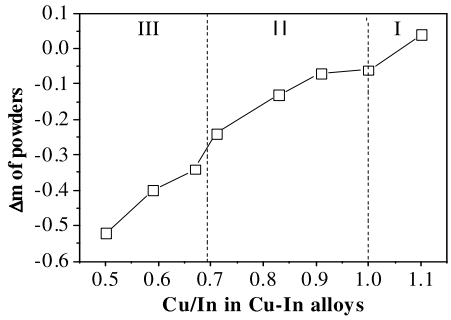

Figure 1. The Cu/In ratio versus molecularity Δm**.**

The selenium concentration of the synthesized powders, determined polarographically and by EDS, as the function of the molecularity Δm is presented in Fig.2. Selenium content in the powders increases with decreasing molecularity and changes from 49% up to about 54%.

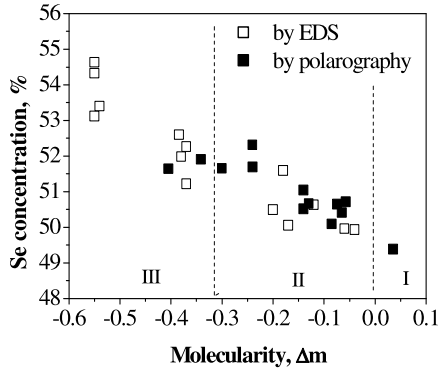

Figure 2. Selenium content in powder as function of molecularity Δm.

Figure 1. and figure 2. show that there are three regions of Cu/In ratios. Each region is characterized by different crystal growth equilibrium and with the different composition of powders. The approximate borders of those regions are marked with dashed lines in Fig. 1 and Fig. 2. The border of II/III region coincides with the changes of the type of conductivity. According to the polarographic analysis, the bulk composition of powder crystals in the III region indicates that we have a two-phase material containing probably $CuInSe_2$ and In_2Se_3. Single-phase $CuInSe_2$ monograin powders can be produced in the II region ($0.67<Cu/In<1$). XRD measurements indicate that in the I region ($Cu/In>1$) also CuSe phase can be detected.

PL study of $CuInSe_2$ powders

Fig. 3 shows the PL spectra of CIS powders with different indium content. The change of In content in CIS influences the shape of PL curve and the positions of peaks in spectra. A broad asymmetric band characterizes the typical PL spectrum of In-rich CIS with the maximum around 0.93 eV. The PL In-rich samples (Cu/In<0.83) exhibit two broad bands with peak positions at ~0.86 and 0.93eV. The broad band at ~ 0.86 eV is probably related to the recombination through deep intrinsic defect levels (~245 meV) that are caused by indium interstitials (In_i) or In_{Cu} [12, 13]. The relative intensity of the latter band increases with the increasing indium content, which seems to be a prerequisite for the creation of corresponding defects. The wide PL peak at about 0.99 eV dominates the PL spectra of Cu-rich powders.

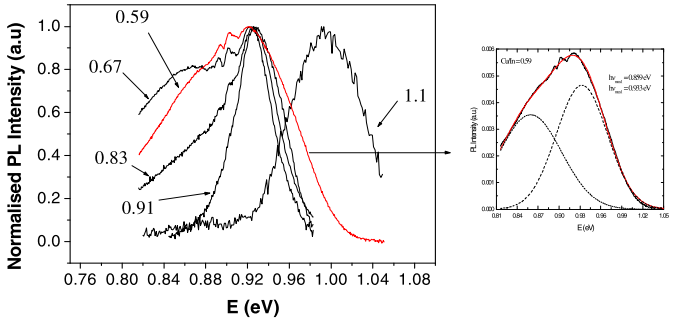

Figure 3. PL spectra of Cu-rich, near stoichiometric and In-rich $CuInSe_2$ at 9K. The Cu/In ratio of precursor Cu-In alloys is shown numerically

Electrical resistance and conductivity type

Fig. 4 shows the electrical resistance of $CuInSe_2$ grains as the function of Cu/In molar ratio of precursor Cu-In alloys. All measured grains were in sizes within 112-150 μm. The measurement data of grains with compositions corresponding to n-type region are represented by solid squares, while p-type ones are shown as open squares. As the Cu/In ratio increases from 0.5 to 1.1, the grain resistance decreases from 2×10^7 to 8×10^2 Ω. Accordingly, the resistance of the materials increases with In content. This is typical for semiconductor materials with high doping levels – the mobility of charge carriers decreases. The change of conductivity type occurs in the region of the Cu/In ratio values of 0.67-0.71. Within this region, the materials consist of crystals with both different types of conductivity. In that region materials selenium content is rather high (about 52 %) and according to EDS analysis, materials consist of crystals with different compositions: with Cu/In=0.92 and Cu/In=0.66. Based on these results the crystal growth takes place in multiphase conditions.

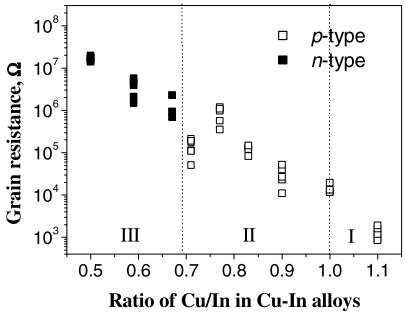

Figure 4. Grain resistance in dependence of Cu/In ratio in material. Sizes of measured grains were within 112-150 μm.

CONCLUSIONS

We determined the preparation conditions for $CuInSe_2$ monograin powder growth in the molten fluxes of different chemical nature. We found that flux material allows the growth of In-rich $CuInSe_2$ monograin powders. The single-phase powder crystals can be synthesized from precursor Cu-In alloys with Cu/In ratio values between 1> Cu/In>0.7. The powders from initial Cu-In alloy with Cu/In<0.67 were found to consist of crystals with different compositions: Cu/In=0.92 and Cu/In=0.66. Accordingly, we had multiphase growth conditions. Selenium content in the grown powders increases almost linearly with the decreasing Cu/In ratio of the materials.

The samples with nearly stoichiometric or slightly In-rich compositions showed p-type conductivity and exhibited PL spectrum with dominant peak at 0.93 eV. In contrast, the samples with Cu/In<0.7 had n-type conductivity and exhibited two broad bands in PL curve with the peak positions at 0.86eV and 0.93eV.

ACKNOWLEDGEMENTS

Financial support of European Union by Energy Program and of Estonian Science Foundation under contracts No. 5139, 5149, 6179 and 5914 is gratefully acknowledged.

REFERENCES

1. M.Altosaar, A.Jagomägi, M.Kauk, M.Krunks, J.Krustok, E.Mellikov, J. Raudoja, T.Varema, *Thin Solid Films* **431-432**, 466 (2003).

2. M. Altosaar, M. Danilson, M. Kauk, J. Krustok, E. Mellikov, J. Raudoja, K. Timmo, T. Varema, *Solar Energy Materials & Solar Cells,* In Press, Corrected Proof, Dec. (2004)
3. M.Altosaar, E.Mellikov, *Jpn. J. Appl. Phys.,* **39**, 65 (2000)
4. T. Gödecke, T. Haalboom, F. Ernst, *Z. Metallkd.* **91,** 622 (2000)
5. R. Noufi, R. Axton *Appl. Phys. Lett.* **45,** 668 (1984)
6. R. Herberholz, U. Rau, H. W. Schock, T. Haalboom, T. Gödecke, F. Ernst, C. Beilharz, K. W. Benz, D. Cahen, *Eur. Phys. J. AP* **6**, 131 (1999)
7. Z. A. Shukri, C. H. Champness, *Journal of Crystal Growth,* **191**, 97 (1998)
8. Yi-Chia Chen, Chin C. Lee, *Thin Solid Films* **283**, 243 (1996)
9. M. Elding- Ponten, L. Stenberg, S. Lidin, *J. Alloys & Comp.* **261**, 162 (1997)
10. N. Orbey, G. A. Jones, R. W. Birkmire and T. W. Fraser Russell , Copper Indium alloy transformations, *Journal of Phase Equilibria*, **21**, 509, (2000)
11. A.V. Mudryi, V.F. Gremenok, I.A. Victorov, V.B. Zalesski, F.V. Kurdesov, V.I. Kovalevski, M.V. Yakushev, R.W. Martin, *Thin Solid Films* **431 –432**, 193 (2003)
12. M.V. Yakushev, A.V. Mudryi , V.F. Gremenok , E.P. Zaretskaya , V.B. Zalesski, Y.Feofanov, R.W. Martin, *Thin Solid Films* **451 –452**, 133 (2004)

PAPER III

K. Timmo, M. Altosaar, J. Raudoja, E. Mellikov, T. Varema, M. Danilson, M. Grossberg, The effect of sodium doping to $CuInSe_2$ monograin powder properties. *Thin Solid Films*, Vol. 515(2007) 5887-5890.

Available online at www.sciencedirect.com
ScienceDirect
Thin Solid Films 515 (2007) 5887–5890
thin solid films
www.elsevier.com/locate/tsf

The effect of sodium doping to $CuInSe_2$ monograin powder properties

K. Timmo *, M. Altosaar, J. Raudoja, E. Mellikov, T. Varema, M. Danilson, M. Grossberg

Department of Materials Science, Tallinn University of Technology, Ehitajate tee 5, 19086 Tallinn, Estonia

Available online 19 January 2007

Abstract

The effect of sodium doping to the electrical and photoluminescence properties of $CuInSe_2$ monograin powders was studied. Sodium was added in controlled amounts from 5×10^{16} cm^{-3} to 1×10^{20} cm^{-3}. The photoluminescence spectra of Na-doped stoichiometric $CuInSe_2$ powders had two bands with peak positions at 0.97 and 0.99 eV. The photoluminescence bands showed the shift of peak positions depending on the Na doping level. Peak positions with maximum energy were observed if added sodium concentration was 1×10^{19} cm^{-3}. This material had the highest carrier concentration 2×10^{17} cm^{-3}. In the case of stoichiometric $CuInSe_2$ (Cu:In:Se=25.7:25.3:49.0), Na doping at concentrations of 3×10^{17} cm^{-3} and higher avoided the precipitation of Cu–Se phase. Solar cells output parameters were dependent on the Na doping level. Sodium concentration 3×10^{18} cm^{-3} resulted in the best open-circuit voltage.

Keywords: $CuInSe_2$; Sodium; Photoluminescence; Solar cells

1. Introduction

Monograin layers are perspective for the development of low priced solar cells. Monograin powders of $CuInSe_2$ have been applied as absorber material in monograin layer solar cells [1]. The isothermal growth of $CuInSe_2$ monograin powders in the presence of liquid phase of a suitable solvent material (flux) leads to the formation of semiconductor materials with single-crystalline grain structure and narrow-disperse granularity, so called monograin powders [2]. In this process the chemical nature of the liquid (molten) phase of used solute material impacts certain properties of the obtained absorber material.

In the case of vacuum deposited $Cu(In,Ga)Se_2$ thin film solar cells, the presence of Na in the absorber correlates with numerous changes in material and device quality. The observed changes include improvements in the open-circuit voltage [3,4], preferential grain orientation [4], increased grain size and carrier concentration [5,6].Using the photoluminescence (PL) measurements, Kimura et al. [7] found that by Na incorporation the compensation of $CuInSe_2$ was reduced due to the suppression of donor-type defects.

In this paper we focus on the effects of Na doping on the electrical and photoluminescence properties of $CuInSe_2$ monograin powders with stoichiometric composition. In order to clarify the influence of sodium doping on the parameters of $CuInSe_2$ monograin layer devices, the synthesized materials doped with Na were used as absorber materials in solar cells.

2. Experimental

$CuInSe_2$ monograin powders used in the present study was synthesized from Cu–In alloy and elemental Se in the liquid phase of CuSe as the flux material in evacuated quartz ampoules. The growth processes of $CuInSe_2$ in CuSe is described in [2]. For doping with Na the synthesized material was heat-treated in the presence of InI as a flux at 800 K for 48 h in addition of sodium as NaI. Solution of NaI in deionizated water was dosed in controlled amounts in the range of 5×10^{16}–1×10^{20} cm^{-3}. By sequential diluting we kept the amount of doping solution constant. The doped materials were dryed and vacuum-sealed into quartz ampoules. After annealing, the ampoules were cooled to room temperature in water. The flux was removed by 3.7% aqueous solution of HCl.

The surface morphology and composition of single powder crystals were analyzed by the scanning electron microscopy (SEM) and the energy dispersive X-ray spectroscopy. Materials were characterised by electrical measurements.

For the photoluminescence measurements, the excitation source was a He–Cd laser with the wavelength of 441 nm. The

* Corresponding author.
E-mail address: timmokas@yahoo.com (K. Timmo).

0040-6090/$ - see front matter © 2007 Elsevier B.V. All rights reserved.
doi:10.1016/j.tsf.2006.12.087

powder crystals were mounted inside a closed cycle He cryostat (T=9–300 K). The PL spectra was recorded with a computer-controlled SPM-2 grating monochromator (f=0.4 m). The signal was detected with InGaAs detector using the conventional lock-in technique.

All the as-grown absorber materials were annealed in sulphur vapour at 800 K for 18 h before solar cell production. More processing details could be found in [8]. For monograin layer formation the monolayer of unisize $CuInSe_2$ powder crystals covered with chemically deposited CdS was sedimentated into thin layer of epoxy resin without the contamination of the upper surfaces of crystals. After polymerization of epoxy, i-ZnO and conductive ZnO:Al were deposited by RF-sputtering. The solar cell structure was completed by the evaporation of 1–2 μm thick In grid contacts onto the ZnO window layer. After glueing the structures on glass substrates, the back contact area of crystals covered by epoxy was opened by etching with H_2SO_4 and by additional abrasive treatment. Graphite paste was used as back contact. Monograin layer solar cells on the basis of Na-doped $CuInSe_2$ monograin powders were characterised with current–voltage and capacitance–voltage measurements.

3. Results and discussion

3.1. Photoluminescence study of $CuInSe_2$ powders

The photoluminescence spectra of all monograin materials show a broad band with its maximum around 0.99 eV (Fig. 1). This band consists of two subbands with peak positions at 0.97 and 0.99 eV. The peak position of the PL band at 0.99 eV depends on the dosed sodium doping level as it is seen in Fig. 2. The peak position shifts to higher energy values with increasing sodium concentration up to 1×10^{19} cm^{-3}. With futher increase in sodium doping level the sharp decrease of the PL peak energy values was observed.

It was found in [3] that Na does not create any shallow acceptor level in $CuInSe_2$, but it can form a solid solution with $CuInSe_2$ in the form of $Na_xCu_{1-x}InSe_2$ with higher bandgap energy than the base material. For $CuGaSe_2$ in [9], there was proposed the formation of a quaternary Na–Cu–Ga–Se compound on the base of defect-chalcopyrite structure in which Cu vacancies are partially filled by Na atoms. To explain the obtained results we propose, analogically to the above

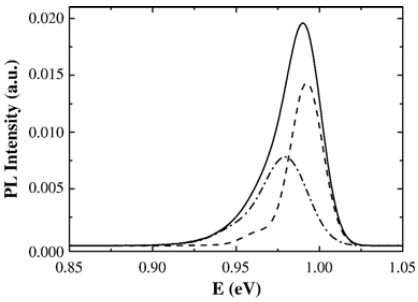

Fig. 1. The PL spectrum of Na-doped $CuInSe_2$ monograin powder. Dosed [Na]=3×10^{18} cm^{-3}.

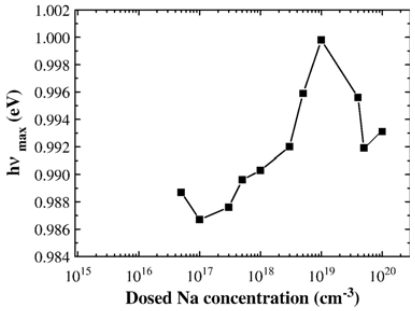

Fig. 2. The peak position of the PL band in dependence on the dosed sodium doping.

mentioned studies, the formation of a solid solution of $CuInSe_2$ with Na with slightly higher bandgap energy on the surface of our crystals. SEM photo indicates to the segregation of an unknown phase in our sodium doped samples (Fig. 3).

The bandgap energy of a quaternary $Na_xCu_{1-x}InSe_2$ solid solution increases with increasing sodium doping level. At doping concentrations higher than 10^{19} cm^{-3}, the PL peak position sharply shifts to lower values of energies. The bandgap energy of ternary compounds is sensitive to the high concentration of defects [10]. The potential fluctuations due to randomly distributed defects cause the widening of the defect levels and the local perturbation of electron potential. Thus, the peak position of the PL band shifts towards lower energies at higher defect concentrations. The increase in the half-width of the PL bands with Na concentration also indicates to the increase of defect density.

3.2. Solar cell parameters

The solar cells with undoped and doped with sodium up to 1×10^{17} cm^{-3} absorber materials had low value of shunt resistance (Fig. 4). These materials were etched with 10% KCN aqueous solution. After KCN etching we were able to measure the solar cell parameters. The solution is known as selective etchant for Cu–Se binary phases [11]. Therefore we suppose that the segregation of the Cu–Se phase occurs in powders with added Na concentration less than 3×10^{17} cm^{-3}.

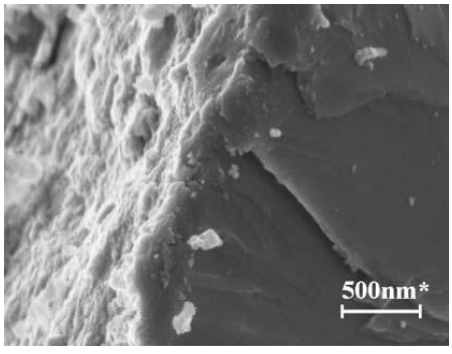

Fig. 3. SEM image of a broken $CuInSe_2$ crystal with sodium content 10^{19} cm^{-3}.

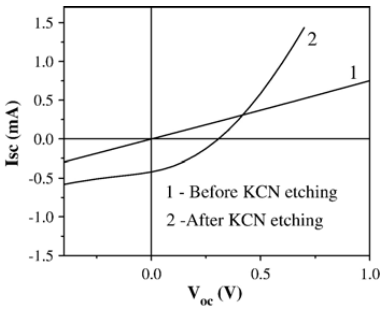

Fig. 4. *I–V* curves of $CuInSe_2$ solar cells without sodium and low sodium concentrations before and after KCN etching.

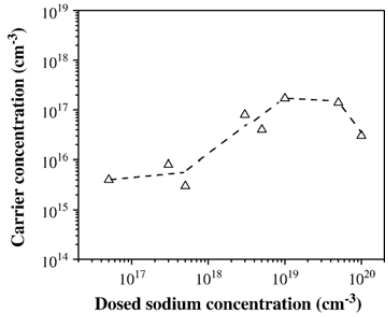

Fig. 6. The carrier concentration in dependence of the dosed sodium doping level.

It is known that sodium incorporation widens the range of the α-($CuInSe_2$) phase existance in the phase diagram [12]. In our case, the increase of sodium content in $CuInSe_2$ widens the single phase area of $CuInSe_2$ towards Cu-rich compositions starting from the doping level of 3×10^{17} cm^{-3}. In materials without Na or with low Na concentration levels up to 1×10^{17} cm^{-3}, the Cu–Se phase segregation is possible.

The values of the open-circuit voltage of solar cells (Fig. 5) increase with increasing dosed sodium concentration from 5×10^{16} cm^{-3} to 3×10^{18} cm^{-3}. At higher than 3×10^{18} cm^{-3} values of Na concentrations the open-circuit voltage decrease and stay constant. Sodium concentration 3×10^{18} cm^{-3} was found to result in the best open-circuit voltage.

At low concentrations, at first Na eliminates the In_{Cu} defects that act as traps for the majority carriers. Thus, the effective hole density increases [3,7]. However, as the Na concentration increases to the level where the most of the In_{Cu} defects have been eliminated, it starts to remove the acceptor V_{Cu}. This process reduces the hole density [3]. That may cause a reduction in the cell performances at Na contents higher than 3×10^{18} cm^{-3}.

3.3. Carrier concentration

Carrier concentration was determined by room-temperature capacitance–voltage measurements (Fig. 6). We found that the maximum carrier concentration 2×10^{17} cm^{-3} was in materials with doped sodium content of 1×10^{19} cm^{-3}. Further increase in sodium content resulted in decreased carrier concentration. As seen in Fig. 5, the same tendency can be observed in the values of open-circuit voltage.

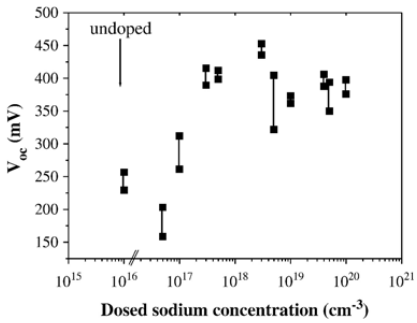

Fig. 5. The open-circuit voltage of solar cells in dependence of the dosed sodium doping.

4. Conclusions

The PL spectra of Na-doped CIS powders showed that the peak position of the PL band shifted depending on the Na doping level. The peak position of the PL band with maximum energy was observed when sodium concentration was 1×10^{19} cm^{-3}. The material with the same sodium concentration had the highest carrier concentration 2×10^{17} cm^{-3}. It has been found that in the case of stoichiometric $CuInSe_2$ (Cu:In:Se=25.7:25.3:49.0) Na doping avoided the precipitation of Cu–Se phase at dosed Na concentration 3×10^{17} cm^{-3} and higher. The obtained results were explained by formation of a solid solution of $CuInSe_2$ with Na containing compound with slightly higher bandgap energy on the surface of crystals. Solar cells output parameters were dependent on the Na doping level of the absorber material. Sodium concentration 3×10^{18} cm^{-3} was found to result in the best open-circuit voltage.

Acknowledgements

Financial support of the European Union by Energy program and Estonian Science Foundation under contracts No. 6160 and 6179 is gratefully acknowledged. The authors would also like to thank Mrs. O. Volobujeva for her help with the SEM studies.

References

[1] M. Altosaar, A. Jagomägi, M. Kauk, M. Krunks, J. Krustok, E. Mellikov, J. Raudoja, T. Varema, Thin Solid Films 431–432 (2003) 466.
[2] M. Altosaar, E. Mellikov, Jpn. J. Appl. Phys. 39 (2000) 65.
[3] Su-Huai Wei, S.B. Zhang, A. Zunger, J. Appl. Phys. (1999) 85.
[4] D. Braunger, D. Hariskos, G. Bilger, U. Rau, H.W. Schock, Thin Solid Films 361–362 (2000) 161.
[5] M.A. Contreras, B. Egaas, P. Dippo, J. Webb, J. Granata, K. Ramanathan, S. Asher, A. Swartzlander, R. Noufi, 26th IEEE Photovoltaic Specialists Conference, 1997, p. 359.

[6] B.M. Keyes, F. Hasoon, P. Dippo, A. Balcioglu, F. Abulfotuh, 26th IEEE Photovoltaic Specialists Conference, 1997, p. 479.
[7] R. Kimura, T. Nakada, P. Fons, A. Yamada, S. Niki, T. Matsuzawa, K. Takahashi, A. Kunioka, Sol. Energy Mater. Sol. Cells 67 (2001) 289.
[8] M. Kauk, M. Altosaar, J. Raudoja, K. Timmo, M. Grossberg, T. Varema, K. Ernits, Proc. SPIE, Optical Materials and Applications, vol. 5946, 2005, p. 224.
[9] V. Nadenau, G. Lippold, U. Rau, H.W. Schock, J. Cryst. Growth 233 (2001) 13.
[10] A.P. Levanyuk, V.V. Osipov, Sov. Phys., Usp. 24 (1981) 187.
[11] R. Scheer, T. Walter, H.W. Schock, M.L. Fearheiley, H.J. Lewerenz, Appl. Phys. Lett. 63 (1993) 3294.
[12] R. Herberholz, U. Rau, H.W. Schock, T. Gödecke, F. Ernst, C. Beilharz, K.W. Benz, D. Cahen, Eur. Phys. J. AP 6 (1999) 131.

PAPER IV

K.Timmo, M. Altosaar, J. Raudoja, M. Grossberg, M. Danilson, O.Volobujeva, E.Mellikov, Chemical etching of $Cu_2ZnSn(S,Se)_4$ monograin powder, 35th IEEE Photovoltaic Specialists Conference, Honolulu, Hawaii, June 20-25, 2010: Conference Proceedings 1982 - 1985.

CHEMICAL ETCHING OF $Cu_2ZnSn(S,Se)_4$ MONOGRAIN POWDER

K.Timmo, M.Altosaar, J.Raudoja, M.Grossberg, M.Danilson, O.Volobujeva, E.Mellikov
Department of Materials Science, Tallinn University of Technology, Tallinn, Estonia

ABSTRACT

$Cu_2ZnSn(S,Se)_4$ (CZTS,Se) monograin powders were synthesized in the liquid phase of molten KI as flux material from binary compounds in evacuated quartz ampoules. Monograin powders were subjected to various chemical treatments with several etchants (HCl, KCN, NH_4OH and Br in methanol (Br_2-MeOH)) to modify the crystal surface. Polarographic analyses of leaching solutions showed that Sn and Se were removed preferably by HCl etching. Treatment with 10% KCN dissolved mainly Cu, Sn and chalcogen, and ammonia solution removed selectively Cu and chalcogen in an approximate ratio of 1:2. From XPS measurements we found that after etching with 1% Br_2-MeOH the material surfaces were Sn-rich. The prepared monograin powders were used as absorber materials in monograin layer solar cells: ZnO/CdS/CZT(S,Se)/graphite. A combination of chemical treatments before the deposition of CdS led to the best parameters of $Cu_2ZnSn(S,Se)_4$ monograin layer solar cells. The here achieved efficiencies of solar cells were above 4%.

INTRODUCTION

The quaternary compounds Cu_2ZnSnS_4 and $Cu_2ZnSnSe_4$ are new interesting semiconductor materials as absorber layer in solar cells. The most of their elemental components are abundant in the earth's crust and they have semiconductor properties such as *p*-type conductivity, direct band gaps and high absorption coefficients ($>10^4$ cm^{-1}) [1]. Typical methods for thin film production, such as sputtering and PVD in the case of $Cu_2ZnSnSe(S)_4$ materials, lead to inhomogeneous and multiphase composition of the layer films [2, 3]. Monograin growth in molten fluxes results in a homogeneous composition of the CZTSe powder material [4]. In the process of the monograin growth the formation of monograins of a semiconductor compound takes place in the liquid phase of the used flux material. The criteria for the monograin growth is the following: the volume of the molten phase V_L between grains has to exceed the limit of sintering - $V_L \geq 0.6\ V_S$, where V_S is the volume of solid phase. In this case the liquid phase separates the initial solid particles from each other and the individual single crystals grow [5]. Due to the solubility, the precursors and the formed CZT(S,Se) may partially dissolve in the molten flux salt at the used recrystallization temperature and some part of it can re-precipitate on the surface of the formed crystals during the cooling period. These precipitations change the surface morphology and the composition of the absorber crystal surface. On the other hand, it is well known that the active interface of *p*-type absorber and *n*-type buffer layer plays a key role for the solar cell performace. Therefore, an in depth understanding of the chemical treatment of CZT(S,Se) monograin powder crystals' surfaces with different etchants is very important for tailoring the absorber crystal's surface composition and finaly the parameters of solar cells on their base.

In this paper we present some results of our studies on chemical etching of CZT(S,Se) monograin powders.

EXPERIMENTAL

$Cu_2ZnSn(S,Se)_4$ monograin powders were synthesized from Cu(S,Se), Zn(S,Se) and Sn(S,Se) precursors in molten KI. The ground precursors were sealed in evacuated quartz ampoules and annealed at 1000 K. The growth process was stopped by quenching the ampoules in water. The flux material was removed by leaching with deionizated water. These leaching solutions contained also some amorphous phase. The amorphous precipitates were separated, dried and analyzed polarographically and by energy dispersive x-ray analysis (EDX). The grown monograin powders were divided into several parts and each of them passed through different etching procedures. As etchants we used concentrated HCl, 10% aqueous solution of KCN, 1% Br_2-MeOH (bromine in methanol) solution and 2M NH_4OH solution. All the chemical etchings were performed at room temperature. The composition of the leaching solutions was analyzed polarographically. The surface morphology of the powder crystals before and after etching were studied by high resolution scanning electron microscope (SEM) equipped with an In-Lens SE detector for topographic imaging and energy and angle selective backscattered electron detector (EsB) for compositional contrast. The bulk and surface chemical composition of the monograins was analyzed using EDX. The phase composition was studied by room temperature (RT) micro-Raman spectroscopy. The changes in surface composition of materials was determined using X-ray photoelectron spectroscopy (XPS). The photovoltaic properties of graphite/$Cu_2ZnSn(S,Se)_4$/CdS/ ZnO solar cell structures were characterised by currant-voltage (*I-V*) measurements under 100mW/cm^2 illumination.

RESULTS

$Cu_2ZnSn(S,Se)_4$ monograin powder crystals had tetragonal shape with rounded grain edges (see Fig. 1).

978-1-4244-5892-9/10/$26.00 ©2010 IEEE

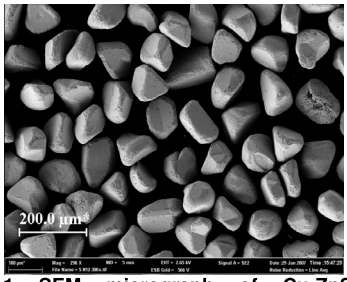

Figure 1 SEM micrograph of $Cu_2ZnSn(S,Se)_4$ monograin powder.

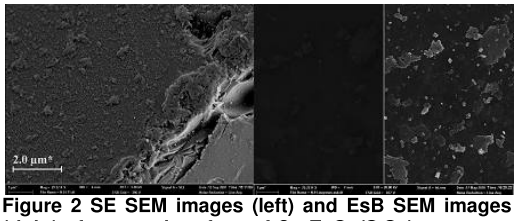

Figure 2 SE SEM images (left) and EsB SEM images (right) of a crystal surface of $Cu_2ZnSn(S,Se)_4$ as-grown monograin powder.

SE and EsB SEM images exposed the inhomogeneity of crystals` surface of as-grown $Cu_2ZnSn(S,Se)_4$ monograin powders (see Fig. 2). The comparison of the crystals' surface composition with the bulk by using EDX revealed that the surface of as-grown CZT(S,Se) crystals is Sn-rich while the bulk of crystals is Zn-rich (see Table 1).

Material	Cu/Zn+Sn	Zn/Sn	Se+S/Met
Crystals` surface	0.94	0.86	1.01
Crystals bulk	0.88	1.03	1.03

Table 1 Compositions of chemically untreated CZT(S,Se) crystals' surfaces and their bulk (polished cross-section of powder crystals) as determined by EDX.

The difference in the surface and the bulk compositions can be taken as a hint of material precipitation from components dissolved in the flux at the growth-temperature onto the surface of the grown crystals during cooling.

After the removal of the flux by deionizated water the remaining solid phase consists of well formed crystallites of CZT(S,Se) and an amorphous material that was originally dissolved in KI at the recrystallization temperature and then precipitated during cooling. The composition of the amorphous deposit was analysed by EDX as Cu : Zn : Sn : S+Se = 24.74 : 3.02 : 19.83 : 52.62. This elemental composition indicates the existence of surface compounds like $Cu_2Sn(S,Se)_3$ and $Sn(S,Se)_2$.

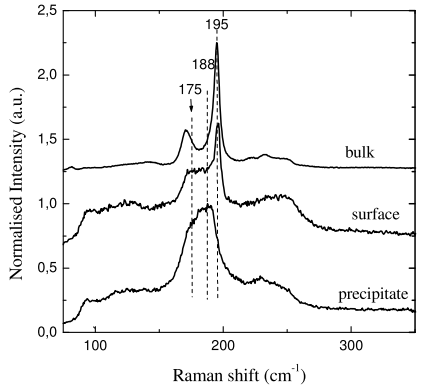

Figure 3 Raman spectra of a $Cu_2ZnSnSe_4$ crystal's bulk (polished cross-sections of crystals), the crystal's surface and the solid precipitate.

Figure 3 shows normalised RT Raman spectra of the surface and the bulk of $Cu_2ZnSnSe_4$ monograins, together with a normalised Raman spectrum of precipitated material. The polished $Cu_2ZnSnSe_4$ monograins were used to determine Raman spectra of the bulk material. Two dominating modes of $Cu_2ZnSnSe_4$ [6] can be found at 195 and 171 cm^{-1} in the Raman spectra of the bulk of crystals. These modes can also be found in the spectra of the monograin surface. However, there are some additional modes around 188 cm^{-1} and 175 cm^{-1} in the Raman spectra of the crystal's surface, indicating the presence of other phases on the crystals' surface. These additional peaks are also present in the Raman spectra of the precipitate, which confirms our assumption that a part of the material dissolved in the molten phase could precipitate onto the crystals' surface in the cooling process. The Sn-rich chemical composition of the crystals' surface and a Raman peak around 188 cm^{-1} give us the base to suppose that $SnSe_2$ (A_1 mode at 186 cm^{-1} [7]) is a main component of the precipitate.

In order to remove other phases from the CZT(S,Se) monograins' surfaces and to improve the active interface of the *p*-type $Cu_2ZnSn(S,Se)_4$ solar cell performance, chemical treatments with several etchants (HCl, KCN, Br_2-MeOH and NH_4OH) were performed.

From SEM micrographs of the CZT(S,Se) surface after treatment with different etchants (see Fig. 4) we found that the $Cu_2ZnSn(S,Se)_4$ crystal surfaces are rough and covered with microparticles after etching with HCl. We were unable to determine the elemental composition of these microparticles by EDX due to their very small size. Etching with NH_4OH results in relatively flat surfaces with some structure. The surfaces of KCN-etched crystals seem to be quite smooth without any precipitates. After

etching with Br_2-MeOH the surfaces of CZT(S,Se) monograins were covered by crater-like areas with microparticles on their edges. Additional etching of the Br_2-MeOH treated powders with KCN removes these precipitates and leads to clean crystal surfaces.

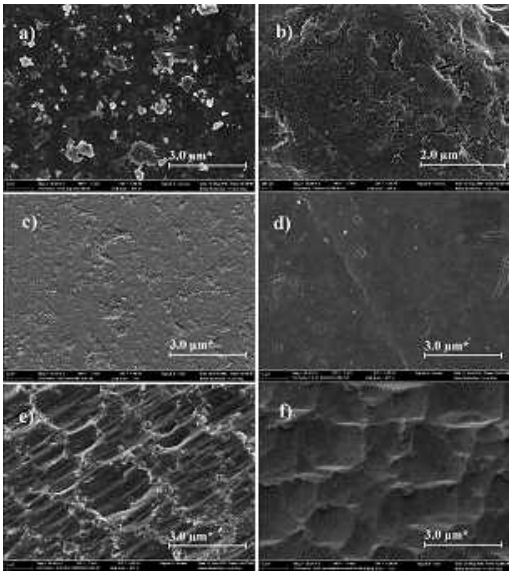

Figure 4 SEM micrographs of as-grown $Cu_2ZnSnSe_4$ monograin powder surfaces (a)and after treatment with b) HCl, c) NH_4OH, d) KCN, e) Br_2-MeOH, and f) Br_2-MeOH+KCN etchants.

A polarographic analysis (see Table 2) of the leaching solutions indicates that Sn and chalcogen are removed preferably by HCl-etching probably due to complexation of tin as $[SnCl_4]^{2-}$. The KCN etching is known as a process to preferably remove Cu-Se binary phases [8]. In our experiments with KCN treatment we also found Sn in the leaching solutions of the $Cu_2ZnSn(S,Se)_4$ monograin materials. Ammonia solution removes selectively Cu and chalcogen in an approximate ratio 1:2.

Etchant	Cu	Zn	Sn	Se
KCN	1.0	no	0.36	1.5
HCl	1.0	0.11	5.8	6.5
NH_4OH	1.0	0.17	no	2.2
Br_2-MeOH	1.0	0.83	0.66	0.33

Table 2 Composition of elements in leaching solution as determined polarographically.

Figure 5 shows XPS spectra of the as-grown and Br_2-MeOH-etched $Cu_2ZnSn(S,Se)_4$ monograins surfaces. We can see that Br_2-MeOH-etching decreases the intensity of Cu2p, CuLMM peaks and increases the intensity of the Sn and O1s peaks. Zn2p and ZnLMM peaks are almost undetectable after etching with Br_2-MeOH. Changes in the monograin surface composition after Br_2-MeOH-etching can be understood using the Zn 2p, Cu 2p, Sn 3d, O1s, S 2p and the Se 3d core levels. The relative atomic concentrations of zinc, copper, tin and selenium were determined from integrated peak areas of high-resolution XPS core level spectra. The S 2p peak area was determined by core level curve-fitting procedures since they overlap with the Se 3p core level. The composition of the $Cu_2ZnSn(S,Se)_4$ monograin surface after Br_2-MeOH was analysed by XPS as Cu: Zn : Sn : S+Se : O = 1.23 : 1.16 : 37.05 : 12.83 : 47.72 at.%. Comparison of the XPS spectra of as-grown and Br_2-MeOH-etched samples allows to conclude that Br_2-MeOH-etching mainly removes Cu and Zn as was found also from the polarographic analysis of the leaching solutions.

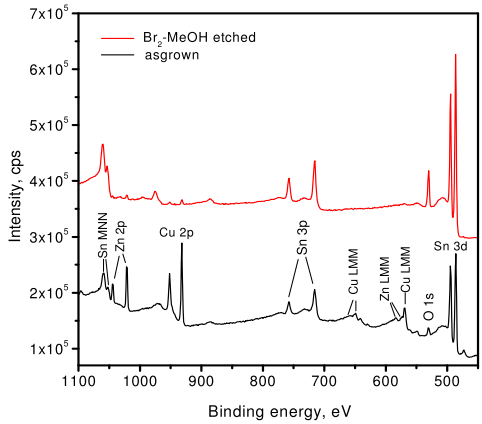

Figure 5 XPS spectra of the as-grown and Br_2-MeOH etched $Cu_2ZnSn(S,Se)_4$ monograin surfaces.

Some results of I-V measurements of solar cells made from chemically treated $Cu_2ZnSn(S,Se)_4$ monograin powders are given in Table 3.

Etchant used	V_{oc}, mV	I_{sc}, mA/cm^2	FF,%
None	300	10	40
Conc. HCl	342	11.5	48
2M NH_4OH	422	10.5	44
10% KCN	490	13.5	49
1% Br_2-MeOH	563	8.5	54
1% Br_2-MeOH +10% KCN	575	13.75	55

Table 3 Performance characteristics of $Cu_2ZnSn(S,Se)_4$ monograin layer solar cells made from etched absorber crystals.

It can be seen that the parameters of monograin layer solar cells improves by etching the powder crystals. Cells made from materials treated in combined etching procedures showed the highest values of V_{oc}, I_{sc} and fill

factor. The here achieved efficiencies of the best solar cells were in the order of 4 %. Higher efficiencies were obtained after further optimized surface treatments.

CONCLUSIONS

We found that the surface and the bulk compositions of as-grown CZT(S,Se) monograin powder crystals were not identical. The analysis of leaching solutions showed that Sn and chalcogen are removed preferably by HCl etching. Leaching solutions after KCN-etching contain Cu, Sn and chalcogen. Aqueous ammonia solutions do not remove Sn from CZT(S,Se) surface. The Raman spectra of the surface after etching with HCl and KCN are similar to the spectrum of the bulk material. From XPS measurements we found that etching with 1% Br_2-MeOH results in Sn-rich material surfaces. The combination of chemical treatments before the deposition of CdS gave the best $Cu_2ZnSn(S,Se)_4$ monograin layer solar cells with efficiencies in the order of 4 %.

ACKNOWLEDGEMENTS

Financial support of Estonian Ministry of Education and Research by Contract No. T099, Estonian Scientific Foundation under Contract No. 7678 and Enterprise Estonia is gratefully acknowledged. This work has been partially supported by graduate school „Functional materials and processes“ recieving funding from the European Social Fund under project 1.2.0401.09-0079 in Estonia." The authors would like to thank also Mrs. Karin Kerm for her help with polarographic studies.

REFERENCES

[1] K. Ito, T. Nakazawa, “Electrical and optical properties of stannite-type quaternary semiconductor thin films”, *Jpn. J. Appl. Phys*. **27**, 1988, pp. 2094-2097.

[2] T.M. Friedlmeier et al., “Growth and Characterization of Cu_2ZnSnS_4 and $Cu_2ZnSnSe_4$ Thin Films for Photovoltaic Application”, *Inst. Phys. Conference Ser. No*. **152***: Proceedings of the 11th ICTMC*, *Salford*, 1997, pp. 345.

[3] T. Tanaka et al., “Preparation of Cu_2ZnSnS_4 thin films by hybrid sputtering”, *Journal of Physics and Chemistry of Solids*. **66**, 2005, pp. 1978–1981.

[4] M. Altosaar, J. Raudoja, K. Timmo, M. Danilson, M. Grossberg, M. Krunks, T. Varema, E. Mellikov, “$Cu_2ZnSnSe_4$ Monograin Powders for Solar Cell Application”, *Proceedings of the 2006 IEEE WCPEC-4*, 2006, pp. 468-470.

[5] E. Mellikov, J. Hiie, M. Altosaar, “Producibility of II-VI Materials and Devices”, *SPIE Proceedings*. **222**, 1994, pp. 177-185.

[6] M. Altosaar, J. Raudoja, K. Timmo, M. Danilson, M. Grossberg, J. Krustok and E. Mellikov, “$Cu_2Zn_{1-x}Cd_xSn(Se_{1-y}S_y)_4$ solid solutions as absorber materials for solar cells”, *Phys. Stat. Sol. (a)*, **205**, 2008, pp. 167–170.

[7] G. Lucovsky, J.C. Mikkelsen, W.Y. Liang, R.M. White, R.M. Martin, “Optical phonon anisotropies in the layer crystals SnS_2 and $SnSe_2$”, *Phys. Rev. B 4*, **14**, 1976, pp. 1663-1669.

[8] R. Scheer, T. Walter, H.W. Schock, M.L. Fearheiley, H.J. Lewerenz, “$CuInS_2$ based thin film solar cell with 10.2% efficiency”, *Appl. Phys. Lett*. **63**, 1993, pp. 3294-3296.

PAPER V

M. Altosaar, J. Raudoja, **K. Timmo**, M. Danilson, M. Grossberg, J. Krustok and E. Mellikov, $Cu_2Zn_{1-x}Cd_xSn(Se_{1-y}S_y)_4$ solid solutions as absorber materials for solar cells, *Physica Status Solidi A - Applications and Materials Science,* 205 (1) (2008) 167-170.

phys. stat. sol. (a) **205**, No. 1, 167–170 (2008) / **DOI** 10.1002/pssa.200776839

physica status solidi a
www.pss-a.com
applications and materials science

$Cu_2Zn_{1-x}Cd_xSn(Se_{1-y}S_y)_4$ solid solutions as absorber materials for solar cells

M. Altosaar*, J. Raudoja, K. Timmo, M. Danilson, M. Grossberg, J. Krustok, and E. Mellikov

Institute of Materials Science, Tallinn University of Technology, Ehitajate tee 5, 19086 Tallinn, Estonia

Received 2 May 2007, accepted 24 October 2007
Published online 15 January 2008

PACS 78.30.Fs, 78.55.Hx, 81.10.Fq, 81.70.Jb, 84.60.Jt

* Corresponding author: e-mail altosaar@staff.ttu.ee, Fax: +3726203367

$Cu_2Zn_{1-x}Cd_xSn(Se_{1-y}S_y)_4$ monograin powders with different x- and y-values were prepared from binary compounds in the liquid phase of flux material (KI) in evacuated quartz ampoules. All the materials had uniform composition and p-type conductivity. PL spectra (10 K) of the as grown $Cu_2Zn_{1-x}Cd_xSn(Se)_4$ monograin powders showed one PL band with peak position around 0.85 eV which shifted linearly to the lower energy side with increasing Cd content. Cu_2ZnSnS_4 material showed asymmetrical PL band at 1.31 eV attributed to band-to-tail recombination. RT Raman spectra of $Cu_2ZnSnSe_4$ revealed two main peaks at 196 cm^{-1} and 173 cm^{-1} and a third less intensive peak with varying peak position in the region 231–253 cm^{-1}. Raman spectra of Cu_2ZnSnS_4 showed an intensive peak at 338 cm^{-1} and additional peaks at 287 cm^{-1} and 368 cm^{-1}. Narrow sieved fractions of grown powders were used as absorber materials in monograin layer (MGL) solar cell structures: graphite/$Cu_2Zn_{1-x}Cd_xSn(Se_{1-y}S_y)_4$/CdS/ZnO. The best so far solar cell that was based on the $Cu_2Zn_{0.8}Cd_{0.2}SnSe_4$ had open circuit voltage 422 mV, short circuit current 12 mA/cm^2 and fill factor 44%.

1 Introduction Quaternary compounds Cu_2ZnSnS_4, $Cu_2ZnSnSe_4$ and $Cu_2CdSnSe_4$ are new interesting semiconductor materials for absorber layer in thin film solar cells. The most of their elemental constituents are abundant on the earth's crust and they have semiconductor properties such as p-type conductivity, direct band gaps and high absorption coefficients ($>10^4$ cm^{-1}) [1]. Almost all investigations on solar cells are based on Cu_2ZnSnS_4 absorbers. The overview of progress in Cu_2ZnSnS_4 thin film solar cell development has been given by Katagiri [2]. The highest conversion efficiency of Cu_2ZnSnS_4 solar cells is till now 5.74% [3]. The methods for thin film production such as sputtering and PVD in the case of quaternary materials lead to inhomogeneous composition of layers [4, 5]. As a rule, monograin growth in molten fluxes results in homogeneous material. In our previous report [6], we showed, that $Cu_2ZnSnSe_4$ monograin powders with tailored chemical composition could be prepared by isothermal recrystallization of initial binary compounds in molten fluxes. $Cu_2ZnSnSe_4$ powder crystals grown in molten KI had tetragonal shape with rounded grain edges. By XRD analysis the powders had stannite structure (space group $I\bar{4}2m$). The ZnO/CdS/$Cu_2ZnSnSe_4$/graphite monograin layer solar cells had low fill factors (25–30) and the barrier height of their p–n junction was around 250 mV [6]. The present research was performed with the aim to gain better understanding of the reasons of low efficiency of $Cu_2ZnSnSe_4$ monograin layer solar cells by comparing the properties of absorber materials on the base of solid solutions $Cu_2Zn_{1-x}Cd_xSn(Se_yS_{1-y})_4$. Therefore $Cu_2Zn_{1-x}Cd_xSnSe_4$ monograin materials with $x = 0$, 0.2, 0.33, 0.5 and $Cu_2ZnSn(Se_{1-y}S_y)_4$ powders with $y = 1$, 0.5, 0 were prepared and studied.

2 Experimental

2.1 Powder preparation The $Cu_2Zn_{1-x}Cd_xSn(Se_yS_{1-y})_4$ powder materials were synthesized from CuSe(S), ZnSe(S), CdSe(S) and SnSe(S) precursors in molten KI. The binary compounds in stoichiometric relation of $Cu_2Zn(Cd)SnSe(S)_4$ and KI were mixed and ground in planetary ball mill. The mixture was degassed and sealed into quartz ampoules. The recrystallization temperature was 1000 K. Crystal size was controlled by the temperature and duration of the recrystallization process. Crystals

of the synthesized powders were released from flux by washing with deionizated water. More details about this process can be found elsewhere [8]. Polycrystalline Cu_2SnSe_3 was synthesized by melting of CuSe and SnSe in a vacuum ampoule at 1170 K.

2.2 Characterization The bulk composition of powders was determined by energy dispersive spectro scopy (EDS). The shape and surface morphology of crystals were studied with the help of high-resolution scanning electron microscope (SEM) Zeiss ULTRA 55. Photoluminescence (PL) was excited by a He–Cd laser with the wavelength of 441 nm. Powder samples were mounted inside a closed cycle He cryostat ($T = 9–300$ K). The PL spectra were recorded with a computer-controlled SPM-2 grating monochromator ($f = 0.4$ m). The signal was detected with an InGaAs detector using the conventional lock-in technique. The room temperature (RT) micro-Raman spectra were recorded by using a Horiba LabRam HR high-resolution spectrometer equipped with a multichannel detection system in the backscattering configuration. The incident laser light with the wavelength of 532 nm was focused on samples within a spot of 1 μm in diameter and the spectral resolution of the spectrometer was about 0.5 cm^{-1}.

2.3 Solar cell preparation Narrow granulometric fractions of the grown powders were used as absorber material in MGL solar cell structures: graphite/$Cu_2Zn_{1-x}Cd_xSn(Se_yS_{1-y})_4$/CdS/ZnO [6, 7]. $Cu_2Zn_{1-x}Cd_xSn(Se_yS_{1-y})_4$ powder crystals were covered with CdS thin layer by chemical bath deposition. For MGL formation a monolayer of sieved, nearly unisize grains was bound into a thin layer of epoxy resin, so that the contamination of upper surfaces of crystals with epoxy was avoided. After polymerization of epoxy, ZnO window layer was deposited onto front side of MGL by RF-sputtering. Solar cell structures were completed by vacuum evaporation of 1–2 μm thick In grid contacts onto the ZnO window layer. After glueing the structures on glass substrates, the back contact area of crystals covered with epoxy was opened by etching epoxy with H_2SO_4 followed by an additional abrasive treatment. The back contact was made using graphite paste.

3 Results and discussion

3.1 Powder preparation and characterization $Cu_2Zn_{1-x}Cd_xSnSe_4$ materials were prepared with $x = 0$, 0.2, 0.33, 0.5 and $Cu_2ZnSn(Se_{1-y}S_y)_4$ powders with $y = 1$, 0.5, 0. EDS scanning over polished individual powder crystals showed homogeneous distribution of constituent elements.

Ratio of Cu to other metals Cu/Zn(Cd) + Sn was 0.85–0.9, Zn/Sn = 1.04 and Se/metals ratio ≥1. PL spectra of pure $Cu_2ZnSnSe_4$ ($x = 0$) and Cu_2ZnSnS_4 ($y = 1$) are presented in Fig. 1. The PL spectrum of Cu_2ZnSnS_4 (see Fig. 1) is similar to that one described by Tanaka et al. [9]. They attributed the detected broad PL band between

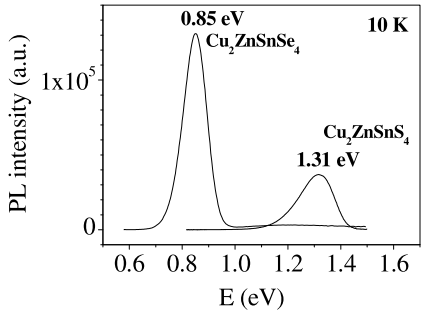

Figure 1 PL spectra of $Cu_2ZnSnSe_4$ and Cu_2ZnSnS_4 monograin powders.

1.1–1.45 eV to donor–acceptor pair recombination. The asymmetrical shape of this band and our temperature and excitation power density dependant measurements of this band showed that the PL band might also originate from band-to-tail (BT) recombination as it was observed in ternaries [10]. A blue shift of the PL band of magnitude about 15 meV per decade with excitation power density was detected while in the case of DA pair recombination the shift is usually smaller. Details of these measurements will be published elsewhere. The PL spectrum of $Cu_2ZnSnSe_4$ shows one nearly symmetrical band with the band maximum at 0.85 eV. The peak position $h\nu_{max}$ (see Fig. 2) and the full width of half maximum (FWHM) of the band shifted with increasing Cd content in $Cu_2Zn_{1-x}Cd_xSnSe_4$ linearly to lower energy side: from $h\nu_{max} = 0.85$ eV ($x = 0$) to 0.77 eV ($x = 0.5$) and from FWHM = 0.09 eV ($x = 0$) to 0.078 eV ($x = 0.5$), correspondingly. By Matsushita et al. [11] the band gap value of $Cu_2ZnSnSe_4$ is 1.44 eV and observed PL emission at 0.85 eV cannot originate from this compound. We tried to identify the possible source of this band by Raman measurements. RT Raman spectra of $Cu_2Zn_{1-x}Cd_xSnSe_4$ revealed two main peaks at 196 cm^{-1} and 173 cm^{-1} (see Fig. 3), which positions did not change noticeably with x, and a third, less intensive peak with varying peak position in the region of 231–253 cm^{-1}. In this region there were peaks in all Raman spectra of $Cu_2Zn_{1-x}Cd_xSnSe_4$ materials. From initial binary compounds, SnSe does not have Raman peaks

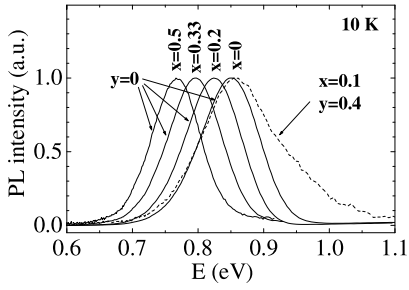

Figure 2 PL spectra of $Cu_2Zn_{1-x}Cd_xSn(Se_{1-y}S_y)_4$.

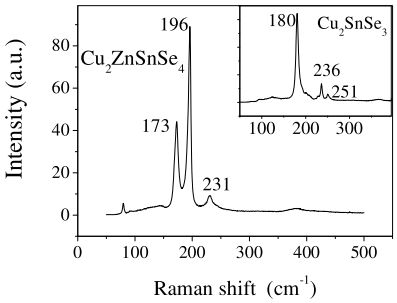

Figure 3 Raman spectrum of $Cu_2ZnSnSe_4$ monograin powder. Raman spectrum of polycrystalline Cu_2SnSe_3 is shown in the upper right corner.

in this region, but ZnSe has a peak at 253 cm^{-1} and CuSe at 260 cm^{-1}.

Cu_2SnSe_3 is the most probable ternary compound in this system. In Cu_2SnSe_3 spectra there are also Raman peaks in the above-mentioned region (see Fig. 4). At the moment the attribution of the Raman peaks in the region of 231–253 cm^{-1} remains questionable and Raman spectra do not give base for unambiguous identification of the bright PL emission at 0.85 eV. The PL spectrum of Cu_2SnSe_3 showed one asymmetrical band at 1.33 eV and so excluded this compound also from the list of probable source of 0.85 eV PL band. The Raman spectra of Cu_2ZnSnS_4 showed the most intensive peak at 338 cm^{-1} and the other peaks at 287 cm^{-1} and 368 cm^{-1} (see Fig. 4) that are close to the values found in [12].

3.2 Solar cell characterization Quantum efficiency (QE) curves of solar cells on the base of Cd containing $Cu_2Zn_{1-x}Cd_xSnSe_4$ showed a shift to the longer wavelengths with increasing Cd content as it is seen in Fig. 5. The highest value of open circuit voltage (V_{oc} = 422 mV) was achieved with $Cu_2Zn_xCd_{1-x}SnSe_4$ material with x = 0.2 (see Fig. 6). By Matsushita et al. the band gap values of $Cu_2ZnSnSe_4$ and $Cu_2CdSnSe_4$ are 1.44 eV and 0.96 eV correspondingly [11]. The temperature dependence of V_{oc}

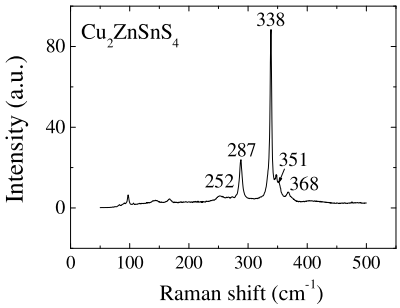

Figure 4 Room temperature Raman spectrum of Cu_2ZnSnS_4 monograin powder.

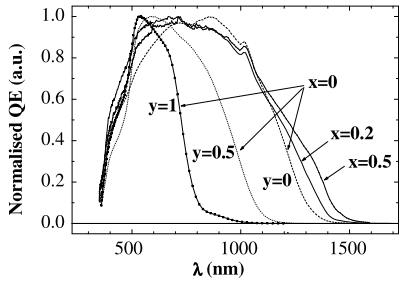

Figure 5 Normalized spectral response curves of $Cu_2Zn_{1-x}Cd_xSn(Se_{1-y}S_y)_4$ solar cells.

gave the barrier height of the junction Φ = 758 meV. This value is much lower than that one possible with an absorber material with the band gap value being a little bit lower than 1.44 eV, as it should be for $Cu_2Zn_xCd_{1-x}SnSe_4$ with x = 0.2. PL spectra of $Cu_2ZnSnSe_4$ (see Fig. 2) showed a band with the band maximum at 0.85 eV. The measured PL spectrum of used SnSe showed the PL band maximum at 0.67 eV. At the same time the QE curves showed a regular shift with increasing Cd content (with increasing x) to the longer wavelength region and with increasing sulphur content (with increasing y) to the shorter wavelength side (see Fig. 5). Considering all these facts we assume that a narrow band gap compound or a solid solution formed on the surface of $Cu_2Zn_{1-x}Cd_xSnSe_4$ limits the efficient work of solar cells at the moment. It is also possible that $Cu_2ZnSnSe_4$ itself has smaller than given in [11] band gap value. Further investigations should clarify the origin of the PL band of $Cu_2ZnSnSe_4$ at 0.85 eV.

4 Conclusions $Cu_2Zn_{1-x}Cd_xSn(Se_{1-y}S_y)_4$ monograin powders were synthesized and characterised by PL and Raman measurements. The results of PL and Raman measurements combined with solar cell parameters enabled to conclude that a narrow band gap compound or a solid solution formed on the surface of $Cu_2Zn_{1-x}Cd_xSnSe_4$ limits the efficient work of solar cells or $Cu_2ZnSnSe_4$ itself has lower than 1.44 eV bandgap.

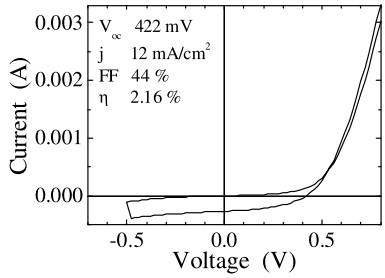

Figure 6 I–V curve of $Cu_2(Zn_{0.8}Cd_{0.2})SnSe_4$ MGL solar cell. The efficiency is given to the active area of solar cell.

Acknowledgements Financial support of the European Union from the Energy Program, PV-EST project (Contract ENK5-CT-2002-80664) and of Estonian Science Foundation under contracts Nos. 6160, 6554 and 6179 is gratefully acknowledged. The authors would also like to thank Mrs. O. Volobujeva for her help in the SEM studies and EDS analysis and Dr. T. Varema and Dr. M. Kauk for their help in the MGL solar cell formation.

References

[1] K. Ito and T. Nakazawa, Jpn. J. Appl. Phys. **27**, 2094 (1988).
[2] H. Katagiri, Thin Solid Films **480/481**, 426 (2005).
[3] K. Jimbo, R. Kimura, S. Yamada, W. S. Maw, H. Araki, K. Oishi, and H. Katagiri, Thin Solid Films **515**, 5997 (2007).
[4] T. M. Friedlmeier et al., Proceedings of the 11th ICTMC, Salford, UK 1997, Inst. Phys. Conference Ser. No. 152, (1997), p. 345.
[5] T. Tanaka et al., J. Phys. Chem. Solids **66**, 1978 (2005).
[6] M. Altosaar, J. Raudoja, K. Timmo, M. Danilson, M. Grossberg, M. Krunks, T. Varema, and E. Mellikov, Proceedings of the 2006 IEEE WCPEC-4, Hawaii, 7–12 May 2006.
[7] M. Altosaar et al., Thin Solid Films **431/432**, 466 (2003).
[8] K. Timmo, M. Altosaar, M. Kauk, J. Raudoja, and E. Mellikov, Thin Solid Films **515**, 5884 (2007).
[9] K. Tanaka, Y. Miyamoto, H. Uchiki, K. Nakazawa, and H. Araki, phys. stat. sol. (a) **203**, 2891 (2006).
[10] J. Krustok, H. Collan, M. Yakushev, and K. Hjelt, Phys. Scr. Vol. T **79**, 179 (1999).
[11] H. Matsushita, T. Maeda, A. Katsui, and T. Takizawa, J. Cryst. Growth **208**, 416 (2000).
[12] M. Himmrich and H. Haeuseler, Spectrochim. Acta A, Mol. Spectrosc. **47**, 933 (1991).

PAPER VI

K. Timmo, M. Altosaar, J. Raudoja, K. Muska, M. Pilvet, M. Kauk, T. Varema, M. Danilson, O. Volobujeva, E. Mellikov, Sulfur-containing $Cu_2ZnSnSe_4$ monograin powders for solar cells, *Solar Energy Materials & Solar Cells* 94 (2010) 1889-1892.

Solar Energy Materials & Solar Cells 94 (2010) 1889–1892

Contents lists available at ScienceDirect

Solar Energy Materials & Solar Cells

journal homepage: www.elsevier.com/locate/solmat

Sulfur-containing $Cu_2ZnSnSe_4$ monograin powders for solar cells

K. Timmo*, M. Altosaar, J. Raudoja, K. Muska, M. Pilvet, M. Kauk, T. Varema, M. Danilson, O. Volobujeva, E. Mellikov

Department of Materials Science, Tallinn University of Technology, Ehitajate tee 5, Tallinn 19086, Estonia

ARTICLE INFO

Article history:
Received 19 November 2009
Received in revised form
10 June 2010
Accepted 22 June 2010

Keywords:
$Cu_2ZnSnSe_4$
Cu_2ZnSnS_4
Solid solutions
Solar cell
Monograin growth

ABSTRACT

$Cu_2ZnSn(Se_{1-x}S_x)_4$ monograin powders with different x values were prepared from binary compounds in the liquid phase of flux material (KI) in evacuated quartz ampoules at 1000 K. Narrow granulometric fractions of the grown powders were used as absorber materials in monograin layer solar cells: graphite/$Cu_2ZnSn(Se_{1-x}S_x)_4$/CdS/ZnO. The values of V_{oc} increased with increase in content of sulfur in the absorber from 283 mV for $x=0$–660 mV for $x=0.85$.

1. Introduction

The Cu_2-II–IV–VI_4 quaternary compounds Cu_2ZnSnS_4 (CTZS) and $Cu_2ZnSnSe_4$ (CZTSe) are novel absorber materials for solar cells, alternatives to $CuIn(S,Se)_2$ due to their p-type conductivity, high absorption coefficients ($>10^4\,cm^{-1}$) and direct band gap close to the optimum value for terrestrial solar energy conversion. Several research groups have found that $Cu_2ZnSnSe_4$ has band gap energies from 1.44 to 1.56 eV [1–4] and Cu_2ZnSnS_4 from 1.45 to 1.51 eV [1,5,6]. At present, to our knowledge the best conversion efficiency of the CZTS thin film solar cells reported has been 6.77%, achieved using a three-source rf co-sputtering system for metal film deposition followed by annealing in sulphur containing atmosphere [7].

In our previous reports [8,9] we showed that monograin powders of $Cu_2ZnSnSe_4$ and $Cu_2ZnSn(Se_{1-x}S_x)_4$ solid solutions with $x=0.5$ can be prepared by isothermal crystallization from initial binary compound precursors in molten potassium iodide. The high temperature (970–1000 K) synthesis and homogenization in molten phase of flux material resulted in uniform composition of powder crystals of these complex multicomponent compounds. $Cu_2ZnSnSe_4$ powder crystals grown in molten KI have stannite structure (space group $I\bar{4}2m$). The first monograin layer solar cells with the layer structure of ZnO/CdS/$Cu_2ZnSnSe_4$/graphite had low values of solar cell parameters and their conversion efficiency was 1.8% [8]. The following research on solid solutions of $Cu_2Zn_{1-x}Cd_xSn(Se_yS_{1-y})_4$ [9] was performed with the aim to gain better understanding of the reasons for the low efficiency of the $Cu_2ZnSnSe_4$ monograin layer solar cells. The results of PL and Raman measurements combined with a detailed analysis of the solar cell parameters enabled us to conclude that $Cu_2ZnSnSe_4$ actually has a band gap much lower than 1.44 eV as reported by Matsushita et al. [3]. According to the PL results, it is proposed that the band gap energy of CZTSe is around 1.02 eV at $T=10$ K [10]. In the present paper we report further the results of studies on solid solutions of $Cu_2ZnSn(Se_{1-x}S_x)_4$ in the form of monograin powders.

2. Experimental

$Cu_2ZnSn(Se_{1-x}S_x)_4$ (CZTSSe) monograin powders with different x values were synthesized from CuSe(S), ZnSe(S) and SnSe(S) in appropriate relations as precursors for CZTSSe in molten KI. The ground initial substances were sealed into evacuated quartz ampoules and annealed at 1000 K. The processes of formation and growth of semiconductor compound CZTSSe crystals took place in the liquid phase of KI as flux material. The crystal size was controlled by the temperature and duration of the crystallization process. The growth process was stopped by quenching the ampoules in cold water. Crystals of the synthesized powders were released from KI flux by washing with deionizated water. Narrow granulometric fractions of the grown powders obtained by sieving were used as absorber material in monograin layer (MGL) solar cell structures: graphite/$Cu_2ZnSn(Se_xS_{1-x})_4$/CdS/ZnO [11].

The bulk composition of powder crystals was determined by energy dispersive X-ray spectroscopy (EDS). The shape and surface morphology of crystals were studied with the help of a

* Corresponding author. Tel.: +372 620 3362; fax: +372 620 3367.
E-mail address: timmokas@yahoo.com (K. Timmo).

0927-0248/$ - see front matter © 2010 Elsevier B.V. All rights reserved.
doi:10.1016/j.solmat.2010.06.046

high-resolution scanning electron microscope (SEM) Zeiss ULTRA 55. XRD patterns were recorded by a Bruker AXS D5005 diffractometer using monochromatic Cu Kα radiation in the 2θ interval of $15-78^\circ$ in steps of 0.04° and counting times of 2 s/step.

The photovoltaic properties of graphite/$Cu_2ZnSn(Se_xS_{1-x})_4$/CdS/ZnO structures were characterized by I–V measurements with 100 mW/cm^2 tungsten halogen illumination from 4 mm^2 graphite contact spots. Spectral response measurements were performed with the help of a computer-controlled SPM-2 monochromator and a 100 W tungsten halogen lamp. All temperature-dependent measurements were made with the help of a closed-cycle He cryostat ($T=10$–300 K).

3. Results

3.1. Composition and structure

$Cu_2ZnSn(Se_{1-x}S_x)_4$ materials were prepared with $x=0$, 0.25, 0.45, 0.75, 0.85 and 1. The ratio of Cu to other metals Cu/(Zn+Sn) was 0.925 and the Zn to Sn ratio was 1.0.

Monograin growth in molten KI resulted in homogeneous composition of the $Cu_2ZnSn(Se_{1-x}S_x)_4$ powders in the region of sulfur content $x=0$–$x=0.85$. This was concluded from analyzing XRD data and EDS scans over polished individual CZTSSe ($0 \le x \le 0.85$) powder crystals. For $x=1$, some synthesized powder crystals consisted of several phases, as can be seen from the SEM photos and from the distribution of constituent elements (Fig. 1).

Here, the results of EDS analysis also indicate the presence of separate phases besides the Cu_2ZnSnS_4 phase: Cu_2SnS_3 ([Cu]=32.9%, [Sn]=17.2%, [S]=49.8%), SnS ([Sn]=51.5%, [S]=48.45%) and ZnS ([Zn]=50%, [S]=50%). The results of XRD investigations confirm that in addition to the dominating CZTS phase, powders contain SnS in small quantities (Fig. 2).

The XRD pattern did not confirm the existence of Cu_2SnS_3 and ZnS. It means that the concentrations of Cu_2SnS_3 and ZnS are lower than the sensitivity of the XRD analysis ($\pm 2\%$) or the distribution of these phases is inhomogeneous in the synthesized material. One possible explanation for the excistence of different phases in synthesized pure CZTS ($x=1$) is that the homogeneity range of Cu_2ZnSnS_4 is much narrower than that of $Cu_2ZnSnSe_4$, resulting therefore in a higher probability for the formation of other phases during the synthesis and the growth process of the Cu_2ZnSnS_4 ($x=1$) monograin powders of the same initial composition as the other $Cu_2ZnSn(Se_{1-x}S_x)_4$ materials ($0 \le x \le 0.85$).

X-ray diffraction patterns of the $Cu_2ZnSn(Se_{1-x}S_x)_4$ monograin powders with different Se/S concentration ratios are shown in Fig. 3.

The diffraction peaks were identified as belonging to the Cu_2ZnSnS_4 compound ($x=1$) with kesterite structure (space group $I\bar{4}$) and to the $Cu_2ZnSnSe_4$ ($x=0$) with stannite structure (space group $I\bar{4}2m$) [3,12]. The reflection Miller indexes were assigned according to Matsushita et al. [3]. The ratio of reflections intensities was in correspondence to those measured by Olekseyuk et al. [12]. An exchange of Se with S shifts the peak positions from the stannite structure to the kesterite structure. At a ratio of S to Se of 85:15 mole% the XRD pattern shows a splitting of peaks, which could be a sign of existance of two crystal phases at the same time. More detailed investigations are necessary to confirm these results.

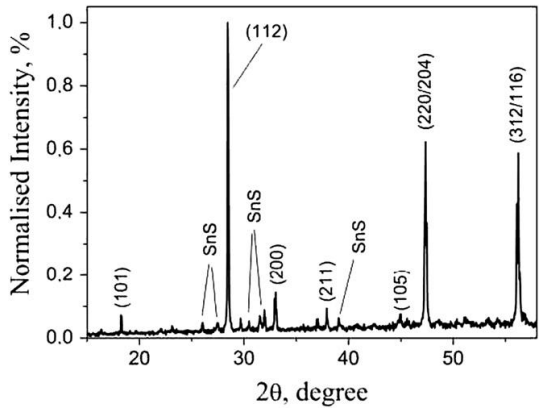

Fig. 2. X-ray diffraction pattern of the Cu_2ZnSnS_4 monograin powder.

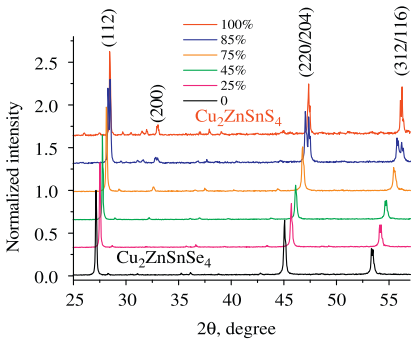

Fig. 3. XRD patterns of $Cu_2ZnSn(Se_{1-x}S_x)_4$ monograin powders with different x values.

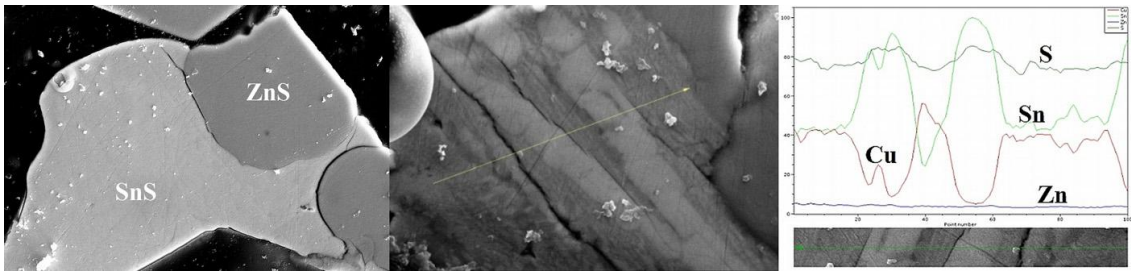

Fig. 1. EDS scanning over polished individual $Cu_2ZnSn(S,Se)_4$ powder crystal.

3.2. Solar cell characterization

The prepared monograin powders were used as absorber materials in monograin layer (MGL) solar cell structures: ZnO/CdS/CZTSSe/graphite, where every crystal works as an individual solar cell. All the as-grown powders were post-heat-treated for improving the crystal surface structure. Solar cells showed uniform distribution of solar cell parameters over the whole working area of the $1 \times 1.5\ cm^{-2}$ samples (Fig. 4). Open circuit voltages of $Cu_2ZnSn(Se_{1-x}S_x)_4$ monograin layer solar cells increased with increase in sulfur content in the monograin powders, from 283 mV for $x=0$–660 mV for $x=0.85$ (Fig. 5.). The pure Cu_2ZnSnS_4 absorber material resulted in lower V_{oc} (541 mV) probably due to secondary phases being formed. An increase of the open circuit voltage values points to a widening of the band gap of $Cu_2ZnSn(Se_{1-x}S_x)$ with increase in S concentration. Solar cell structures based on monograin powders with a S/Se concentration ratio of 85 mole% sulfur to 15 mole% selenium yielded the highest values of the open circuit voltage. The $Cu_2ZnSn(S,Se)_4$ solid solution with 75 mole% sulfur and 25 mole% selenium gave the best solar cell with parameters: $V_{oc}=622$ mV, $I_{sc}=15.87$ mA/cm^2, $FF=60\%$, $\eta=5.9\%$.

The normalized quantum efficiency (QE) spectra of solar cells on the base of $Cu_2ZnSn(Se_{1-x}S_x)_4$ monograin powders show the shift of the absorption edge to shorter wavelengths as well a change in the short wavelengths response with increase in S content in the absorber material as shown in Fig. 6.

Temperature-dependent open circuit voltage measurements were performed to determine the barrier height of the p–n junction ($q\Phi_B$) (Fig. 7). The barrier height of the solar cells

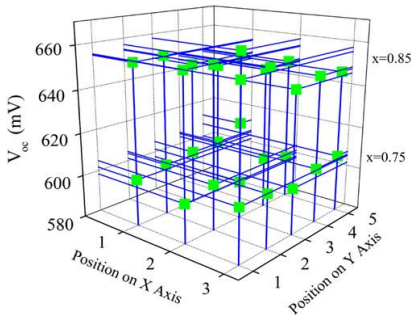

Fig. 4. Distribution of V_{oc} values of two different $Cu_2ZnSn(Se_{1-x}S_x)_4$ solar cells with $x=0.75$ and $x=0.85$ over a 1 cm (x-axis) by 1.5 cm (y-axis) cell measured in equal distances. Area of every point is 4 mm^2.

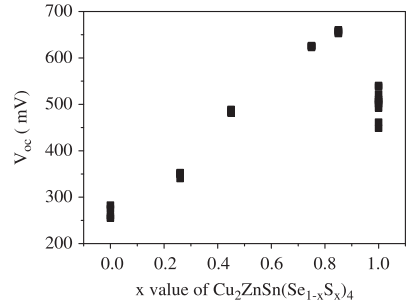

Fig. 5. Maximum V_{oc} values of $Cu_2ZnSn(Se_{1-x}S_x)_4$ monograin layer solar cells in dependence of Se displacement by S. Data points describe measurement results from graphite back contacts of 4 mm^2 of 1×1.5 cm^2 cell.

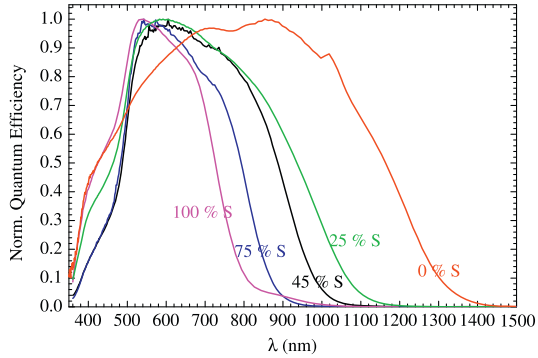

Fig. 6. Normalized quantum efficiency spectra of MGL solar cell devices with different S/Se concentration ratios in the used absorber material.

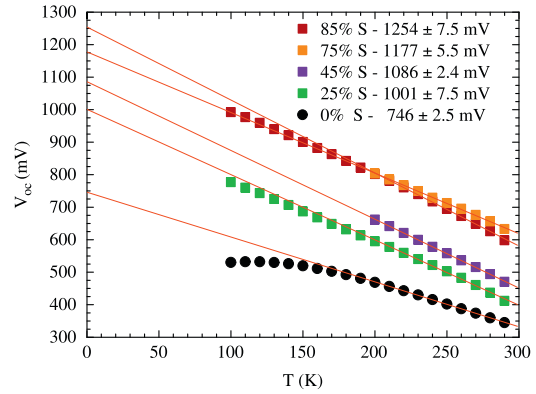

Fig. 7. V_{oc} vs. T for $Cu_2ZnSn(Se_{1-x}S_x)_4$ monograin layer solar cells with different x values in the monograin powders.

increases as expected with increase in the S content in $Cu_2ZnSn(Se_{1-x}S_x)$ monograin powders.

As expected from the increase in open circuit voltage values for increasing sulfur content, the quantum efficiency spectra shift to shorter wavelengths. This increase of the barrier height of solar cells with increase in S content in the absorber material gives us a basis to believe that the $Cu_2ZnSnSe_4$ band gap energy value (in literature 1.44–1.56 eV) should be much lower than the Cu_2ZnSnS_4 band gap energy: 1.45–1.51 eV.

4. Conclusions

Monograin powder technology enables us to grow $Cu_2ZnSn(S,Se)_4$ materials with homogeneous composition usable for monograin layer solar cells. The increasing sulfur content in $Cu_2ZnSnSe_4$ monograin powder absorber materials improves the values of open circuit voltages of MGL solar cells and shifts the QE curves to the higher energy side. Solar cell structures based on monograin powders with a S/Se concentration ratio of 85 mole% sulfur to 15 mole% selenium yielded the highest values of open circuit voltage: 660 mV.

Acknowledgements

This work was supported by the Estonian Ministry of Education and Science under Contract no. T099 and by the

Estonian Science Foundation under Contract no. 6160. The support of the World Federation of Scientists National Scholarship Programme is also gratefully acknowledged.

References

[1] K. Ito, T. Nakazawa, Electrical and optical properties of stannite-type quaternary semiconductor thin films, Jpn. J. Appl. Phys. 27 (1988) 2094–2097.

[2] Rachmat Adhi Wibowo, Woo Seok Kim, Eun Soo Lee, Badrul Munir, Kyoo Ho Kim, Single step preparation of quaternary $Cu_2ZnSnSe_4$ thin films by RF magnetron sputtering from binary chalcogenide targets, J. Phys. Chem. Solids 68 (2007) 1908–1913.

[3] H. Matsushita, T. Maeda, A. Katsui, T. Takizawa, Thermal analysis and synthesis from the melts of Cu-based quaternary compounds Cu–III–IV–VI_4 and Cu_2–II–IV–VI_4 (II=Zn, Cd; III=Ga, In; IV=Ge, Sn; VI=Se), J. Cryst. Growth 208 (2000) 416–422.

[4] G. Suresh Babu, Y.B. Kishore Kumar, P. Uday Bhaskar, V. Sundara Raja, Effect of post-deposition annealing on the growth of $Cu_2ZnSnSe_4$ thin films for a solar cell absorber layer, Semicond. Sci. Technol. 23 (2008) 085023 (12pp).

[5] H. Katagiri, N. Ihigaki, T. Ishida, K. Saito, Characterization of Cu_2ZnSnS_4 thin films prepared by vapor phase sulfurization, Jpn. J. Appl. Phys. 40 (2001) 500–504.

[6] K. Tanaka, N. Moritake, H. Uchiki, Preparation of Cu_2ZnSnS_4 thin films by sulfurizing sol–gel deposited precursors, Sol. Energy Mater. Sol. Cells. 91 (2007) 1199–1201.

[7] H. Katagiri, K. Jimbo, W. Shwe Maw, K. Oishi, M. Yamazaki, H. Araki, A. Takeuchi, Development of CZTS-based thin film solar cells, Thin Solid Films 517 (2009) 2455–2460.

[8] M. Altosaar, J. Raudoja, K. Timmo, M. Danilson, M. Grossberg, M. Krunks, T. Varema, E. Mellikov, $Cu_2ZnSnSe_4$ monograin powders for solar cell application, in: Proceedings of the 2006 IEEE WCPEC-4, Havaii, May 7–12, 2006.

[9] M. Altosaar, J. Raudoja, K. Timmo, M. Danilson, M. Grossberg, J. Krustok, E. Mellikov, $Cu_2Zn_{1-x}Cd_xSn(Se_{1-y}S_y)_4$ solid solutions as absorber materials for solar cells, Phys. Stat. Sol. (a) 205 (2008) 167–170.

[10] M. Grossberg, J. Krustok, K. Timmo, M. Altosaar, Radiative recombination in $Cu_2ZnSnSe_4$ monograins studied by photoluminescence spectroscopy, Thin Solid Films 517 (2009) 2489–2492.

[11] E. Mellikov, D. Meissner, T. Varema, M. Altosaar, M. Kauk, O. Volobujeva, J. Raudoja, K. Timmo, M. Danilson, Monograin materials for solar cells, Sol. Energy Mater. Sol. Cells 93 (2009) 65–68.

[12] I.D. Olekseyuk, L.D. Gulay, I.V. Dydchak, L.V. Piskach, O.V. Parasyuk, O.V. Marchuk, Single cystal preparation and crystal structure of the Cu_2Zn/Cd, $Hg/SnSe_4$ compounds, J. Alloys Compd. 340 (2002) 141–145.

APPENDIX B

ELULOOKIRJELDUS

Ees- ka perekonnanimi:	Kristi Timmo
Sünniaeg ja –koht:	08.12.1979, Võru
E-post:	timmokas@yahoo.com
Hariduskäik	2005 - Tallinna Tehnikaülikool, keemia- ja materjalitehnoloogia teaduskond, doktorantuur 2005 - Tallinna Tehnikaülikool, keemia- ja materjalitehnoloogia teaduskond, magistrikraad 2003 - Tallinna Tehnikaülikool, keemia- ja materjalitehnoloogia teaduskond, bakalaureusekraad 1998 – Võru Kreutzwaldi Gümnaasium, keskharidus
Teenistuskäik	2005 - Tallinna Tehnikaülikool, materjaliteaduse instituut, teadur 2003 – 2005 Tallinna Tehnikaülikool, materjali-teaduse instituut, insener 2001 – 2003 Tallinna Tehnikaülikool, materjali-teaduse instituut, tehniline töötaja
Kaitstud lõputööd	,,Monoterapulbilise $CuInSe_2$ kasvatamine ja tema omaduste kujundamine kaaliumjodiidsulandaja keskkonnas'', magistritöö, juhendaja juhtivteadur Mare Altosaar ,,$CuInSe_2$ monoterapulbrite sünteeskasvatus kaaliumjodiidsulandajas'', bakalaureusetöö, juhendaja vanemteadur Mare Altosaar
Täiendõpe	sept. – dets. 2006 täiendõpe Hahn-Meitneri Instituut, Berliin, Saksamaa veebr. 25 – 27, 2006 Chemistry and physics of photovoltaics, European Union Centre of Excellence in PV materials and Devices, Tallinn, Eesti 21.08.2006 – 25.08.2006 European Union Centre of Excellence in PV materials and Devices, ,,YSSS-2006 on PV", Pärnu, Eesti aug. 27 – sept. 4, 2005 täiendkoolitus, Berliin, Saksamaa

CURRICULUM VITAE

First name and surname:	Kristi Timmo
Date and place of birth:	08.12.1979, Võru
E-mail:	timmokas@yahoo.com
Education	2005 – Tallinn University of Technology, Faculty of Chemistry and Materials Technology, doctoral study 2005 - Tallinn University of Technology, Faculty of Chemistry and Materials Technology, Master of Science in Natural Sciences 2003 - Tallinn University of Technology, Faculty of Chemistry and Materials Technology, Bachelor of Science in Natural Sciences 1998 – Võru Kreutzwald Gymnasium
Professional experience	2005 - Tallinn University of Technology, Department of Materials Science, researcher 2003 – 2005 Tallinn University of Technology, Department of Materials Science, engineer 2001 – 2003 Tallinn University of Technology, technical assistant
Defended dissertations	„Tailoring the properties of $CuInSe_2$ monograin powders in growth process", master thesis, supervisor Leading Research Scientist Mare Altosaar „Synthesis growth of $CuInSe_2$ in potassium iodide", bachelor thesis, supervisor Senior Researcher Mare Altosaar
Training courses	Sept. – Dec. 2006, Hahn-Meitner-Institut Berlin, Germany Febr. 25 – 27, 2006 Chemistry and physics of photovoltaics, European Union Centre of Excellence in PV materials and Devices, Tallinn, Estonia 21.08.2006 – 25.08.2006, European Union Centre of Excellence in PV materials and Devices, ''YSSS-2006 on PV", Estonia Aug. – Sept. 2005, PV Interact, Berlin, Germany

List of publications

1. E. Mellikov,M. Altosaar, J. Raudoja, K. Timmo, O. Volobujeva, M. Kauk, J. Krustok, T. Varema, M. Grossberg, M. Danilson, K. Muska, K. Ernits, F. Lehner, D. Meissner, $Cu_2(Zn_xSn_{2-x})(S_ySe_{1-y})_4$ MONOGRAIN MATERIALS FOR PHOTOVOLTAICS. *Materials challenges on Energy*, (2010), (in press).

2. E. Mellikov, D. Meissner, M. Altosaar, M. Kauk, J. Krustok, A. Öpik, O. Volobujeva, J. Iljina, K. Timmo, I. Klavina, J. Raudoja, M. Grossberg, T. Varema, K. Muska, M. Ganchev, S. Bereznev,M. Danilson, Solar Energy Materials Research at Tallinn University of Technology, *Advanced Materials Research,* (2010), (in press).

3. M. Grossberg, J. Krustok, J. Raudoja, K. Timmo, M. Altosaar, T. Raadik, *Thin Solid Films,* (2010) doi:10.1016/j.tsf.2010.12.099.

4. K. Timmo, M. Altosaar, J. Raudoja, K. Muska, M. Pilvet, M. Kauk, T. Varema, M. Danilson, O. Volobujeva, E. Mellikov, Sulfur-containing $Cu_2ZnSnSe_4$ monograin powders for solar cells, *Solar Energy Materials & Solar Cells*, 94 (2010) 1889–1892.

5. K.Timmo; M.Altosaar; J.Raudoja; M.Grossberg; M.Danilson; O.Volobujeva, E.Mellikov, Chemical etching of $Cu_2ZnSn(S,Se)_4$ monograin powder. 35th IEEE Photovoltaic Specialists Conference, Honolulu, Hawaii, June 20-25, 2010: *Conference Proceedings* 1982 - 1985.

6. M. Grossberg, J. Krustok, K. Timmo, M. Altosaar, Radiative recombination in $Cu_2ZnSnSe_4$ monograins studied by photoluminescence spectroscopy, *Thin Solid Films*, Volume 517, Issue 7, 2 February 2009, 2489-2492.

7. Mellikov, E.; Meissner, D.; Varema, T.; Altosaar, M.; Kauk, M.; Volobujeva, O.; Raudoja, J.; Timmo, K.; Danilson, M. (2009). Monograin materials for solar cells, *Solar Energy Materials & Solar Cells*, 93(1), 65 - 69.

8. Altosaar, M.; Timmo, K.; Danilson, M.; Raudoja, J.; Mellikov, E. Characterization of Cu2ZnSnSe4 monograin layer solar cells. In: Proceedings of the International Conference on Solar Cells: International Conference on Solar Cells IC-SOLACE 2008, 21-23 January, Cochin, India, 2008, 103 - 105.

9. M. Altosaar, J. Raudoja, K. Timmo, M. Danilson, M. Grossberg, J. Krustok and E. Mellikov, $Cu_2Zn_{1-x}Cd_x$ $Sn(Se_{1-y}S_y)_4$ solid solutions as absorber materials for solar cells, *Physica Status Solidi A - Applications and Materials Science*, 205(1), (2008) 167 - 170.

10. M. Kauk, M. Altosaar, J. Raudoja, K. Timmo, T. Varema, M. Danilson, M. Grossberg and E. Mellikov The influence of doping with donor type impurities to the properties of $CuInSe_2$, *Physica Status Solidi C*, 5(2), (2008) 609 - 611.

11. K. Timmo, M. Altosaar, M. Kauk, J. Raudoja, E. Mellikov, $CuInSe_2$ monograin growth in the liquid phase of potassium iodide, *Thin Solid Films*, Volume 515, Issue 15, (2007), 5884-5886.

12. K. Timmo, M. Altosaar, J. Raudoja, E. Mellikov, T. Varema, M. Danilson, M. Grossberg, The effect of sodium doping to $CuInSe_2$ monograin powder properties, *Thin Solid Films*, Volume 515, Issue 15, (2007), 5887-5890.

13. M. Kauk, M. Altosaar, K. Ernits, K. Timmo, A. Jagomägi, M. Grossberg, J. Krustok, T. Varema, E. Mellikov, "Chemical of $CuInSe_2$ absorber surface for monograin layer solar cell application", *Proceedings of EUPVSEC*, 2006, p. 1811-1815.

14. M. Altosaar, J. Raudoja, K. Timmo, M. Danilson, M. Grossberg, M. Krunks, T. Varema and E. Mellikov, $Cu_2ZnSnSe_4$ monograin powders for solar cell application, In: Conference Record of the 2006 IEEE 4th World Conference on Photovoltaic Energy Conversion, Waikoloa, HI, MAY 07-12, 2006. IEEE Electron Devices Society, 2006, 468 - 470.

15. M. Altosaar, M. Danilson, M. Kauk, J. Krustok, E. Mellikov, J. Raudoja, K. Timmo, T.Varema, Further developments in CIS monograin layer solar cells technology, *Solar Energy Materials & Solar Cells* 87 (2005) 25-32.

16. M. Kauk, M. Altosaar, J. Raudoja, K. Timmo, M. Grossberg, T. Varema, E. Mellikov, Growth of $CuInSe_2$ monograin powders with different compositions, *Mater. Res. Soc. Symp. Proc*. Vol. 865 (2005) .

17. M.Altosaar, M.Kauk, L.Kaupmees, J.Raudoja, K.Timmo, Tailoring the composition and properties of CuInSe2 materials for solar cells application, Proc. SPIE Vol. 5946, *Optical Materials and Applications*, 2005, p. 224-229

Patent application:

1. Enn Mellikov, Mare Altosaar, Dieter Meissner, Jaan Raudoja, Kristi Timmo, Semiconductor material and its application as an absorber material for solar cells, international patent application WO2010006623 (Priority No. US61/080836, priority date: 15.07.2008).

DISSERTATIONS DEFENDED AT TALLINN UNIVERSITY OF TECHNOLOGY ON *NATURAL AND EXACT SCIENCES*

1. **Olav Kongas**. Nonlinear dynamics in modeling cardiac arrhytmias. 1998.

2. **Kalju Vanatalu**. Optimization of processes of microbial biosynthesis of isotopically labeled biomolecules and their complexes. 1999.

3. **Ahto Buldas**. An algebraic approach to the structure of graphs. 1999.

4. **Monika Drews**. A metabolic study of insect cells in batch and continuous culture: application of chemostat and turbidostat to the production of recombinant proteins.1999.

5. **Eola Valdre**. Endothelial-specific regulation of vessel formation: role of receptor tyrosine kinases. 2000.

6. **Kalju Lott**. Doping and defect thermodynamic equilibrium in ZnS. 2000.

7. **Reet Koljak**. Novel fatty acid dioxygenases from the corals *Plexaura homomalla* and *Gersemia fruticosa.* 2001.

8. **Anne Paju**. Asymmetric oxidation of prochiral and racemic ketones by using sharpless catalyst. 2001.

9. **Marko Vendelin**. Cardiac mechanoenergetics *in silico*. 2001.

10. **Pearu Peterson**. Multi-soliton interactions and the inverse problem of wave crest. 2001.

11. **Anne Menert**. Microcalorimetry of anaerobic digestion. 2001.

12. **Toomas Tiivel**. The role of the mitochondrial outer membrane in *in vivo* regulation of respiration in normal heart and skeletal muscle cell. 2002.

13. **Olle Hints**. Ordovician scolecodonts of Estonia and neighbouring areas: taxonomy, distribution, palaeoecology, and application. 2002.

14. **Jaak Nõlvak**. Chitinozoan biostratigrapy in the Ordovician of Baltoscandia. 2002.

15. **Liivi Kluge**. On algebraic structure of pre-operad. 2002.

16. **Jaanus Lass**. Biosignal interpretation: Study of cardiac arrhytmias and electromagnetic field effects on human nervous system. 2002.

17. **Janek Peterson**. Synthesis, structural characterization and modification of PAMAM dendrimers. 2002.

18. **Merike Vaher**. Room temperature ionic liquids as background electrolyte additives in capillary electrophoresis. 2002.

19. **Valdek Mikli**. Electron microscopy and image analysis study of powdered hardmetal materials and optoelectronic thin films. 2003.

20. **Mart Viljus**. The microstructure and properties of fine-grained cermets. 2003.

21. **Signe Kask**. Identification and characterization of dairy-related *Lactobacillus.* 2003.

22. **Tiiu-Mai Laht**. Influence of microstructure of the curd on enzymatic and microbiological processes in Swiss-type cheese. 2003.

23. **Anne Kuusksalu**. 2–5A synthetase in the marine sponge *Geodia cydonium*. 2003.

24. **Sergei Bereznev**. Solar cells based on polycristalline copper-indium chalcogenides and conductive polymers. 2003.

25. **Kadri Kriis**. Asymmetric synthesis of C2-symmetric bimorpholines and their application as chiral ligands in the transfer hydrogenation of aromatic ketones. 2004.

26. **Jekaterina Reut**. Polypyrrole coatings on conducting and insulating substracts. 2004.

27. **Sven Nõmm**. Realization and identification of discrete-time nonlinear systems. 2004.

28. **Olga Kijatkina**. Deposition of copper indium disulphide films by chemical spray pyrolysis. 2004.

29. **Gert Tamberg**. On sampling operators defined by Rogosinski, Hann and Blackman windows. 2004.

30. **Monika Übner**. Interaction of humic substances with metal cations. 2004.

31. **Kaarel Adamberg**. Growth characteristics of non-starter lactic acid bacteria from cheese. 2004.

32. **Imre Vallikivi**. Lipase-catalysed reactions of prostaglandins. 2004.

33. **Merike Peld**. Substituted apatites as sorbents for heavy metals. 2005.

34. **Vitali Syritski**. Study of synthesis and redox switching of polypyrrole and poly(3,4-ethylenedioxythiophene) by using *in-situ* techniques. 2004.

35. **Lee Põllumaa**. Evaluation of ecotoxicological effects related to oil shale industry. 2004.

36. **Riina Aav**. Synthesis of 9,11-secosterols intermediates. 2005.

37. **Andres Braunbrück**. Wave interaction in weakly inhomogeneous materials. 2005.

38. **Robert Kitt**. Generalised scale-invariance in financial time series. 2005.

39. **Juss Pavelson**. Mesoscale physical processes and the related impact on the summer nutrient fields and phytoplankton blooms in the western Gulf of Finland. 2005.

40. **Olari Ilison**. Solitons and solitary waves in media with higher order dispersive and nonlinear effects. 2005.

41. **Maksim Säkki**. Intermittency and long-range structurization of heart rate. 2005.

42. **Enli Kiipli**. Modelling seawater chemistry of the East Baltic Basin in the late Ordovician–Early Silurian. 2005.

43. **Igor Golovtsov**. Modification of conductive properties and processability of polyparaphenylene, polypyrrole and polyaniline. 2005.

44. **Katrin Laos**. Interaction between furcellaran and the globular proteins (bovine serum albumin β-lactoglobulin). 2005.

45. **Arvo Mere**. Structural and electrical properties of spray deposited copper indium disulphide films for solar cells. 2006.

46. **Sille Ehala**. Development and application of various on- and off-line analytical methods for the analysis of bioactive compounds. 2006.

47. **Maria Kulp**. Capillary electrophoretic monitoring of biochemical reaction kinetics. 2006.

48. **Anu Aaspõllu.** Proteinases from *Vipera lebetina* snake venom affecting hemostasis. 2006.

49. **Lyudmila Chekulayeva**. Photosensitized inactivation of tumor cells by porphyrins and chlorins. 2006.

50. **Merle Uudsemaa**. Quantum-chemical modeling of solvated first row transition metal ions. 2006.

51. **Tagli Pitsi**. Nutrition situation of pre-school children in Estonia from 1995 to 2004. 2006.

52. **Angela Ivask**. Luminescent recombinant sensor bacteria for the analysis of bioavailable heavy metals. 2006.

53. **Tiina Lõugas**. Study on physico-chemical properties and some bioactive compounds of sea buckthorn (*Hippophae rhamnoides* L.). 2006.

54. **Kaja Kasemets**. Effect of changing environmental conditions on the fermentative growth of Saccharomyces cerevisae S288C: auxo-accelerostat study. 2006.

55. **Ildar Nisamedtinov**. Application of 13C and fluorescence labeling in metabolic studies of Saccharomyces spp. 2006.

56. **Alar Leibak**. On additive generalisation of Voronoï's theory of perfect forms over algebraic number fields. 2006.

57. **Andri Jagomägi**. Photoluminescence of chalcopyrite tellurides. 2006.

58. **Tõnu Martma**. Application of carbon isotopes to the study of the Ordovician and Silurian of the Baltic. 2006.

59. **Marit Kauk**. Chemical composition of CuInSe 2 monograin powders for solar cell application. 2006.

60. **Julia Kois**. Electrochemical deposition of CuInSe2 thin films for photovoltaic applications. 2006.

61. **Ilona Oja Açik**. Sol-gel deposition of titanium dioxide films. 2007.

62. **Tiia Anmann**. Integrated and organized cellular bioenergetic systems in heart and brain. 2007.

63. **Katrin Trummal**. Purification, characterization and specificity studies of metalloproteinases from *Vipera lebetina* snake venom. 2007.

64. **Gennadi Lessin**. Biochemical definition of coastal zone using numerical modeling and measurement data. 2007.

65. **Enno Pais**. Inverse problems to determine non-homogeneous degenerate memory kernels in heat flow. 2007.

66. **Maria Borissova**. Capillary electrophoresis on alkylimidazolium salts. 2007.

67. **Karin Valmsen**. Prostaglandin synthesis in the coral *Plexaura homomalla*: control of prostaglandin stereochemistry at carbon 15 by cyclooxygenases. 2007.

68. **Kristjan Piirimäe**. Long-term changes of nutrient fluxes in the drainage basin of the gulf of Finland – application of the PolFlow model. 2007.

69. **Tatjana Dedova**. Chemical spray pyrolysis deposition of zinc sulfide thin films and zinc oxide nanostructured layers. 2007.

70. **Katrin Tomson**. Production of labelled recombinant proteins in fed-batch systems in *Escherichia coli*. 2007.

71. **Cecilia Sarmiento**. Suppressors of RNA silencing in plants. 2008.

72. **Vilja Mardla**. Inhibition of platelet aggregation with combination of antiplatelet agents. 2008.

73. **Maie Bachmann**. Effect of Modulated microwave radiation on human resting electroencephalographic signal. 2008.

74. **Dan Hüvonen**. Terahertz spectroscopy of low-dimensional spin systems. 2008.

75. **Ly Villo**. Stereoselective chemoenzymatic synthesis of deoxy sugar esters involving *Candida antarctica* lipase B. 2008.

76. **Johan Anton**. Technology of integrated photoelasticity for residual stress measurement in glass articles of axisymmetric shape. 2008.

77. **Olga Volobujeva**. SEM study of selenization of different thin metallic films. 2008.

78. **Artur Jõgi**. Synthesis of 4'-substituted 2,3'-dideoxynucleoside analogues. 2008.

79. **Mario Kadastik**. Doubly charged Higgs boson decays and implications on neutrino physics. 2008.

80. **Fernando Pérez-Caballero**. Carbon aerogels from 5-methylresorcinol-formaldehyde gels. 2008.

81. **Sirje Vaask**. The comparability, reproducibility and validity of Estonian food consumption surveys. 2008.

82. **Anna Menaker**. Electrosynthesized conducting polymers, polypyrrole and poly(3,4-ethylenedioxythiophene), for molecular imprinting. 2009.

83. **Lauri Ilison**. Solitons and solitary waves in hierarchical Korteweg-de Vries type systems. 2009.

84. **Kaia Ernits**. Study of In2S3 and ZnS thin films deposited by ultrasonic spray pyrolysis and chemical deposition. 2009.

85. **Veljo Sinivee**. Portable spectrometer for ionizing radiation "Gammamapper". 2009.

86. **Jüri Virkepu**. On Lagrange formalism for Lie theory and operadic harmonic oscillator in low dimensions. 2009.

87. **Marko Piirsoo**. Deciphering molecular basis of Schwann cell development. 2009.

88. **Kati Helmja**. Determination of phenolic compounds and their antioxidative capability in plant extracts. 2010.

89. **Merike Sõmera**. Sobemoviruses: genomic organization, potential for recombination and necessity of P1 in systemic infection. 2010.

90. **Kristjan Laes**. Preparation and impedance spectroscopy of hybrid structures based on CuIn3Se5 photoabsorber. 2010.

91. **Kristin Lippur**. Asymmetric synthesis of 2,2'-bimorpholine and its 5,5'-substituted derivatives. 2010.

92. **Merike Luman**. Dialysis dose and nutrition assessment by an optical method. 2010.

93. **Mihhail Berezovski**. Numerical simulation of wave propagation in heterogeneous and microstructured materials. 2010.

94. **Tamara Aid-Pavlidis**. Structure and regulation of BDNF gene. 2010.

95. **Olga Bragina**. The role of Sonic Hedgehog pathway in neuro- and tumorigenesis. 2010.

96. **Merle Randrüüt**. Wave propagation in microstructured solids: solitary and periodic waves. 2010.

97. **Marju Laars**. Asymmetric organocatalytic Michael and aldol reactions mediated by cyclic amines. 2010.

98. **Maarja Grossberg**. Optical properties of multinary semiconductor compounds for photovoltaic applications. 2010.

99. **Alla Maloverjan**. Vertebrate homologues of Drosophila fused kinase and their role in Sonic Hedgehog signalling pathway. 2010.

100. **Priit Pruunsild**. Neuronal Activity-Dependent Transcription Factors and Regulation of Human *BDNF* Gene. 2010.

101. **Tatjana Knjazeva.** New approaches in capillary electrophoresis for separation and study of proteins. 2011

102. **Atanas Katerski**. Chemical composition of sprayed copper indium disulfide films for nanostructured solar cells. 2011.